Yosemite National Park
Division of Resources Management and Science

USGS science for a changing world

Quantitative rock-fall hazard and risk assessment for Yosemite Valley, Yosemite National Park, California

April, 2012

Greg M. Stock, Ph.D., P.G.[1], Nicolas Luco, Ph.D.[2], Brian D. Collins, Ph.D., P.E.,[3], Edwin L. Harp, Ph.D.[2], Paola Reichenbach[4], and Kurt L. Frankel, Ph.D.[5]

[1]National Park Service, Yosemite National Park, El Portal, CA 95318
[2]U.S. Geological Survey, Golden, CO 80225
[3]U.S. Geological Survey, Menlo Park, CA 94025
[4]Research Institute for Geo-Hydrological Protection (CNR-IRPI), Perugia, Italy
[5]Georgia Institute of Technology, Atlanta, GA 30332 (deceased)

Cover photo: Rock fall from the northwest face of Half Dome on 27 May 2011. Photo by Peter Girling, used with permission.

TABLE OF CONTENTS

Summary

Rock falls are common in Yosemite Valley, California, posing substantial hazard and risk to the approximately four million annual visitors to Yosemite National Park. Rock falls in Yosemite Valley over the past few decades have damaged structures and caused injuries within developed regions located on or adjacent to talus slopes, highlighting the need for additional investigations into rock-fall hazard and risk. This assessment builds upon previous investigations of rock fall hazard and risk in Yosemite Valley (Wieczorek et al., 1998, 1999; Guzzetti et al., 2003; Wieczorek et al., 2008), and focuses on hazard and risk to structures posed by relatively frequent fragmental-type rock falls (Evans and Hungr, 1999), up to approximately 100,000 m^3 in volume.

Previous rock-fall hazard assessments delineated two primary hazard zones in Yosemite Valley defined by: (1) a line delineating the base of rock-fall talus and other slope movement debris, and (2) a line delineating the shadow angle limit (Wieczorek et al., 1998, 1999). The base of talus line encapsulates all rock debris on the valley floor and provides an important first approximation of the hazard, as evidence of past rockfalls (such as talus) is a generally a positive predictor of future rock fall deposition areas. However, by encapsulating all rock debris on the valley floor, the base of talus line mapped by Wieczorek et al. (1998, 1999) does not discriminate between active rock fall and debris flow deposits and inactive rock avalanche and debris flow deposits. Furthermore, as a hazard approximation, the base of talus line does not address the expected progradation of the talus edge as future rock falls accumulate on the talus slope.

We define a new rock-fall hazard line by integrating the spatial distribution of individual boulders beyond the base of talus with the inferred frequency of boulder deposition in this region. Debris from most rock falls will come to rest on talus slopes, but some rock falls produce boulders that will travel beyond the base of talus and out onto the valley floor, where substantial park infrastructure exists. The boulders that lie farthest beyond the talus edge presumably indicate the maximum extent of fragmental rock-fall debris since the deglaciation of Yosemite Valley about 15,000 years ago. These "outlying" boulders define a hazard zone that accounts for talus slope progradation and is relevant to developed regions in Yosemite Valley adjacent to active talus slopes.

We mapped 258 outlying boulders in 16 study regions throughout Yosemite Valley, and used a statistical approach to define the distances beyond the base of talus that encompass 90% of the outlying boulders in each region. 90^{th}-percentile distances for the study regions range from 7 to 57 m beyond the mapped base of talus. This statistical analysis defines a probability of outlying boulder deposition, with a 90% probability that outlying boulders resulting from future fragmental rock falls will be deposited between the talus edge and this line, and a 10% probability that future rock-fall boulders will be deposited beyond this line. Selection of the 90^{th}-percentile distances, which is based on professional judgment, captures 90% of the population of outlying boulders while properly excluding true statistical – and potentially anomalous – outliers.

The geologic record of the past 15,000 years of outlying boulder deposition give some indication of potential runout distances of future events. However, the frequency of outlying boulder deposition within each study region is not taken into account by the 90th-percentile distances. To explicitly account for frequency, we adjusted the 90th-precentile distances by frequency-related factors derived from cosmogenic exposure dating of outlying boulders and numerical simulations of potential future rock-fall trajectories and runout extents.

Cosmogenic beryllium-10 exposure dating of outlying boulders indicates that outlying boulders tend to result from numerous individual events through time rather than only a few events. The oldest boulder exposure ages approach the timing of deglaciation for Yosemite Valley (~15,000 years), suggesting that 15,000 years is a reasonable time period for the accumulation of outlying boulders for each study region. We calculate annualized frequency of outlying boulders for each study region, and for the union of all of the study regions, by dividing the corresponding number of outlying boulders by 15,000 years.

To evaluate the approximate frequency of potential future rock falls, we used a three-dimensional computer program that simulates rock-fall runout (STONE). The model tracks the trajectories of dimensionless particles and reports them as raster grid cells in a Geographic Information Systems (GIS) database. We performed rock-fall trajectory modeling in which rock falls were simulated from every slope ≥60° in Yosemite Valley. The resulting trajectory maps provide a means of comparing the number of rock-fall trajectories entering each study region in relation to the total number of simulated trajectories across all study regions. We then compared these estimates with the corresponding number of actual mapped outlying boulders in each study region. Based on this comparison, we used the modeled trajectories to apportion the total (across all study regions) annualized frequency of outlying boulders to the individual study regions.

The two estimates of outlying boulder frequency in each study region are both plausible estimates that we give equal weight in our rock-fall hazard assessment. We used the average of these annualized frequencies, each normalized by the width of the respective study regions, and the frequencies based on the observed outlying boulders, to adjust the 90th-percentile distance line inward or outward relative to talus edge. The adjusted hazard line is such that the average recurrence interval for deposition of outlying boulders beyond the line is everywhere approximately 500 years, an interval commonly used for assessing other natural hazards such as earthquakes or floods. Assuming steady deposition through time, this translates to an approximately 0.2% probability of boulder deposition beyond the hazard line in a given year, or a 10% probability of occurrence in 50 years.

The hazard line is thus based on observable, measurable evidence of previous rock falls in the form of the spatial distribution of outlying boulders, but also incorporates additional data on the frequency of occurrence of outlying boulder deposition. The hazard line is generally positioned outboard of the edge of talus line (more toward the

center of Yosemite Valley) mapped by Wieczorek et al. (1998, 1999) except where it crosses regions of presently inactive talus, such as prehistoric rock avalanche deposits, or the distal portions of debris flow fans, which have lower frequencies of occurrence. The line defines a rock-fall hazard zone between the line on the valley floor and the apex of talus slopes.

The hazard line presented here encompasses a zone of deposition for fragmental rock falls in Yosemite Valley up to approximately 100,000 m^3 in volume. It does not account for potential deposition zones of infrequent extremely large rock falls (>100,000 m^3), zones potentially affected by airblasts produced by rock-fall impacts, or zones affected by flyrock (i.e., rock "shrapnel" produced by impacts on talus slopes). This report also does not account for geological hazards associated with debris flows. As previously stated by Wieczorek et al. (1998), because of the configuration of the steep, tall (~ 1 km) valley walls and the relatively narrow (~1 km) valley, there are no absolutely safe or zero probability regions for extremely large rock falls or rock avalanches within Yosemite Valley.

We assessed risk to structures within the rock-fall hazard zone by identifying structures within the line (including visitor accommodations, campsites, employee residences, and communal structures such as amphitheaters) and assembling use data for each structure. We quantified the human exposure to rock-fall hazard in each building or other structure in terms of an expected number of people in each structure at any given moment in time when a rock fall could occur. This was calculated by multiplying the typical number of occupants in each structure by its occupancy rate (i.e., the fraction of year that the structure is occupied). We assumed that all structures in the study regions are equally vulnerable to penetration by rock-fall boulders. We then calculated a risk metric for each structure that is proportional to an annualized expected number of people struck by outlying boulders; this is calculated as the product of an annualized frequency of an outlying boulder striking the structure and the expected number of people in it.

Aggregated risk metrics for each study region reveal two important points: (1) Permanent closure of structures in Curry Village in 2008 reduced the overall risk associated with structures in Yosemite Valley by at least 87%, and (2) following the 2008 closures, the remaining risk associated with structures is highest in Curry Village, Camp 4, and the Curry Village Residential Area, respectively, with lesser degrees of risk in the LeConte-Housekeeping Camp, Sunnyside Bench, Castle Cliffs, Wahhoga, and El Capitan study regions, respectively. Sorting the list of structures by their risk metrics can assist the National Park Service in evaluating infrastructure within the hazard zone and prioritizing planning and mitigation actions.

1.0 Introduction

Rock falls are a type of rapid mass movement common in mountainous regions worldwide. A rock fall is an event that involves independent movement of individual rock fragments that detach from bedrock along new or previously existing discontinuities such as bedding planes, joints, fractures, cleavage, and foliation (Selby, 1993). This type of event is often termed "fragmental" rock fall (Evans and Hungr, 1993). In general, fragmental rock falls involve relatively small detachments (<100,000 m^3), although there is no well-defined volume limit (Evans and Hungr, 1993). However, because they are characterized by high energy and mobility, even relatively small rock falls can pose a substantial hazard. Rock fragments may move initially by creeping, sliding, toppling, or falling (Varnes, 1978), and then subsequently fall from a cliff and proceed down slope by bouncing along ballistic trajectories, or by rolling on bedrock, talus, or debris slopes. When a rock fragment, termed a "boulder", has dissipated sufficient energy through impacts or friction it generally stops on or near the edge of the talus slope, though in some cases can travel far beyond the talus edge (Evans and Hungr, 1993).

A number of geologic factors can lead to a rock fragment on a cliff becoming unstable, including lithology, spacing and orientation of discontinuities, and weathering (Selby, 1993; Dorren, 2003). Rock-fall triggers, which initiate movement of rock fragments, can include earthquakes (Harp and Wilson, 1995; Keefer 1984), freeze-thaw cycles of water (Gardner, 1983; Matsuoka and Sakai, 1999), precipitation and snowmelt (Chau et al., 2003; Wieczorek and Jäger, 1996), temperature changes (Davies et al., 2001, Vargas et al., 2009), and redistribution of stresses (Wieczorek and Jäger, 1996; Wieczorek and Snyder, 2004; Stock et al., 2012a). However, in many cases triggers are not recognized, even when events are closely monitored (Wieczorek and Jäger, 1996; Wieczorek and Snyder, 1999, 2004; Stock et al., 2011, 2012a, b). This greatly complicates efforts to develop time-dependent predictions of rock fall occurrence.

1.1 Geologic setting and rock-fall hazards in Yosemite Valley

Yosemite Valley is located in Yosemite National Park, California (Figures 1, 2). The region is underlain by Late Cretaceous-age granitic rocks of the Sierra Nevada batholith (Bateman, 1992; Calkins et al., 1985). Yosemite Valley has been carved into granitic rocks by both rivers and glaciers, with Pleistocene glacial cycles contributing substantially to creating the steep, approximately 1 km tall walls that form the valley's sides (Matthes, 1930; Huber, 1987). The most recent glaciation (the Last Glacial Maximum, known locally as the Tioga Glaciation) reached a maximum position midway up the valley walls about 18,000 years ago and retreated thereafter (e.g., Bursik and Gillespie, 1993; Phillips et al., 2009). Yosemite Valley is thought to have deglaciated by about 15,000 to 17,000 years ago (Huber 1987; Smith and Anderson, 1992; Stock and Uhrhammer, 2010), leaving behind a relatively flat valley floor free of talus at about the same elevation (within approximately 5 m) as the modern valley floor. This setting provides for remarkable long-term preservation of post-glacial rock-fall deposits on the valley floor.

Figure 1. View of Yosemite Valley in Yosemite National Park, California, looking to the east from "Discovery View". The glacially steepened cliffs of Yosemite Valley experience numerous rock falls each year.

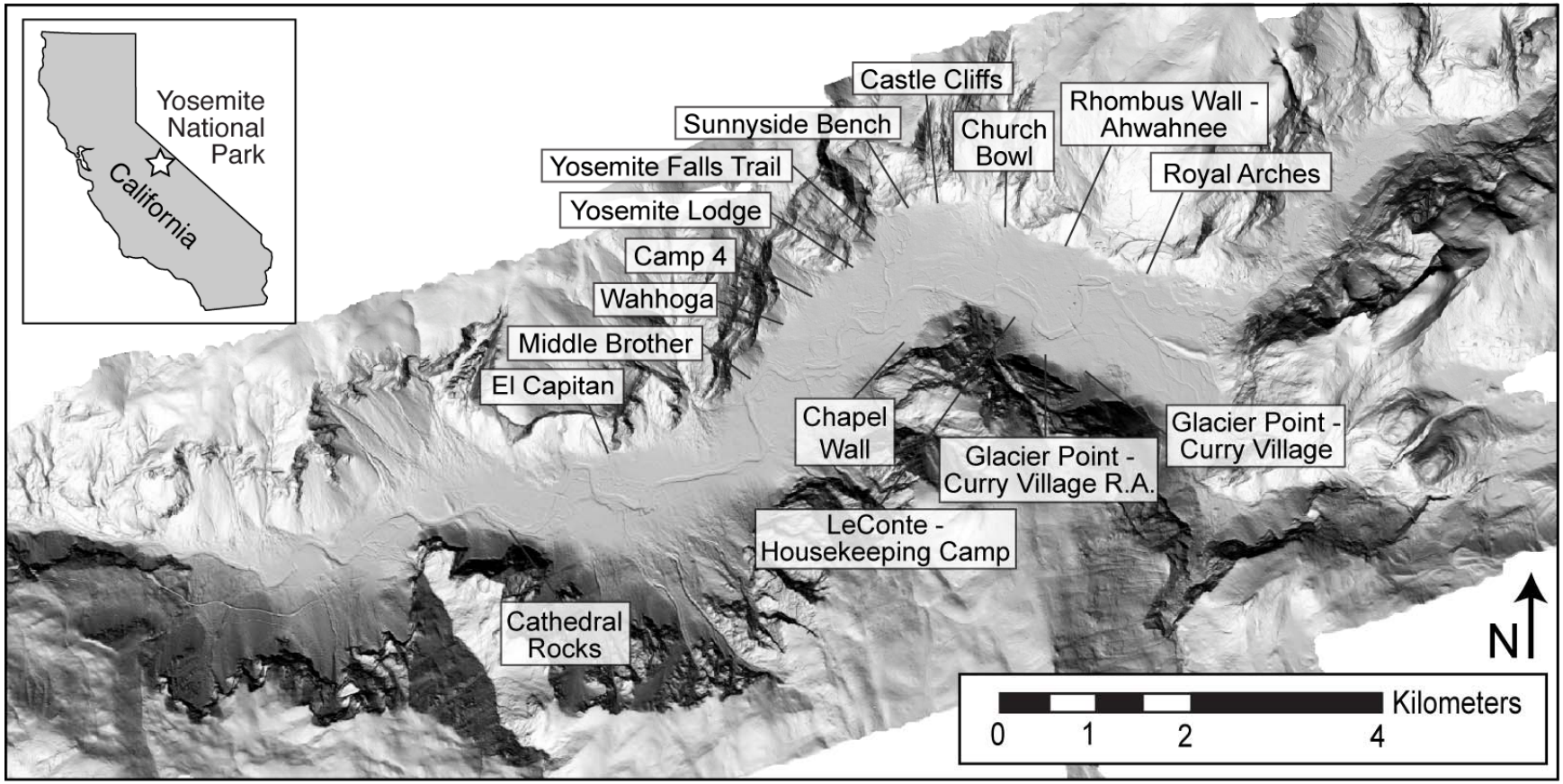

Figure 2. Shaded relief map of Yosemite Valley in Yosemite National Park, California (inset), showing locations of the sixteen study regions discussed in the text.

Since deglaciation, rock falls have left abundant talus deposits around the base of almost all the cliffs of Yosemite Valley. Matthes (1930) first mapped the extent of talus around the edge of the valley, which, in some places, is estimated to be greater than 100 m thick (Wieczorek and Jäger, 1996). At some locations, such as below El Capitan, where a large prehistoric rock avalanche occurred, these deposits extend more than 400 m beyond the base of talus slopes produced by fragmental rock falls and across the valley floor (Stock and Uhrhammer, 2010).

Yosemite Valley experiences many fragmental rock falls each year (Figures 3, 4). A database of historical rock falls and other slope movement events documents 910 events between 1857 and 2011, with the majority of events occurring as rock falls or rock slides in Yosemite Valley (Stock et al., 2012b). Recent (2006-2011) detailed documentation demonstrates that approximately one rock fall occurs each week on average in Yosemite Valley. Based on historic rock-fall frequency-magnitude relations (Wieczorek et al., 1995), a rock fall of approximately 10,000 m^3 occurs each year in Yosemite Valley on average, and at least one rock fall greater than 100,000 m^3 has occurred in historic time (the ~600,000 m^3 1987 Middle Brother rock fall; Wieczorek, 2002; Stock et al., 2012b).

Figure 3. Rock fall from the southeast face of El Capitan on 11 October 2010. The height of the cliff above the talus is approximately 700 m. Photo by Luke Lydiard.

Rock falls in Yosemite Valley range in size from small individual blocks of less than 1 m^3 to rock avalanches up to approximately 11 million m^3 (e.g., Wieczorek et al., 1999, 2000, 2008; Stock et al., 2011, 2012a, b; Zimmer et al., 2012). Rock avalanches pose substantial hazard due to their large size and correspondingly long runout, but their frequency is low, with only six events in Yosemite Valley in the past approximately 15,000 years (Wieczorek et al., 1998, 1999); many cliffs in Yosemite Valley have not

experienced any rock avalanches in that time period. Smaller fragmental rock falls are much more frequent (Stock et al., 2102b), and though they are generally not as hazardous as a rock avalanche, even a rapidly moving small boulder can cause serious injury to people and considerable damage to buildings, vehicles, roads, and other infrastructure.

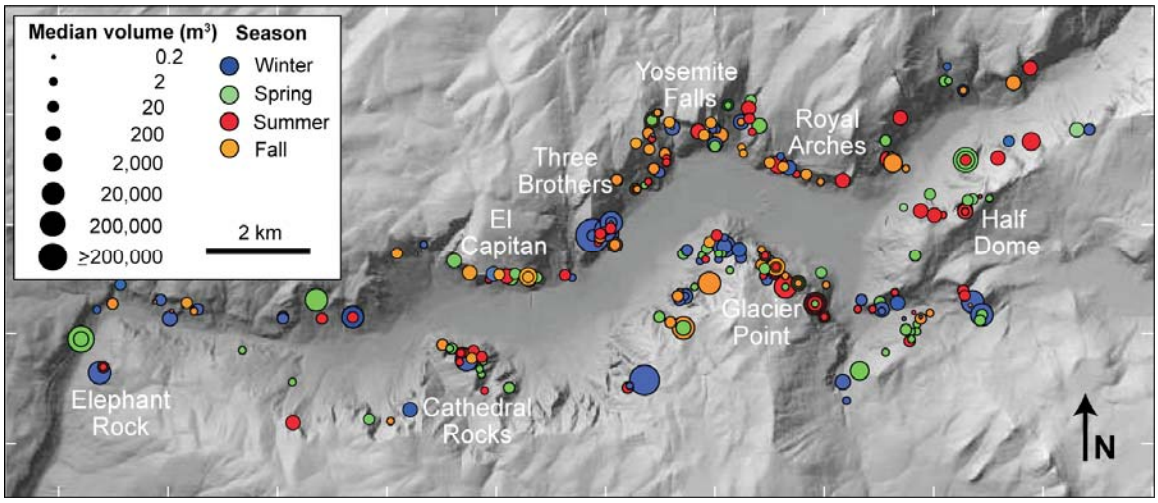

Figure 4. Map of Yosemite Valley showing historical rock falls (1857-2011) for which the location and seasonality of occurrence are known. The greater number of rock falls in eastern Yosemite Valley likely represents a reporting bias (i.e., there more people in eastern Yosemite Valley to report rock falls) rather than a real difference in rock fall activity.

1.2 Need for hazard and risk assessment in Yosemite Valley

Rock falls have long been recognized as a potent natural force in Yosemite (LeConte, 1875; Muir, 1912; Matthes, 1930). However, due perhaps in part to the smaller number of visitors to Yosemite Valley during the late 1800's and early 1900's, recognition that rock falls also pose substantial hazard and risk was slower to take hold. This perception changed drastically following the 16 November 1980 rock fall onto the upper Yosemite Falls Trail, which caused three fatalities and at least 19 injuries (Stock et al., 2012b), representing the greatest mass casualty incident in Yosemite National Park's history. This tragic event marked the beginning of a collaborative relationship between the U.S. Geological Survey and the National Park Service to document and analyze rock falls and rock-fall hazards in Yosemite National Park, with the intent to quantify the hazard posed by rock falls in Yosemite Valley.

It is now recognized that fragmental rock falls pose hazard and resulting risk to the nearly four million annual visitors to Yosemite National Park, the majority of whom (~70%) visit Yosemite Valley. Numerous rock falls have adversely impacted human safety and park infrastructure in Yosemite Valley in historic time. Between 1857 and 2011, there were 15 fatalities and at least 85 injuries from rock falls and other slope movement events (Stock et al., 2012b). Rock falls and rock slides have impacted trails, roads, parking lots, tent cabins, wooden cabins, residences, and other structures in

Yosemite Valley; examples include the 1987 Middle Brother rock fall (Weiczorek, 2002), the 1996 Happy Isles rock fall (Wieczorek et al., 2000), the 1998-1999 Curry Village rock falls (Wieczorek and Snyder, 1999), the 2008 Glacier Point rock falls (Figure 5; Stock et al., 2011), the 2009 Ahwiyah Point rock fall (Zimmer et al., 2012), and the 2009-2010 Rhombus Wall rock falls (Stock et al., 2012a). The 2008 Glacier Point rock falls, which represent the most damaging historical rock fall event with respect to infrastructure (Figure 5), led the National Park Service to permanently close more than 200 buildings within the Curry Village area.

Figure 5. Cabin damage in Curry Village from a fresh, light-colored boulder resulting from the 8 October 2008 rock fall from Glacier Point. Darker-colored prehistoric rock-fall boulders can be seen in the background. Buildings in this region were permanently closed following the rock fall.

1.3 National Park Service policies regarding geological hazard and risk assessment

This report assesses hazard and risk posed by frequent, fragmental-type rock falls within Yosemite Valley in Yosemite National Park. The National Park Service (NPS) is charged with preserving unimpaired the natural and cultural resources and values of the national park system for the enjoyment, education, and inspiration of present and future generations. The mission of the NPS is:

> *"...to conserve the scenery and the natural and historic objects and the wild life therein and to provide for the enjoyment of the same in such manner and by such means as will leave them unimpaired for the enjoyment of future generations."*
> National Park Service Organic Act, 16 U.S.C.1.

In fulfilling this mission, the NPS must balance issues of access against those of safety. Toward this goal, the NPS *"must strive to prevent visitor injuries and fatalities within the limits of available resources. Within this context, visitor risk management does not mean eliminating all dangers, nor can the NPS guarantee visitor safety or be responsible for acts and decisions made by visitors that may result in their injury or illness."* National Park Service Director's Order #50C: Public Risk Management Program.

Further, Director's Order #50C states that Park Superintendents *"should strive to minimize the frequency and severity of visitor incidents by developing a range of appropriate prevention strategies and implementing risk reduction mitigation plans".* Examples of such strategies include *"conducting periodic risk assessments to identify and appropriately mitigate hazards"* and *"integrating safety measures into the design and maintenance of park facilities, as appropriate, feasible, and consistent with NPS and park mandates."* Section 4.1 Management and Incident Reduction, Operational Policies and Procedures

NPS Management Policies (2006) state the following with regard to identifying and managing geologic hazards:

> *"Naturally occurring geologic processes, which the Park Service is charged to preserve unimpaired, can be hazardous to humans and park infrastructure. These include earthquakes, volcanic eruptions, mudflows, landslides, floods, shoreline processes, tsunamis, and avalanches. The Service will work closely with specialists at the U.S. Geological Survey and elsewhere, and with local, state, tribal, and federal disaster management officials, to devise effective geologic hazard identification and management strategies. Although the magnitude and timing of future geologic hazards are difficult to forecast, park managers will strive to understand future hazards and, once the hazards are understood, minimize their potential impact on visitors, staff, and developed areas. Before interfering with natural processes that are potentially hazardous, superintendents will consider other alternatives."* Section 4.8.1.3 Geologic Hazards

NPS Management Policies (2006) also state the following with regard to siting facilities to avoid natural hazards:

> *"The Service will try to avoid placing new visitor and other facilities in geologically hazardous areas. Superintendents will examine the feasibility of phasing out, relocating, or providing alternative facilities for park developments subject to hazardous processes, consistent with other sections of these Management Policies."* Section 4.8.1.3 Geologic Hazards.

> *"The Service will strive to site facilities where they will not be damaged or destroyed by natural physical processes. Natural hazard areas include sites with unstable soils and geologic conditions, fault zones, thermal areas, floodplains, flash-flood zones, fire-prone vegetation, and coastal high-hazard areas. Park development that is damaged or destroyed by a hazardous or catastrophic natural*

event will be thoroughly evaluated for relocation or replacement by new construction at a different location. If a decision is made to relocate or replace a severely damaged or destroyed facility, it will be placed, if practicable, in an area that is believed to be free from natural hazards. In areas where dynamic natural processes cannot be avoided, such as seashores, developed facilities should be sustainably designed (e.g., removable in advance of hazardous storms or other conditions). When it has been determined that facilities must be located in such areas, their design and siting will be based on

- *a thorough understanding of the nature of the physical processes; and*
- *avoiding or mitigating (1) the risks to human life and property, and (2) the effect of the facility on natural physical processes and the ecosystem."*

Section 9.1.1.5 Siting Facilities to Avoid Natural Hazards

Thus, the NPS has clear direction to identify areas potentially subject to geological hazards such as rock falls in Yosemite Valley, and to identify ways to mitigate or otherwise manage these hazards.

The protected status of most of the cliffs in Yosemite Valley (Congressionally-designated Wilderness) and the directive to let natural processes prevail in National Parks limits the amount of direct mitigation that can be performed to reduce the number and magnitude of rock falls in Yosemite Valley. Furthermore, mitigating the very high energies from most rock falls in Yosemite Valley by protective structures such as ditches, fences, or netting is not feasible in most cases. As a result, the most effective mitigation for reducing hazard and risk from rock falls in Yosemite Valley is to minimize exposure to rock falls by locating (or relocating) structures away from regions of potential rock-fall deposition.

2.0 Previous rock-fall hazard and risk assessments in Yosemite Valley

With respect to rock falls and other slope movement events, hazard has been defined as "the probability of occurrence within a specified period of time and within a given area of a potentially damaging phenomenon" (Varnes, 1984). This widely accepted definition incorporates the important concepts of location (i.e., where an event will occur) and time (i.e., when or how frequently an event will occur). Information on both location and time are critical for accurate hazard assessment. With respect to rock falls and other slope movements, risk has been defined as "a measure of the probability and severity of an adverse affect to health, property, or the environment" (Fell et al., 2008). Though a variety of methods exist for assessing risk (e.g., Dai et al., 2002), risk is often estimated by the mathematical product of the probability of an event of a given magnitude occurring and the related consequences of that occurrence (Fell, 1994; Fell et al., 2008).

A variety of methods have been proposed and implemented for assessing rock-fall hazard. Many methods are empirical, drawing on existing inventories of rock falls (e.g., Hungr et al., 1999; Dussauge-Peisser et al., 2002; Dussauge et al., 2003; Guzzetti et al., 2003; Copons and Villaplana, 2008; Corominas and Moya, 2008). These methods

typically only consider the triggering probability of rock falls, without any characterization or modeling of rock-fall runout trajectories or impacts. Other studies have integrated empirical methods with more deterministic models of rock-fall susceptibility and runout (e.g., Evans and Hungr, 1993; Bunce et al., 1997).

More recently, researchers have used Geographic Information Systems (GIS) to perform more quantitative spatial analyses of rock-fall hazard and risk (e.g., Jaboyedoff and Labiouse, 2003, Jaboyedoff et al., 2004; Coe et al., 2005; Derron et al., 2005; Frattini et al., 2008; Ruff and Czurda, 2008; Loye et al., 2009). Hazard studies utilizing GIS benefit from being able to compile and analyze multiple layers of spatial information derived from both field investigations and computer modeling. The results from physically based computer simulations of rock-fall runout provide an important means of characterizing potential rock-fall dynamics and runout distances (Dorren et al., 2003), and in most cases can be easily integrated into GIS. Initial attempts dealt primarily with two-dimensional cross-sections (e.g., Jones et al., 2000), but advances in computing power have allowed more recent models to operate in three-dimensional space, often utilizing high-resolution digital topographic data (e.g., Guzzetti et al., 2002; Agliardi and Crosta, 2003; Crosta and Agliardi, 2003; Dorren and Seijmonsbergen, 2003; Dorren et al., 2004; Tagliavini et al., 2009; Lan et al., 2010).

Wieczorek et al. (1992) provided the first systematic documentation of rock falls and other slope movement events in Yosemite National Park, with a focus on rock falls in Yosemite Valley. This event inventory utilized published and unpublished accounts of rock falls, direct observations from park visitors, employees, and residents, and other records. Wieczorek and Snyder (2004) and Stock et al. (2012b) have subsequently updated the database. These data have been used to assess magnitude-frequency relations for historical rock falls in Yosemite Valley (e.g., Wieczorek et al., 1995; Dussauge-Peisser et al., 2002; Dussauge et al., 2003; Guzzetti et al., 2003).

In support of planning efforts in the 1990's, Wieczorek et al. (1998) performed hazard assessment for select areas in Yosemite Valley (Figure 6). This assessment involved (1) compiling spatial information on the source areas and runout extent of prehistorical (pre-1850 C.E.) and historical rock falls and other slope movements, (2) mapping the base of talus, including extents of debris flows and rock avalanche deposits, and (3) determining the rock-fall shadow angle limit (Figure 6; Wieczorek et al., 1998). Subsequent work by Wieczorek et al. (1999) further refined the extent of talus and the shadow line in Yosemite Valley (Figure 7).

Guzzetti et al. (2003) first applied three-dimensional computer modeling of rock-fall runout to hazard and risk assessment in Yosemite Valley. They calibrated the STONE rock-fall simulation model (Guzzetti et al., 2002) to Yosemite Valley using previously defined geological units, and compared initial simulation results for individual rock falls to actual rock falls mapped in the field (Guzzetti et al., 2003). They also performed a valley-wide rock-fall simulation and assessed hazard and risk along roads and trails in Yosemite Valley (Guzzetti et al., 2003). Wieczorek et al. (2008) subsequently used the STONE model to simulate recent and potential future rock falls

from the Staircase Falls rock-fall source area on Glacier Point, above Curry Village. They determined, based on observations of recent rock falls, mapping of rock debris, and simulations of rock-fall runout distances beneath the Staircase Falls area, that "rock-fall hazard zones extend farther downslope than the extent previously defined by mapped surface talus deposits" (Wieczorek et al., 2008).

In addition to hazard assessment, recent studies in Yosemite Valley have focused on probable rock-fall triggering mechanisms (Wieczorek and Jäger, 1996; Stock et al., 2011; 2012a; Zimmer et al., 2012) and cliff evaluations of rock-fall susceptibility (Matasci et al., 2011; Stock et al. 2011). Both of these subject areas have the potential to further clarify future rock-fall hazard assessment by better defining specific rock-fall sources on the cliffs, and by identifying the conditions under which rock falls from these sources would most likely occur. However, these studies are still in preliminary phases, and results so far indicate that both rock-fall triggering and susceptibility are complex issues. Because of that, and because of the vast scale of potential rock-fall sources in Yosemite Valley (at least 40 km^2 of cliffs with slope angles $\geq 45°$ in Yosemite Valley; Guzzetti et al., 2003), the hazard assessment presented here focuses on those areas on adjacent to talus slopes that are subject to boulder deposition independent of the exact timing or point of origin of future rock falls.

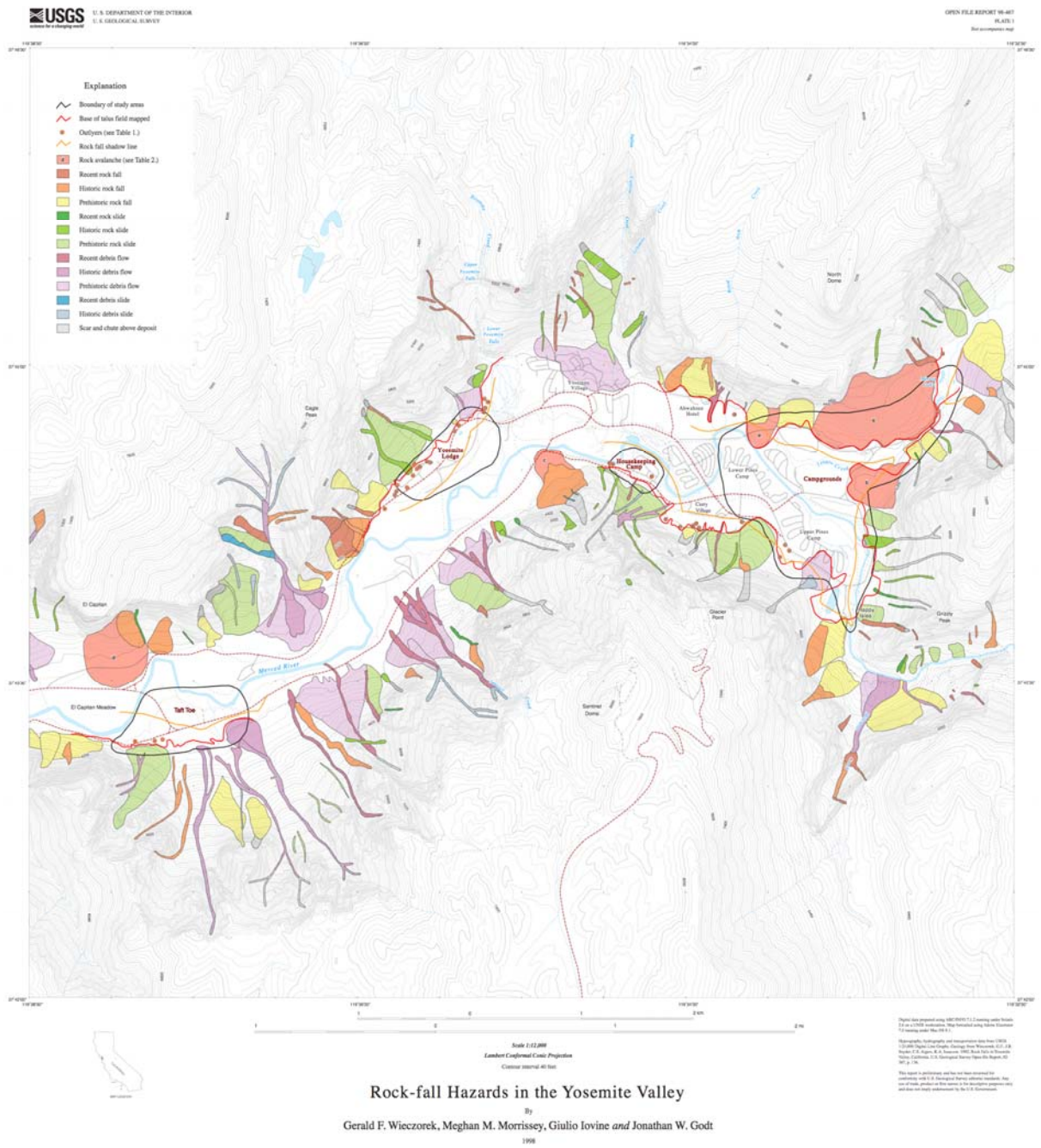

Figure 6. Map showing recent, historic, and prehistoric rock falls and other slope movement events in Yosemite Valley from 1857 to 1998, reproduced from Wieczorek et al. (1998). Note the position of the base of talus (red line), partial rock-fall shadow line (yellow line), and study areas (black lines). Document available online at: http://pubs.usgs.gov/of/1998/ofr-98-0467/

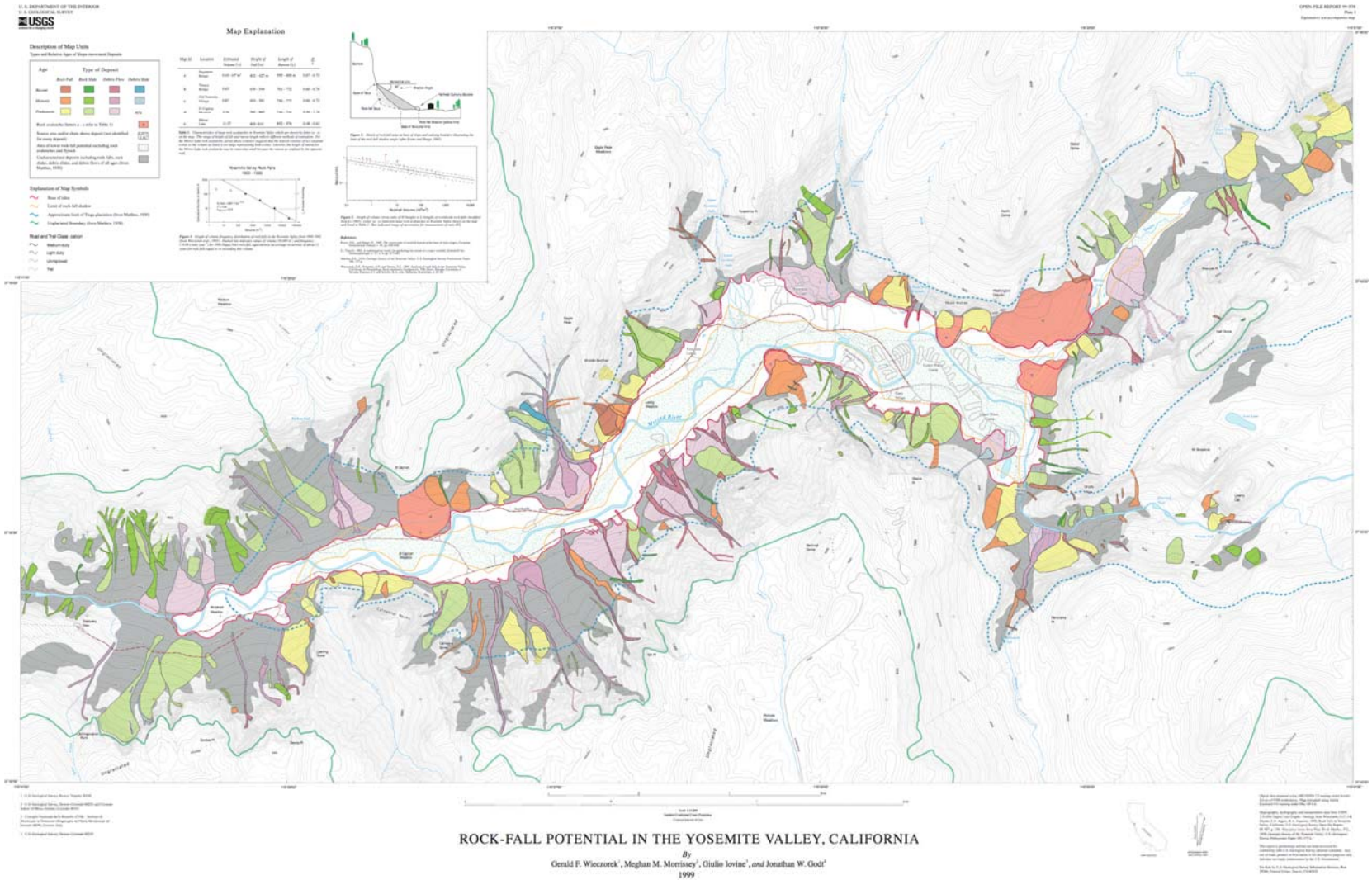

Figure 7. Map showing rock-fall hazard potential based on recent, historic, and prehistoric rock falls and other slope movement events in Yosemite Valley from 1857 to 1998, reproduced from Wieczorek et al. (1999). Note base of talus line (red) and rock-fall shadow line (yellow). Document available online at: http://pubs.usgs.gov/of/1999/ofr-99-0578/

3.0 Existing data sources

The hazard and risk assessment described herein uses both existing and newly collected data for Yosemite Valley. Existing sources include geologic mapping data, airborne laser scanning data (often referred to as Light Detection and Ranging, or LiDAR, data) and visitor use data for risk assessment analysis. New data sources collected as part of this project include mapping and cosmogenic nuclide exposure dating of outlying boulders and simulations of rock-fall trajectories and runouts using computer models. Existing data sources are described in this section, whereas new data sources are described in later sections of this report.

3.1 Geologic mapping data

Data on the bedrock and surficial geology of Yosemite Valley go back nearly a century, to the geologic mapping of Francois Matthes and Frank Calkins of the U.S. Geological Survey (Matthes, 1930; Calkins et al., 1985). These maps detail the geology of the predominantly granitic bedrock of Yosemite Valley, as well as Quaternary surficial deposits such as alluvium, glacial deposits, rock-fall talus, and debris flow (torrent) deposits. Matthes (1930) produced the first map of the base of talus slopes, which was subsequently revised by Wieczorek et al. (1998, 1999). Wieczorek et al. (1998, 1999) also mapped prehistoric, historic, and recent slope movement events such as rock falls, rock slides, rock avalanches, debris slides, and debris flows. These data will be discussed in more detail is Section 4.

3.2 Airborne LiDAR data

In September 2006, airborne LiDAR data were collected for Yosemite Valley and vicinity, an area of approximately 43 km^2. Airborne LiDAR data were collected with an Optech 1233 ALTM scanner mounted in a turbocharged twin engine Cessna 337. Flying heights above ground level ranged from less than 100 m to more than 2 km, with an average height of 1050 m. The average resultant point spacing on the ground was approximately 75 cm. Interpolation of the LiDAR point cloud results in a digital elevation model (DEM) that has approximately 1 m resolution, from which we generated detailed shaded relief (Figure 8), surface slope (Figure 9), and other topographic maps. In addition, the data can be interrogated for analysis of site-specific events when necessary and compared with subsequent data from either airborne or terrestrial LiDAR methods (e.g., Stock et al., 2011; 2012a; Zimmer et al., 2012).

3.3 Infrastructure data

The NPS maintains a complete inventory of infrastructure within Yosemite National Park, including roads, trails, utilities, and approximately 5,000 buildings. This infrastructure was mapped in the field and with aerial photogrammetry, subsequently

digitized and expanded upon in CAD, and exported to ArcGIS. The information available for each building include a name, its address, a global identification code, the region of the Park in which it is located, its function, and the planimetric area of the polygon that depicts the building in plan view.

3.4 Building occupancy data

The NPS and current park concessionaire, Delaware North Corporation (DNC), maintain monthly and/or daily occupancy or "use" data for the major visitor areas in Yosemite Valley, including Camp 4, Backpacker's Campground, Curry Village, Housekeeping Camp, and the Ahwahnee. For the risk assessment described in this report (see Section 5), the NPS and DNC also provided data for the NPS and concessioner employee housing in Yosemite Village and Curry Village, the NPS Wildlife Building, the NPS Videography Office, and the Curry Village Amphitheater. Park partnering organizations provided use data for the District Court House, the LeConte Memorial Lodge, the US Post Office, the Ansel Adams Gallery, AT&T residences, Yosemite Valley school teacher residences, and the Wahhoga Roundhouse. All occupancy rates were based on use data from 2010. For the risk assessment analyses (see Section 5), we used these data to estimate the number of hours per day that each building or site is in use in order to arrive at the expected number of people in it at any given moment in time.

Exposure factors, a key component of the risk assessment described in detail in Section 5, were based on one year (365 days) of use. As most of the structures evaluated are continuously inhabited, the calculated exposure factors accurately represent the year-round occupancy of the structures. However, in some cases (e.g., Camp 4 campsites, LeConte Lodge, and the Curry Village amphitheater) occupancy is strongly seasonal; in these cases the occupancy rate averaged over one year is less than the maximum occupancy during the busy season (summer). Considering that there is not a strong seasonality to rock-fall activity in Yosemite Valley (Stock et al., 2012b), we consider an annual average of exposure to be reasonable.

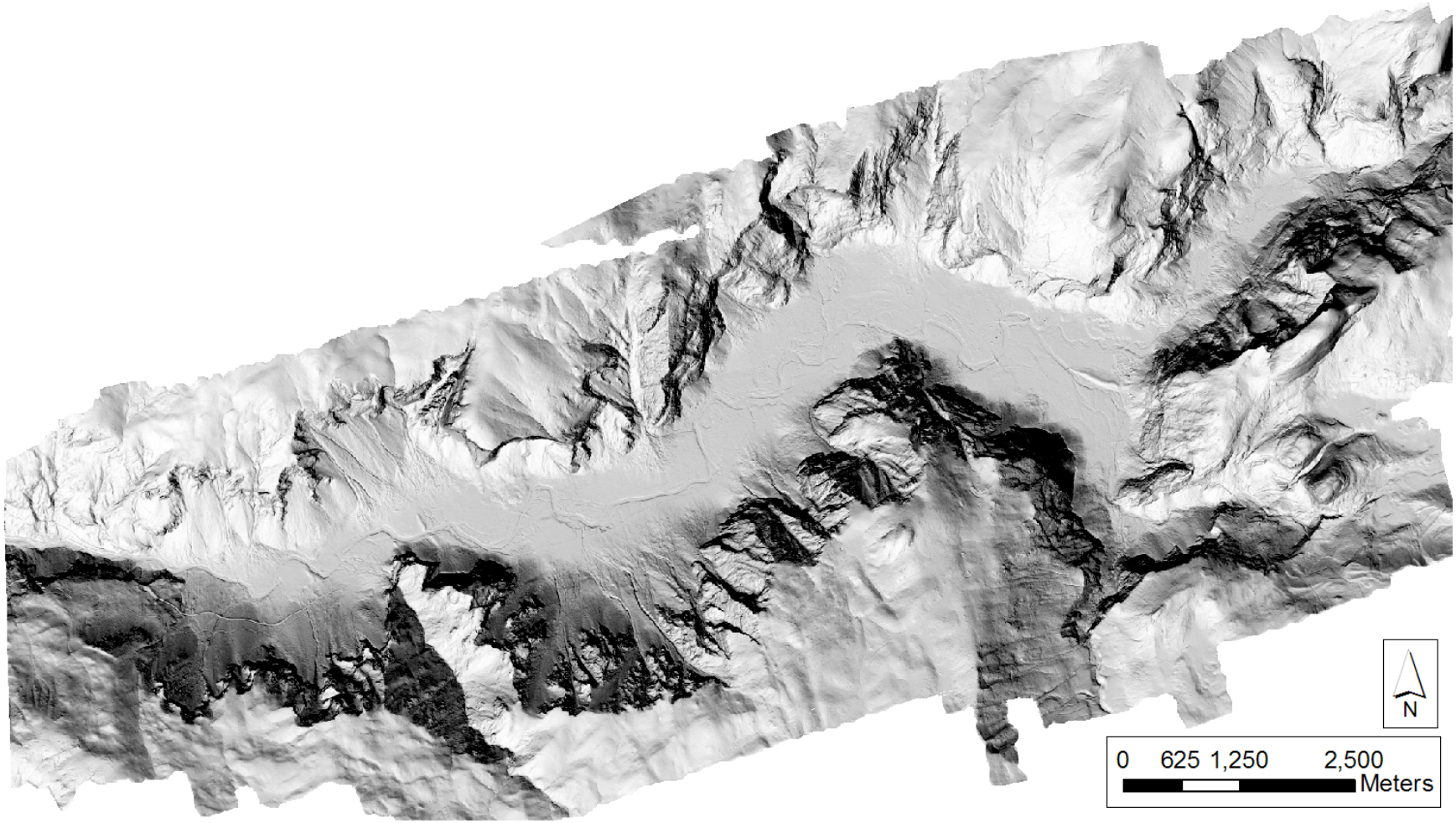

Figure 8. Shaded relief map of Yosemite Valley derived from 1-m digital elevation model (DEM) from airborne LiDAR data. See Figure 2 for general place names and study region locations.

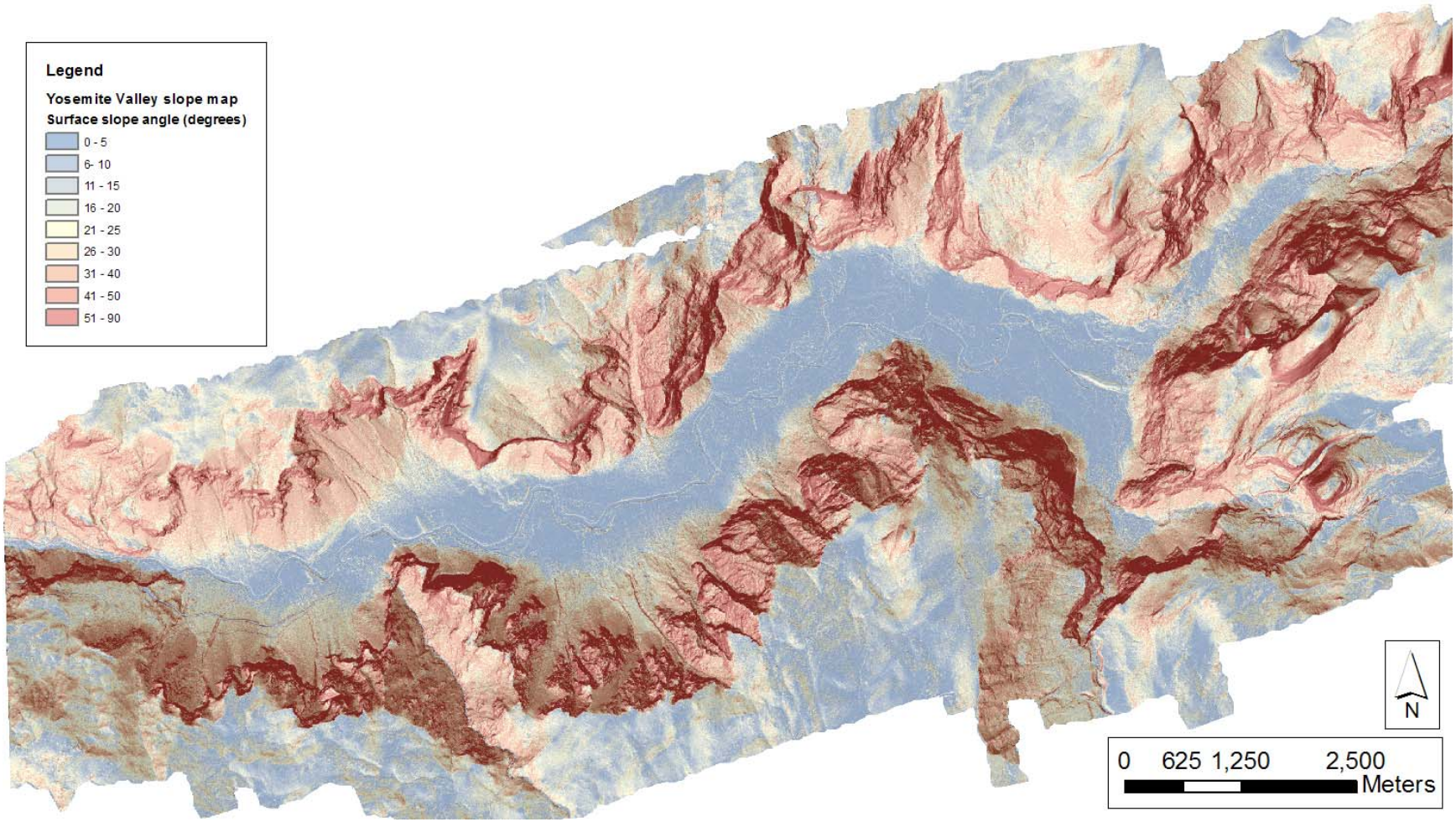

Figure 9. Surface slope map for Yosemite Valley derived from 1-m digital elevation model (DEM) from airborne LiDAR data. The very steep valley walls (red) are easily distinguished from the nearly flat valley floor (blue). See Figure 2 for general place names and study region locations.

4.0 Rock-fall hazard assessment

4.1 Scope and definitions

This report assesses the hazard associated with individual, fragmental rock falls up to volumes of approximately 100,000 m^3, which represents the most common events in Yosemite Valley (Wieczorek et al., 1998; Guzzetti et al., 2003; Dussauge-Peisser et al., 2002; Dussauge et al., 2003). This document does not assess hazards associated with extremely large rock falls (>100,000 m^3) or rock avalanches (infrequent, extremely large mass movement events, sometimes measuring approximately >500,000 m^3 in volume; Wieczorek et al., 1999; Stock and Uhrhammer, 2010), air blasts associated with impacts of large intact rock masses on talus slopes (Morrissey et al., 1999; Wieczorek et al., 2000), or flyrock - small rock fragments produced by rock debris impacts on bedrock ledges or talus boulders that have trajectories independent of the main rock-fall mass (Wieczorek and Snyder, 1999). Research on these phenomena in Yosemite Valley is ongoing, but the existing data are not sufficient to evaluate hazards associated with them at this time. This report also does not specifically address hazards associated with debris flows or debris slides, although the extent of debris flows and slides is accounted for in the base of talus line as mapped by Wieczorek et al. (1998, 1999).

Individual, fragmental-type rock falls (herein referred to simply as "rock falls") deposit rock debris on talus slopes, with some rock falls depositing "outlying" boulders beyond the edge of talus slopes. Outlying boulder deposition may occur, for example, when boulders have sufficient bouncing or rolling energy to not stop earlier on the talus. Identifying and mapping the base of talus slopes and outlying boulders provide information on where past rock falls have occurred; assuming steady rates and magnitudes of rock-fall activity, this information also provides a first-order assessment of the hazard associated with potential future rock falls. This type of information can then be used to aid in decision-making with regard to future planning. This rock-fall hazard assessment is therefore based on defining the limits of these geomorphologic attributes.

We define talus as the accumulation of rock-fall generated boulders at the base of steep cliffs. In general, a sharp slope break is found between the steep cliff bottom and the top of talus and again at the bottom of talus and flatter valley floor. Therefore, a rock fall-dominated talus slope exhibits a characteristic profile (Evans and Hungr, 1993; Figure 10). Finer talus fragments accumulate below the apex of the talus slope, at an angle of approximately 32-38°, although this can vary depending on the talus fragment size. Farther downslope, the talus angle generally decreases. The lowermost part of the talus deposit usually contains the largest boulders because large boulders typically have the greatest total kinetic energy, are less likely to be stopped by obstacles such as trees, and are less likely to become trapped within depressions in the talus slope (Dorren, 2003). At the lowermost part of the talus deposit, the surface slope angle falls to 10 or 20° in most cases (Evans and Hungr, 1993), again depending on the talus fragment size. The very base of the talus slope is marked by an abrupt change in slope angle (typically to <10°) and a substantial reduction in the number of talus fragments; beyond the base of

the talus slope the slope is no longer completely covered by talus fragments, having only widely scattered "outlying" boulders (Evans and Hungr, 1993).

Widely scattered boulders are found beyond the edge of talus slopes throughout Yosemite Valley (Figures 11-14). Compared to the many thousands of boulders comprising the talus slopes, these outlying boulders are few in number; however, given their position on the valley floor and often within developed regions, these "outlying" boulders present a greater risk than rock falls that deposit solely on the talus slope where there is little infrastructure.

Following Wieczorek et al. (1998, 1999), we define outlying boulders as any rock-fall generated debris of substantial size (>0.5 m^3) that travels beyond the limits of the talus deposits. As previously discussed, the adopted definition of outlying does not include small fragments of flyrock, which are more difficult to map in the field and to quantify through computer simulations. In general, outlying boulders may travel along many different paths and trajectories depending on their type of motion (falling, bouncing, sliding, or rolling) and on the geometric configuration of both the adjacent cliffs and talus slopes that they must travel along. The distribution of these respective outlying boulders beneath the different cliffs and talus slopes, and their temporal frequency, can be used to help quantify the rock-fall hazard that exists beyond the base of talus within each study region. Such quantification can assist the National Park Service to make decisions with respect to existing and potential future infrastructure adjacent to talus slopes in Yosemite Valley.

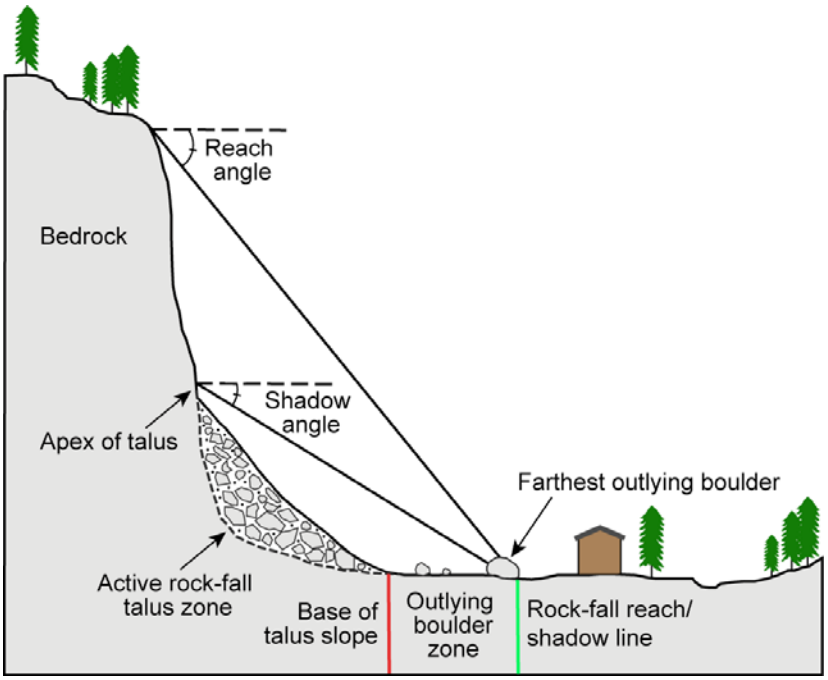

Figure 10. Schematic diagram showing a typical rock-fall talus slope morphology, the base of talus (red line), the outlying boulder zone, and the farthest outlying boulder, illustrating the determination of reach angle, rock-fall shadow angle, and rock-fall shadow limit (green line). Figure modified from Wieczorek et al. (1998, 1999, 2008) and Evans and Hungr (1993).

Figure 11. Outlying boulders in the Camp 4 study region. The large boulder on the right, one of the largest outlying boulders in Yosemite Valley, has an approximate volume of 2,500 m^3 and a cosmogenic beryllium-10 exposure age of 4.44 ± 0.42 thousand years (see Section 4.7).

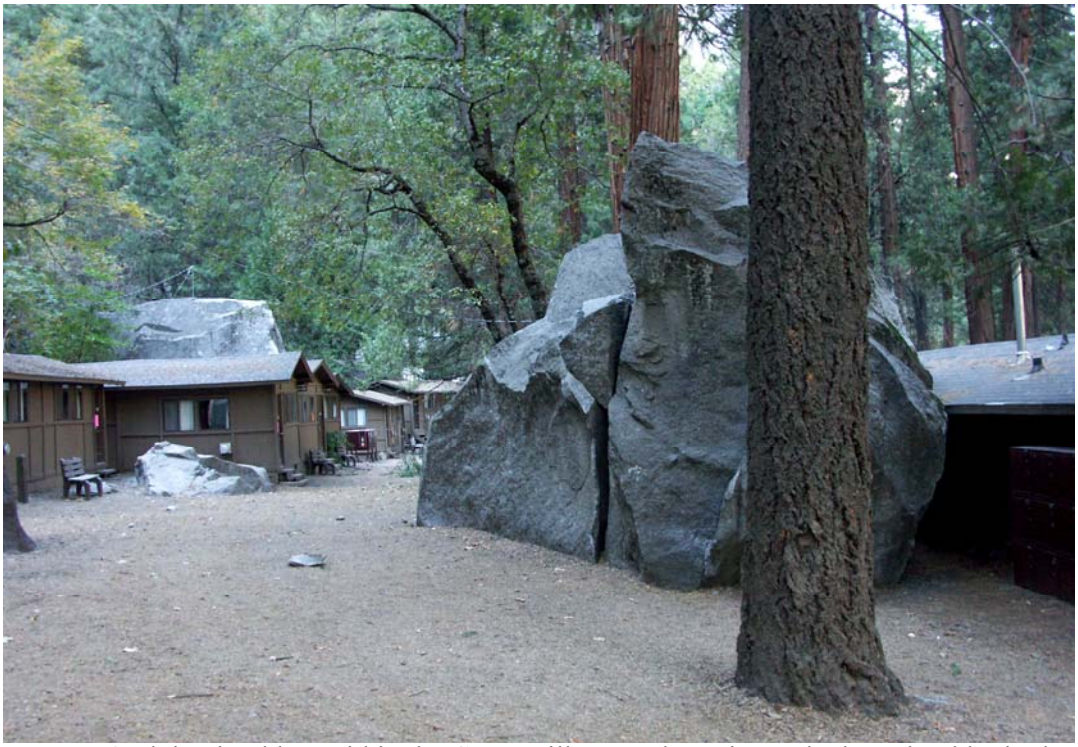

Figure 12. Outlying boulders within the Curry Village study region. The large boulder in the foreground has an approximate volume of 240 m^3 and a cosmogenic beryllium-10 exposure age of 8.45 ± 0.84 thousand years (see Section 4.7). Buildings within this region of Curry Village were permanently closed in 2008 following the 8 October 2008 rock fall.

Figure 13. Outlying boulders in the Curry Village Residential Area study region. The larger boulder in the left background has an approximate volume of 112 m^3 and a cosmogenic beryllium-10 age of 7.37 ± 0.72 thousand years (see Section 4.7). The smaller boulder in the center foreground has an approximate volume of 9 m^3 and a cosmogenic beryllium-10 exposure age of 0.71 ± 0.08 thousand years.

Figure 14. Outlying boulder within the Chapel Wall study region. Note people on boulder for scale. This boulder has an approximate volume of 1,000 m^3 and a cosmogenic beryllium-10 exposure age of 2.63 ± 0.25 thousand years (see Section 4.7).

4.2 Delineating the base of talus slopes

A line delineating the base of talus slopes in Yosemite Valley was first mapped by Matthes (1930), and was subsequently revised by Wieczorek et al. (1998, 1999) based on detailed field mapping. Although referred to as the "base of talus", the line reported by Wieczorek et al., (1998, 1999) encompasses all rock debris of slope-movement origin on the floor of Yosemite Valley, including debris flow deposits as well as those originating from rock falls, rock slides, and rock avalanches.

For the purposes of this hazard assessment, we generally adopt the base of talus line reported by Wieczorek et al. (1998, 1999), recognizing that regions with existing rock debris are generally regions where future debris deposition is possible, and hence where geological hazard exists. We have revised the base of talus line of Wieczorek et al., (1998, 1999) using a combination of even more detailed field mapping with GPS and GIS. Utilizing the 1 m DEM, we also prepared detailed surface slope maps (e.g., Figure 9) that help identify the base of talus as defined by prominent slope changes. Overall, our modifications to the base of talus line defined by Wieczorek et al. (1998, 1999) were relatively minor.

4.3 Rock-fall reach and shadow angles

To compensate for a lack of subsurface data on the full extent of post-glacial rock falls, and also for the fact that the talus edge can reasonably be expected to prograde farther into the valley as the talus slope builds in height with future rock falls, Wieczorek et al. (1998, 1999) assessed rock-fall hazard beyond the base of talus slopes using the rock-fall shadow concept (Figure 9; Evans and Hungr, 1993). From an energy standpoint, a rock falling from a source on a cliff will travel down the slope and stop at a point below the cliff, with a so-called energy line connecting the rock-fall source and the point of deposition. This defines an angle from horizontal known as the Fahrböschung (Heim, 1932; Schiedegger, 1973; Evans and Hungr, 1993), which can be used to delineate hazard zones (e.g, Jaboyedoff and Labiouse, 2003). However, areas such as Yosemite Valley pose a challenge for using this technique because the cliffs are very tall and because past (prehistoric) rock-fall source areas that generated outlying boulders are often difficult or impossible to accurately locate on the cliffs. Lacking exact source area information, researchers often identify a "reach angle", which is the angle from horizontal between the farthest outlying boulder and the top of the adjacent cliff (Figure 10; Corominas, 1996).

Unlike reach angles, rock-fall shadow angles are keyed to the apex of the adjacent talus slope rather than a rock-fall source area or the top of the cliff. The rock-fall shadow angle is determined by the angle from horizontal between the farthest outlying boulder and the apex of the talus slope (Figure 10; Evans and Hungr, 1993). Based on analyses of 25 outlying boulder locations, Wieczorek et al. (1998, 1999) selected a minimum shadow angle of 22° to define the rock-fall shadow line in Yosemite Valley (Figures 6, 7). This value generally compares reasonably well with shadow angle values reported by

Evans and Hungr (1993) for other areas with known rock fall potential. However, it is reasonable to expect that the rock-fall shadow angle would not be the same everywhere in Yosemite Valley due to variable heights and morphologies of the talus slopes and adjacent cliff faces, and thus the position of the shadow limit could vary outboard of talus slopes.

According to Wieczorek et al. (1998, 1999), their shadow line was extrapolated from the talus apex to the floor of Yosemite Valley, resulting in a line on the valley floor representing the shadow limit. However, in some locations (e.g., Yosemite Village) the mapped shadow limit exceeds the farthest outlying boulders by several hundred meters horizontally (Figures 15-22), suggesting that in some locations the 22° angle was projected from a point on the cliff above the talus apex; no explanation for this discrepancy is provided. As a result, the shadow limit line reported by Wieczorek et al. (1998, 1999) extends much farther than frequent fragmental-type rock falls have traveled in the past, and is better suited for characterizing potential runout from infrequent, extremely large rock falls. For this reason, the rock-fall shadow line of Wieczorek et al. (1998, 1999) has not been used directly in the hazard assessment detailed in this report, except for reference with respect to the hazard line defined herein.

4.4 Mapping of outlying boulders

We mapped 520 boulders along or beyond the base of talus within the 16 study regions in Yosemite Valley (Figure 2, Figures 15-22). We did not map outlying boulders at several locations in Yosemite Valley because the origins of boulders in those locations could not be confidently determined, i.e., the boulder positions could not be reliably attributed to individual fragmental rock falls, and could instead have resulted from other processes such as debris flows or glacier deposition. Regions excluded from mapping consisted of debris flow fans, such as those emanating from Eagle Creek, Indian Canyon, and LeConte Gully, and regions adjacent to moraines, such as regions west of El Capitan and Bridalveil Fall that have obvious glacially-deposited erratics. We also excluded specific regions dominated by deposits defined as "rock avalanches" by Wieczorek et al. (1999), such as those located at El Capitan, Sugarpine Bridge, Curry Village, and Old Yosemite Village. Although rock talus and outlying boulders do also result from rock avalanches, their deposition is very likely influenced by dynamics unique to very large mass movements (e.g., Scheidegger, 1973; Hsu, 1975; Nicoletti and Sorriso-Valvo, 1991), and thus they have a different origin than outlying boulders that result from smaller, individual fragmental rock falls, which are more typical in Yosemite Valley and are the focus of this study.

We mapped boulders in the field using differential Global Positioning System (GPS), specifically a Trimble Juno handheld instrument with an external receiver. Where possible, we made GPS measurements in the center of boulders; otherwise we made them on the downslope side of boulders, facing the center of the valley. We collected data in UTM coordinates and corrected the raw data for satellite "drift" using local Plate Boundary Observatory base station data collected from a position approximately 5-10 km

distant. We estimate the accuracy of our corrected measurements to be ± 2 m. We also collected information on approximate boulder length, width, and height. These values, especially boulder height, are minimum values because many boulders are partially buried in surficial sediments. We calculated approximate boulder volumes based on the exposed dimensions, and these too are considered minimum values. The mean boulder volume for outlying boulders beyond the base of talus is 67 m^3.

We plotted the positions of mapped boulders in a GIS, and found that of the 520 boulders mapped in the field, 258 were found to lie beyond the base of talus, and could thus be considered to be "outlying" (Figures 10, 15; Evans and Hungr, 1993; Wieczorek et al., 1998, 1999). The remaining 262 boulders were located within the previously mapped base of talus (e.g., Figures 15-22). For all boulders, we estimated the approximate steepest paths that the boulders could have taken down the talus slope to reach their positions near or beyond the edge of the talus slope. These paths were estimated by evaluating the local talus slope morphology and drawing lines perpendicular to elevation contours on the talus slope (Figures 15-22). For those boulders mapped as being beyond the edge of talus, we determined outlying distance values by measuring from the edge of talus to each boulder along that boulder's estimated path.

4.5 Measuring rock-fall reach and shadow angles

With the individual outlying boulder locations and approximate steepest paths down the talus slopes, we measured reach and shadow angles for all mapped boulders. This was performed in a GIS by determining the elevations of the boulder and the talus apex on either end of estimated trajectory, measuring the horizontal distance between these points, and calculating the shadow angle. We also measured reach and shadow angles in the field with an inclinometer where conditions allowed, with similar results.

Mean reach angles for each study region range from 41° to 56° (Table 1), with a mean reach angle for all study regions of 50°. The variation in shadow angles between study sites is likely due to variable heights and morphologies of the talus slopes and adjacent cliff faces. Mean shadow angles for each study region range from 16° to 30° (Table 1), with a mean shadow angle for all study regions of 25°. As with the reach angles, the variation in shadow angles between study sites is likely due to variable heights and morphologies of the talus slopes and adjacent cliff faces. For example, two sites with small shadow angles (Yosemite Lodge and Sunnyside Bench) have very small talus accumulations, with apices only a few meters above the valley floor.

The mean shadow angle value of 25° for all study regions generally compares well with the shadow angle of 22° determined by Wieczorek et al. (1998, 1999) based on only 25 boulders. It also compares well with a mean shadow angle of 27.5° calculated for talus slopes in British Columbia (Evans and Hungr, 1993). However, as discussed previously, the projected shadow limit line of Wieczorek et al. (1999) does not appear to be everywhere keyed to talus apices, as its position on the valley floor far exceeds even the maximum outlying boulder position in many regions (Figures 15-22).

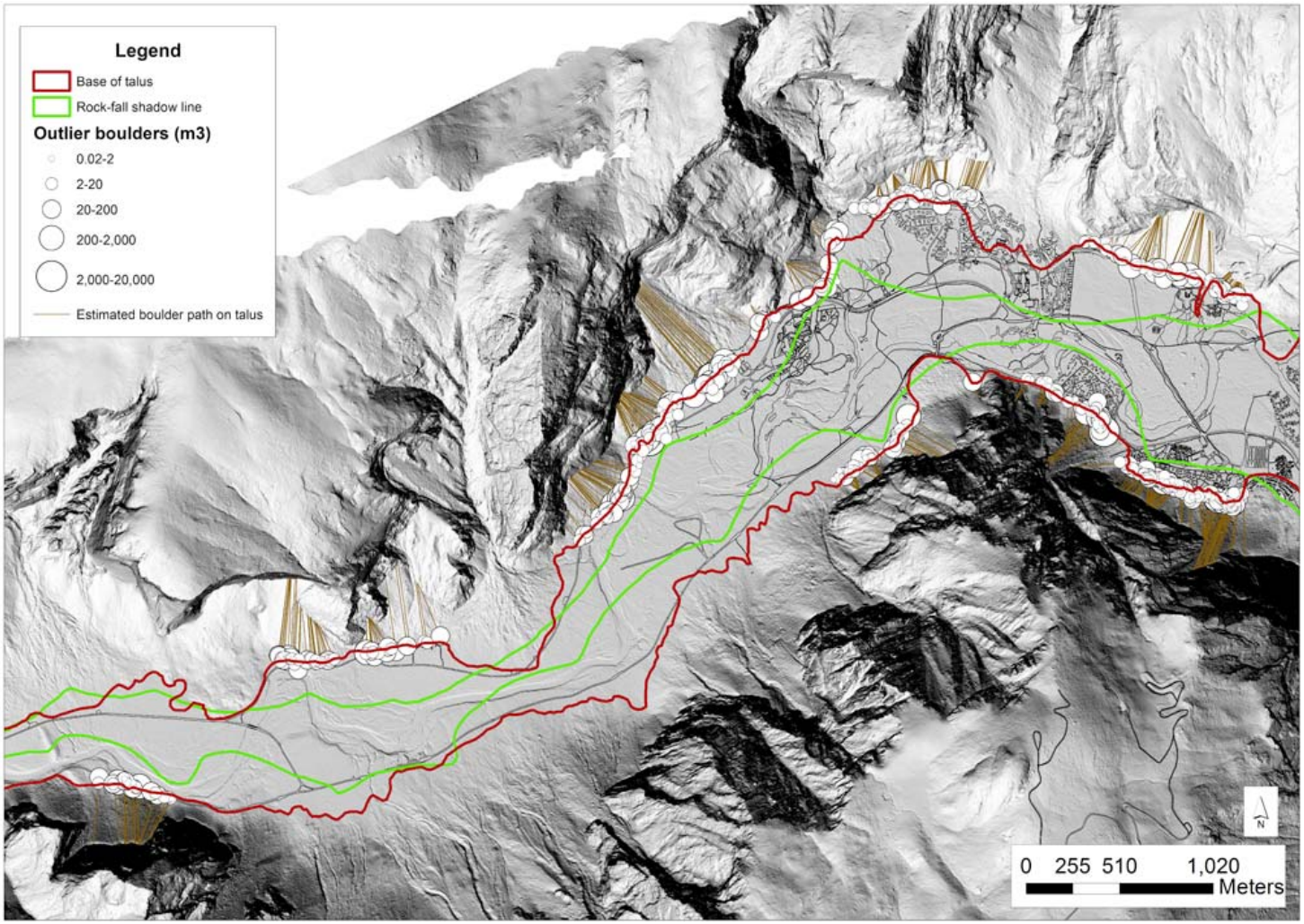

Figure 15. Mapped outlying boulders (white circles) adjacent to or beyond the base of talus slopes within the study regions in Yosemite Valley. Outlying boulders were not mapped in regions characterized by debris flows, rock avalanches, or glacial deposits. The positions of the revised base of talus (red line) and rock-fall shadow limit (green line) of Wieczorek et al. (1998, 1999) are shown for reference.

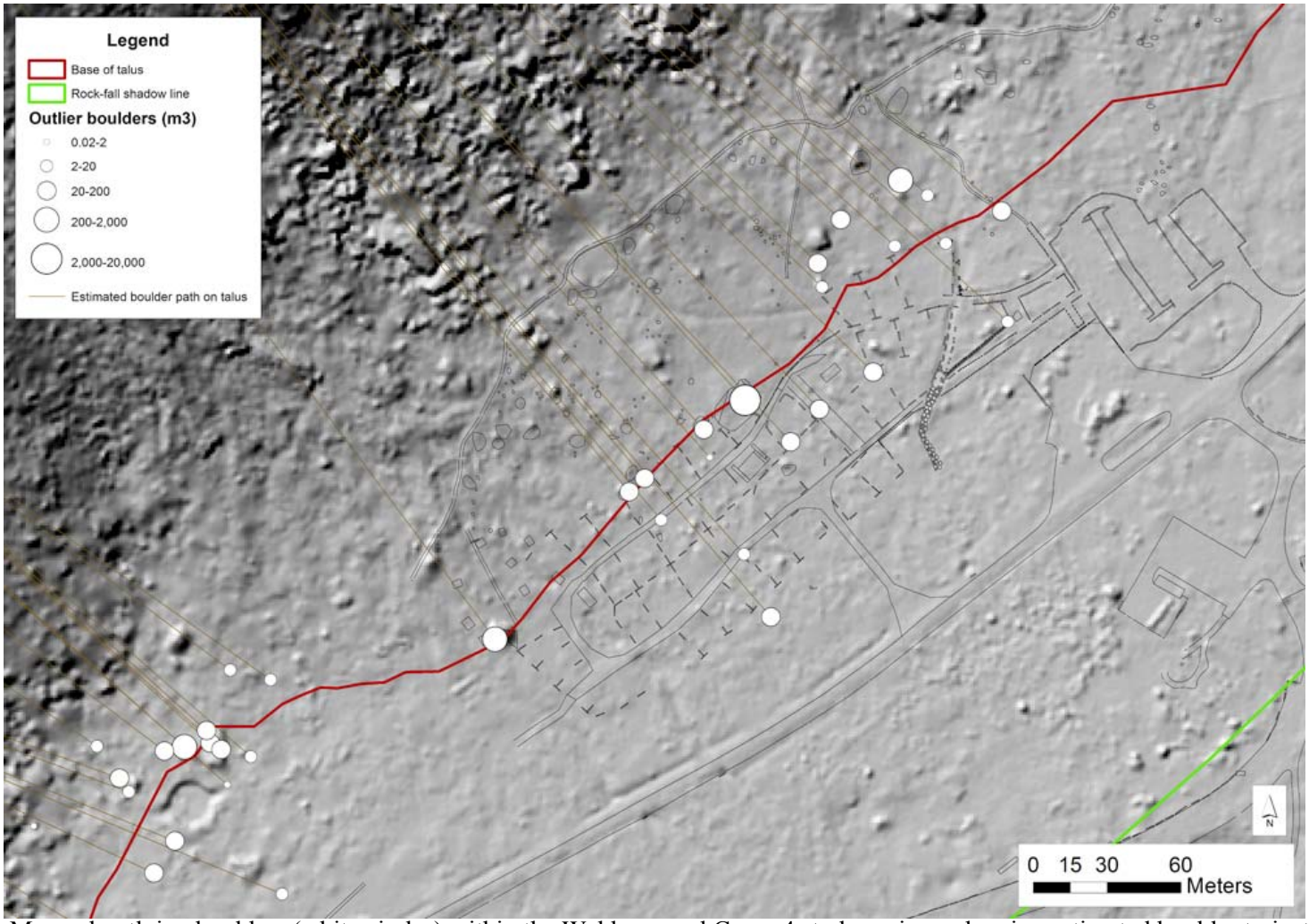

Figure 16. Mapped outlying boulders (white circles) within the Wahhoga and Camp 4 study regions, showing estimated boulder trajectories (brown lines). Outlying boulder distances beyond the revised base of talus (red line) are measured along the approximate steepest boulder path on the adjacent talus slope. The position of rock-fall shadow limit (green line) mapped by Wieczorek et al. (1998, 1999) is well beyond the farthest extent of outlying boulders.

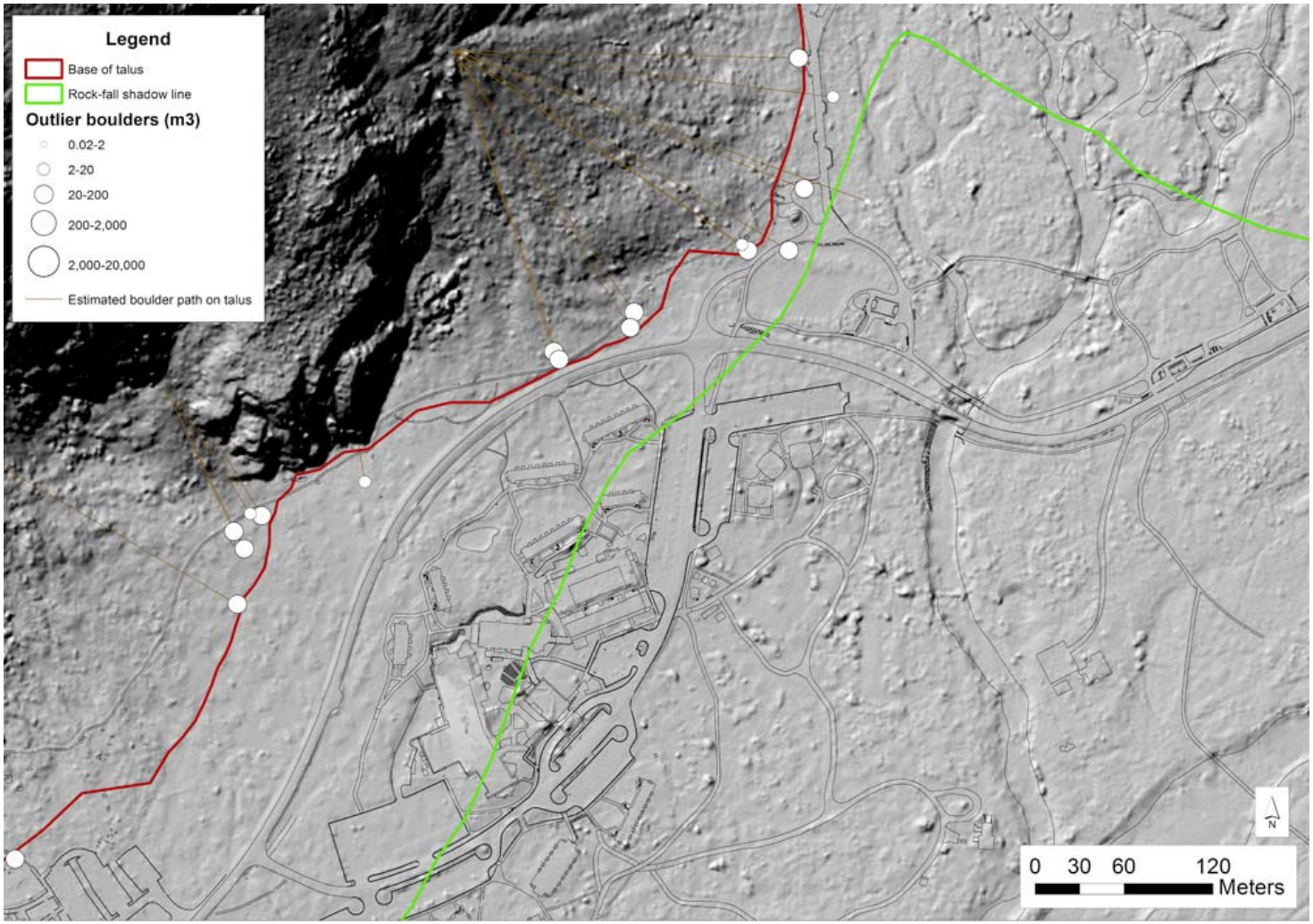

Figure 17. Mapped outlying boulders (white circles) within the Yosemite Lodge and Yosemite Falls Trail study regions, showing estimated boulder trajectories (brown lines). Outlying boulder distances beyond the revised base of talus (red line) are measured along the approximate steepest boulder path on the adjacent talus slope. The position of rock-fall shadow limit (green line) mapped by Wieczorek et al. (1998, 1999) is well beyond the farthest extent of outlying boulders.

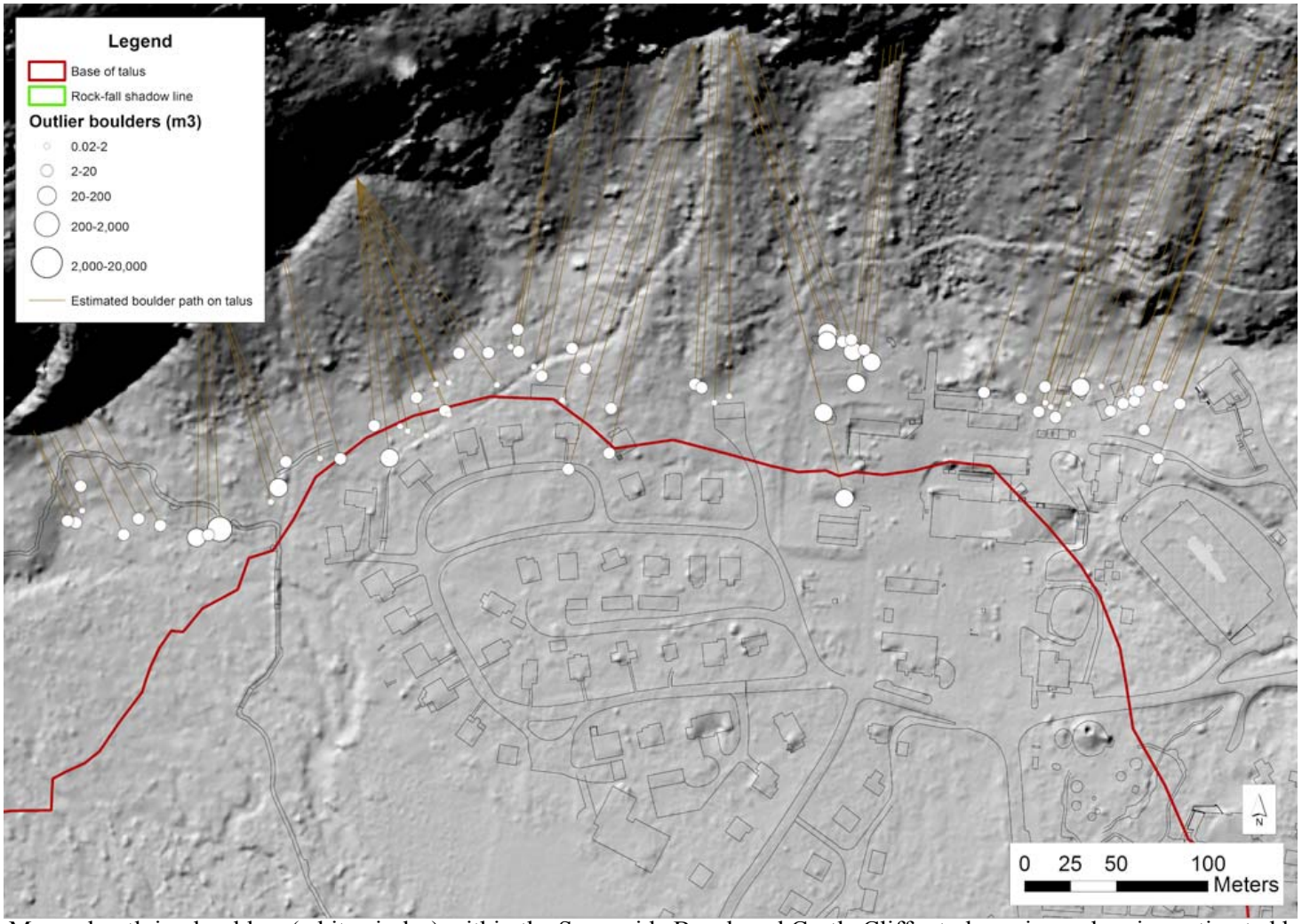

Figure 18. Mapped outlying boulders (white circles) within the Sunnyside Bench and Castle Cliffs study regions, showing estimated boulder trajectories (brown lines). Outlying boulder distances beyond the revised base of talus (red line) are measured along the approximate steepest boulder path on the adjacent talus slope. The rock-fall shadow limit mapped by Wieczorek et al. (1998, 1999) is off the page to the south well beyond the farthest extent of outlying boulders.

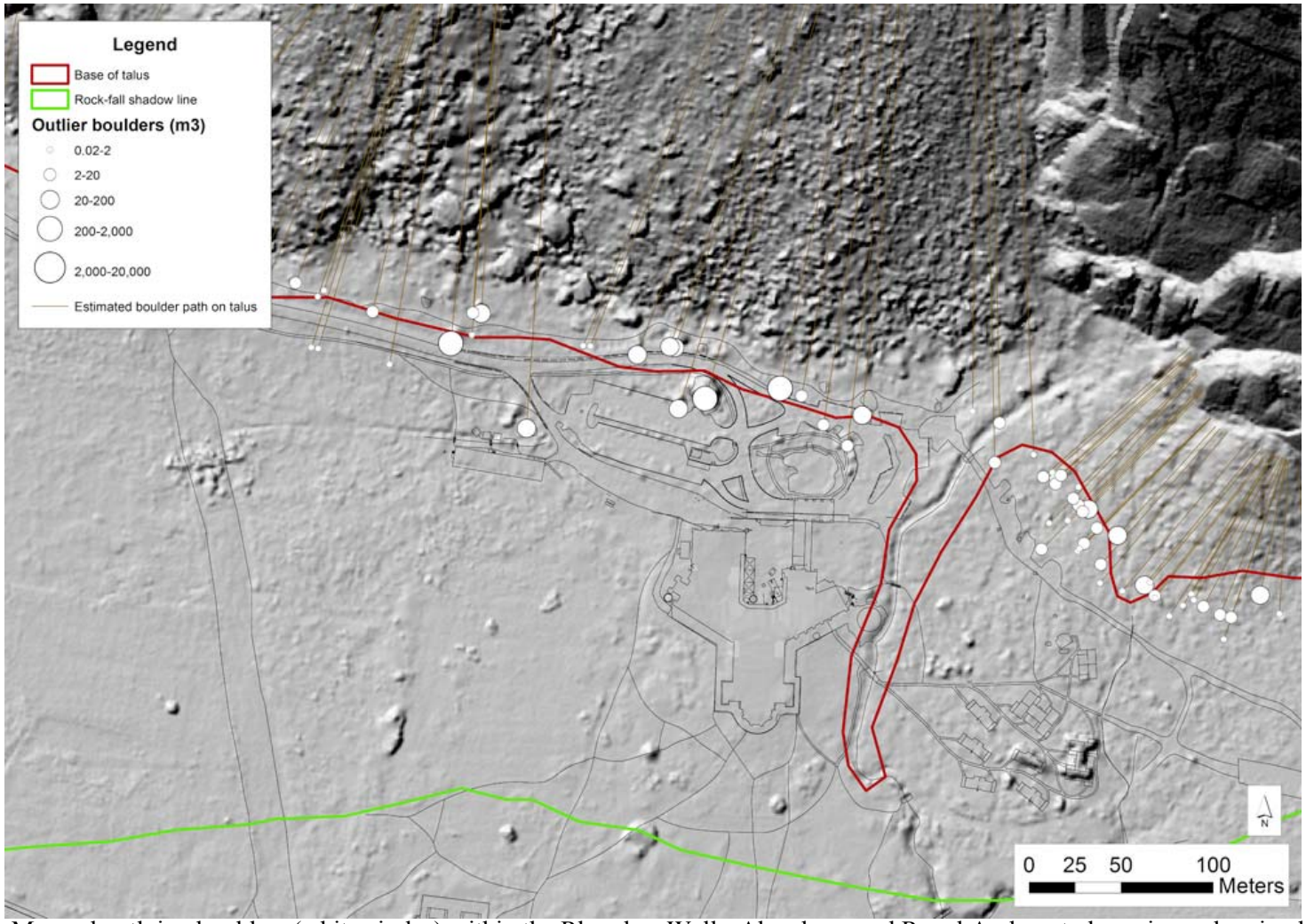

Figure 19. Mapped outlying boulders (white circles) within the Rhombus Wall - Ahwahnee and Royal Arches study regions, showing boulder estimated trajectories (brown lines). Outlying boulder distances beyond the revised base of talus (red line) are measured along the approximate steepest boulder path on the adjacent talus slope. The position of rock-fall shadow limit (green line) mapped by Wieczorek et al. (1998, 1999) is well beyond the farthest extent of outlying boulders. The narrow "finger" within the base of talus line in the center-right is a debris flow channel.

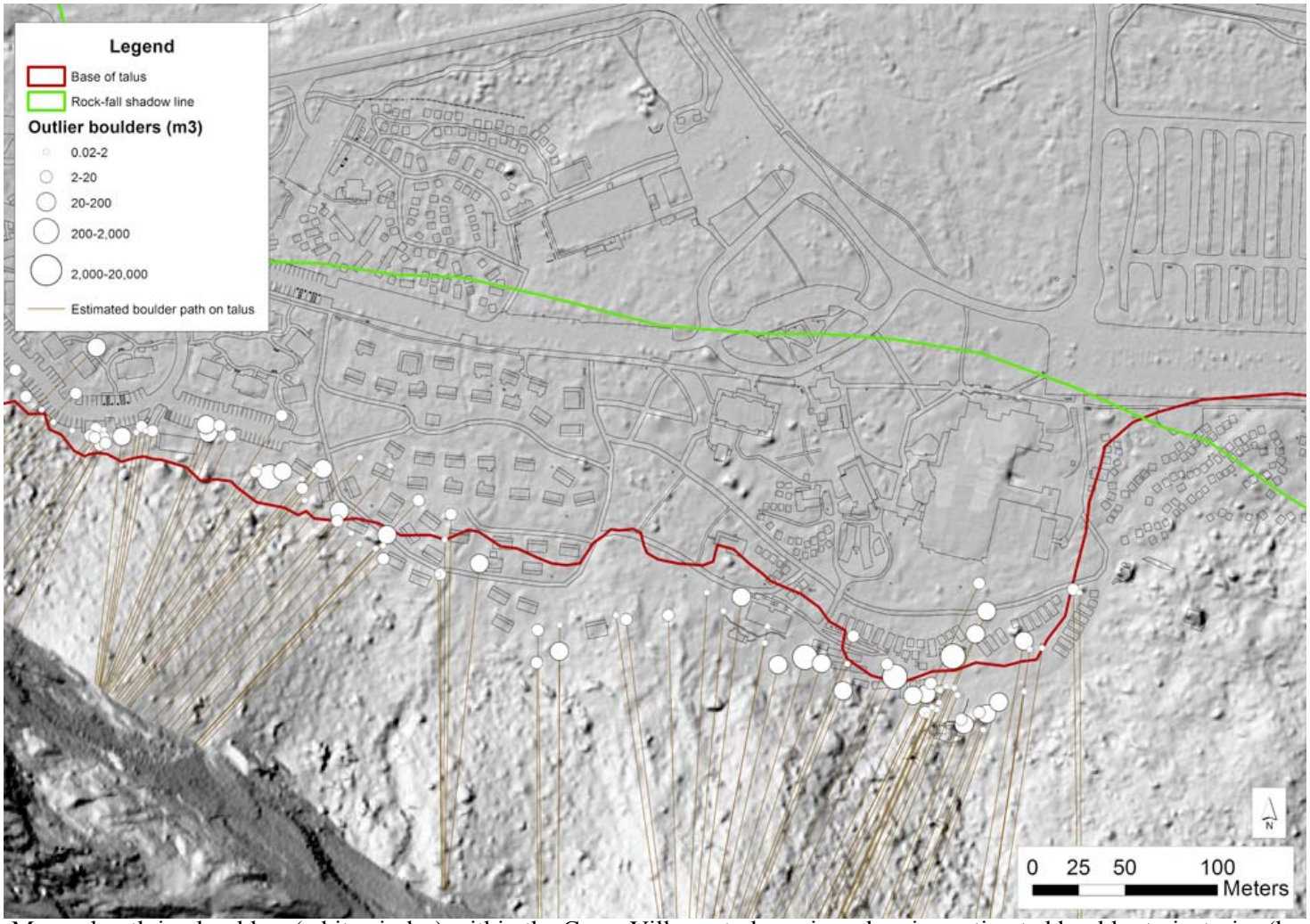

Figure 20. Mapped outlying boulders (white circles) within the Curry Village study region, showing estimated boulder trajectories (brown lines). Outlying boulder distances beyond the revised base of talus (red line) are measured along the approximate steepest boulder path on the adjacent talus slope. The position of rock-fall shadow limit (green line) mapped by Wieczorek et al. (1998, 1999) is well beyond the farthest extent of mapped outlying boulders. The northward extension of the base of talus line on the far right includes a rock avalanche deposit.

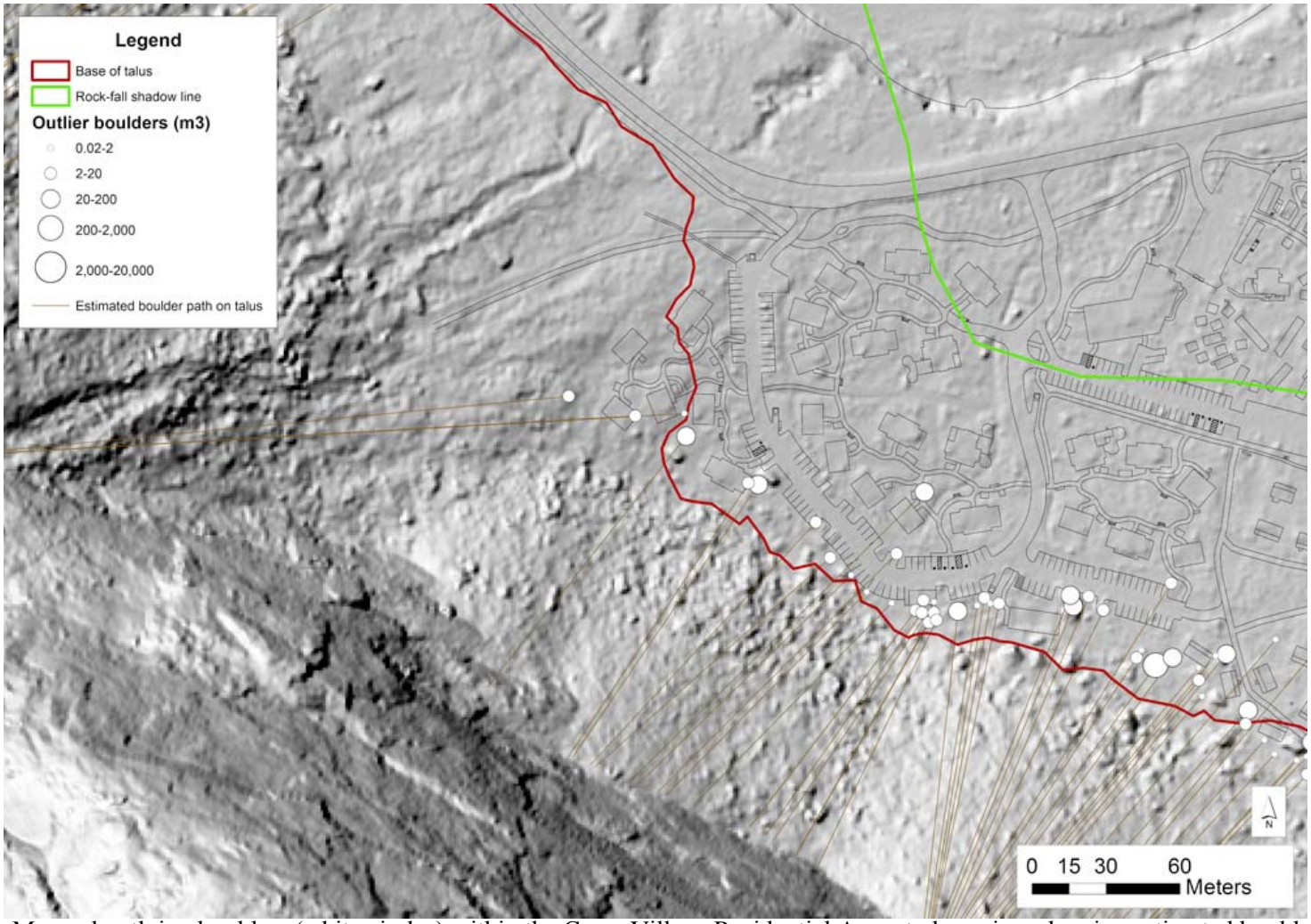

Figure 21. Mapped outlying boulders (white circles) within the Curry Village Residential Area study region, showing estimated boulder trajectories (brown lines). Outlying boulder distances beyond the revised base of talus (red line) are measured along the approximate steepest boulder path on the adjacent talus slope. The position of rock-fall shadow limit (green line) mapped by Wieczorek et al. (1998, 1999) is well beyond the farthest extent of outlying boulders.

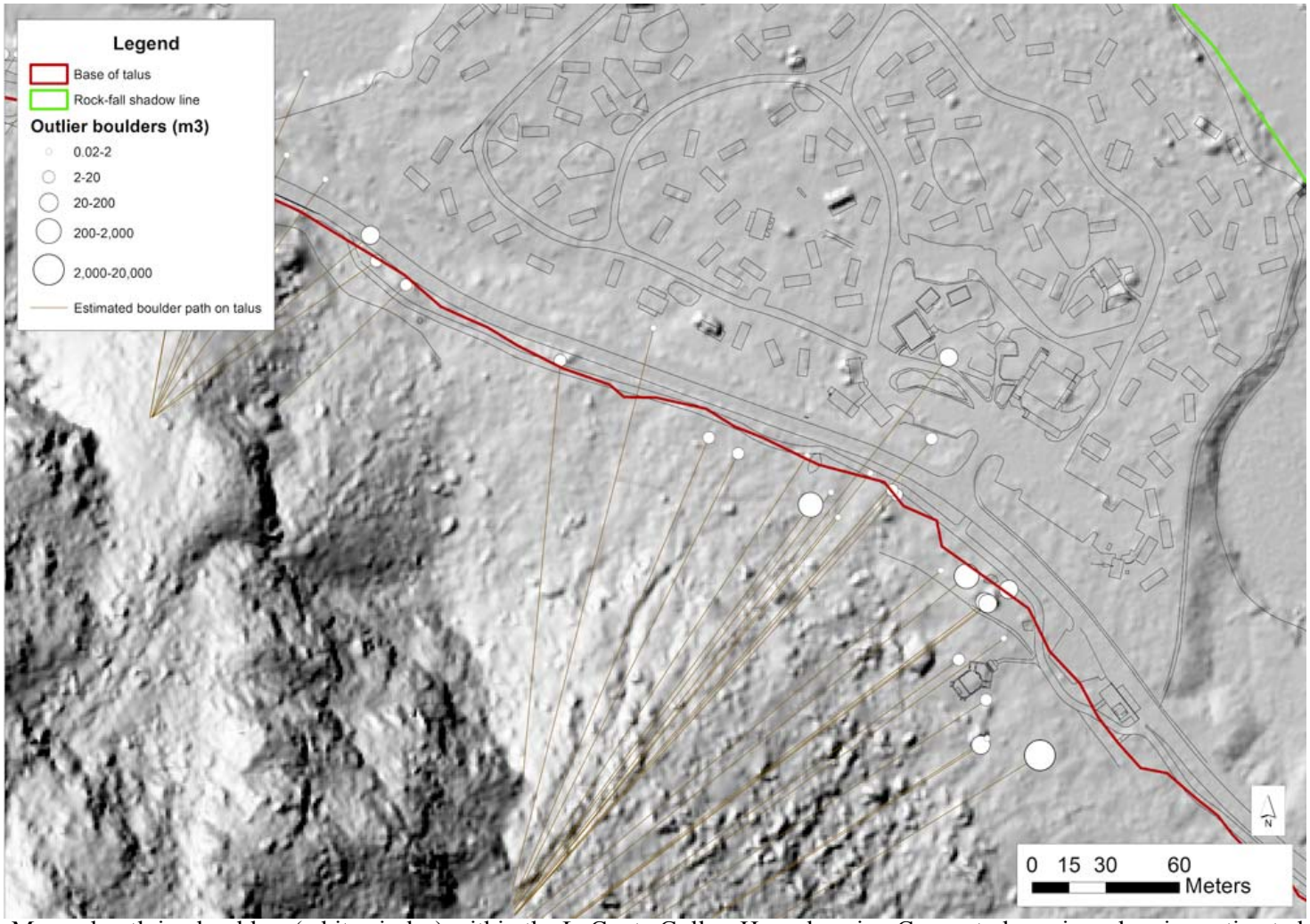

Figure 22. Mapped outlying boulders (white circles) within the LeConte Gully - Housekeeping Camp study region, showing estimated boulder trajectories (brown lines). Outlying boulder distances beyond the revised base of talus (red line) are measured along the approximate steepest boulder path on the adjacent talus slope. The position of rock-fall shadow limit (green line) mapped by Wieczorek et al. (1998, 1999) is well beyond the farthest extent of outlying boulders.

4.6 Defining an initial hazard line based on spatial distributions of outlying boulders

To further delineate the level of rock-fall hazard beyond the base of talus, we use the spatial distribution of the outlying boulders to provide an initial estimate of the size hazard zone of likely outlying boulder deposition. This distance estimate depends only on the spatial locations of rock-fall outlying boulders; we modify this distance using rock-fall frequency data in a subsequent section of this report. We calculated the 90th-percentile of the distances using a cumulative distribution of boulder distances for each study region (e.g., Figure 23 for the El Capitan study region). For study regions in which only one or two outlying boulders were mapped and therefore of limited statistical use, we use the maximum outlying boulder distance as a proxy for the 90th-percentile distance.

The meaning of a 90th-percentile in a hazard sense is that, at the 90th-percentile distance (32 m in the case of the El Capitan study region; Figure 23), there is a 10% probability that an outlying boulder from a future rock fall will exceed this distance. This assumes that the future distribution of outlying boulder deposition is similar to that which has occurred during the past 15,000 years; although this is likely to be the case, we specifically address this issue through the use of computer simulations of potential future rock falls, described in Section 4.8.

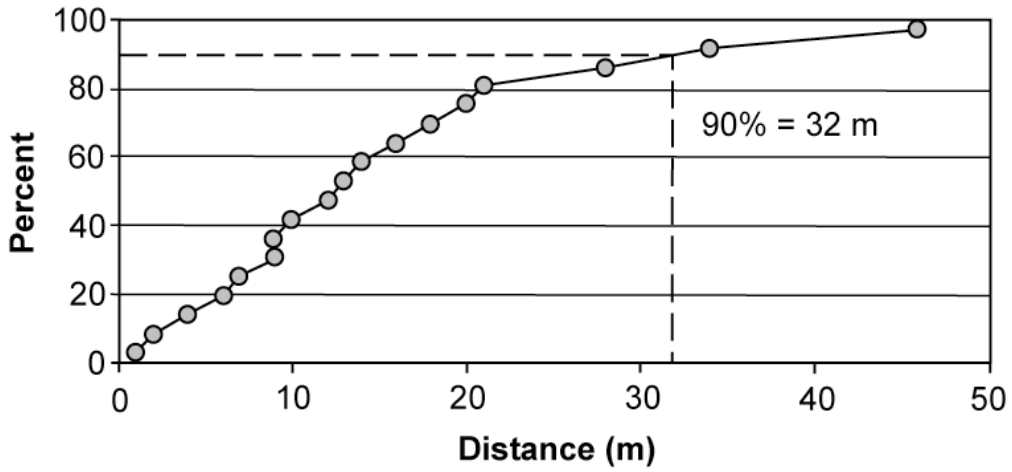

Figure 23. Cumulative distribution function of outlying boulder distance beyond the mapped base of talus for the El Capitan study region. The 90th-percentile distance is 32 m.

Comparison of the 90th-percentile limits for the different study regions reveals significant variation (Table 1; Figure 24), demonstrating that there are substantial differences in the distance that outlying boulders can travel beyond the base of talus slopes within the different study regions. This likely relates to topography of the cliffs and the talus slopes above the different study regions. For example, study regions such as Yosemite Lodge and Church Bowl are positioned beneath topographic spurs that tend to divert rock falls from high on the cliff away from these regions (and into other study

regions). This leads to a smaller number of outlying boulders in those study regions, and also generally small outlying distances because the boulders are derived from low on the cliffs immediately adjacent to the study region.

For some study regions, the different percentile distances vary widely; for example, the 80th-percentile distance for the El Capitan study region is 21 m, whereas the 95th-percentile distance is nearly twice that, at 41 m. Selection of the 90th-percentile distances, as opposed to the 80th-percentile or the 100th-percentile, for example, is based on professional judgment. Selection of the 90th-percentile distance captures 90% of the population of outlying boulders while properly excluding true statistical and potentially anomalous outliers that might otherwise exert undue influence on the position of the hazard line. For example, the 90th-percentile distance for the Three Brothers study region is 48 m, but the maximum outlying boulder distance there is 80 m (Table 1). If this one maximum boulder is excluded, the next farthest outlying boulder distance is 60 m, much closer to the 90th-percentile distance. Because the farthest boulder 80 m beyond the talus edge is positioned in isolation far beyond the other boulders in the study region, the frequency with which boulders are deposited that far beyond the base of talus must be very low (approximately 1 event in 15,000 years; see the discussion in section 4.7.2). This illustrates the undue influence that a solitary boulder – a true statistical outlier – can have on the overall distance analysis. It is for this reason that we select the 90th-percentile distance rather than the 100th-percentile distance as a starting point for the hazard line determination. However, ultimately the final hazard line is scaled outward or inward from the 90th-percentile distance based on frequency information described below, so that the final hazard line everywhere represents a 1/500 year annual exceedance probability.

Table 1. Outlying boulder metrics, mean reach and shadow angles, maximum outlying boulder distances, and 90th percentile outlying boulder distances for Yosemite Valley study regions.

Study region	Number of outlying boulders	Mean boulder volume (m^3)	Mean reach angle (degrees)	Mean shadow angle (degrees)	Maximum outlying boulder distance (m)	90th-percentile outlying boulder distance (m)
El Capitan	18	83	54	27	46	32
Three Brothers	36	121	54	25	80	48
Wahhoga	8	60	51	25	65	54
Camp 4	12	255	45	28	76	57
Yosemite Lodge	1	85	45	18	21	21[a]
Yosemite Falls Trail	6	74	46	28	63	55
Sunnyside Bench	9	7	54	17	27	23
Castle Cliffs	1	30	47	23	12	12[a]
Church Bowl	3	13	49	22	7	7[a]
Rhombus Wall - Ahwahnee	11	97	52	30	49	35
Royal Arches	36	9	51	16	39	27
Glacier Point - Curry Village	25	37	56	23	60	42
Glacier Point – Curry Village Residential Area	26	15	53	26	52	28
LeConte Gully – Housekeeping Camp	16	95	41	27	60	41
Chapel Wall	36	33	48	23	46	42
Cathedral Rocks	14	56	56	26	44	42

[a]There were not sufficient data for these study regions to calculate the 90th-percentile distance, so we take the maximum distance (the distance from the base of talus to the farthest outlying boulder).

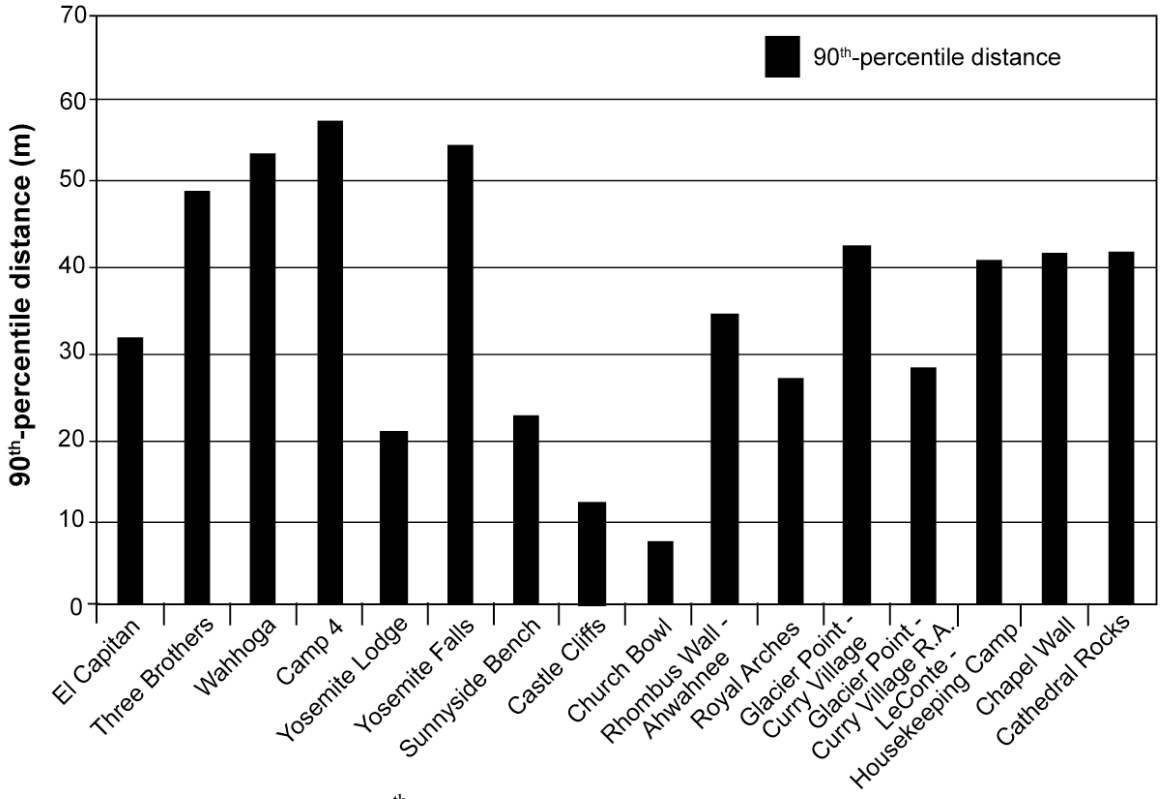

Figure 24. Comparison of the 90th percentile distances of boulders beyond the talus edge for study regions in Yosemite Valley.

The 90th-percentile distances beyond the base of talus provide a first-order approximation of likely deposition zones for outlying boulders. These distances, as measured beyond the mapped base of talus, are the basis for a preliminary hazard zone that accounts for rock falls that produce rock-fall deposits that travel beyond the base of talus slopes. However, how frequently a future rock fall will generate an outlying boulder within each study region is not taken into account by the 90th-percentile distances. For example, if this frequency of outlying boulders is relatively high in a particular region, over time relatively many boulders may travel beyond the edge of talus there, presenting a relatively higher hazard. Conversely, if the frequency of outlying boulders is relatively low in a particular region, then the overall hazard beyond the edge of talus there may be relatively lower. As an example, the Chapel Wall and Cathedral Rocks study regions both have 90th-percentile distances of 42 m (Table 1). However, the Chapel Wall study region has more than twice as many boulders than the Cathedral Rocks study area (Table 1), even when the number of boulders is normalized by the study region areas. Thus, the frequency of outlying boulder deposition within the Chapel Wall study region is greater than that in the Cathedral Rocks study area.

To explicitly account for the frequency of outlying boulders generated within each study region, we adjusted the 90th-percentile distances by frequency-related factors

described in the following sections. As a result, the adjusted distances are such that the overall hazard beyond the adjusted hazard line is the same in all of the study regions.

4.7 Determining the frequency of past outlying boulder deposition

Areas within the active talus zone, outlying boulder zone, and beyond are all potentially hazardous, although the degree of hazard depends upon the period of time that might elapse between return events in those areas. As stated in Section 1, information on rock-fall frequency is critical in order to fully evaluate hazard (Varnes, 1984). As described above, rock-fall recurrence intervals may be estimated from historical frequency-magnitude relations, but these are limited by the relatively short historical time period and do not contain specific information about the recurrence of events that produce outlying boulders beyond the base of talus slopes. Determining the age of outlying boulders beyond the base of the talus slope is therefore important for assessing the timing of boulder deposition in this zone, as well as for evaluating assumptions regarding the nature of boulder deposition, e.g., whether outlying boulders represent individual rock-fall events or whether many outlying boulders result from the same event.

Yosemite Valley presents a unique and ideal setting for determining the frequency of outlier boulder deposition. Deglaciation occurred approximately 15,000 to 17,000 years ago (Huber, 1989; Wieczorek and Jäger, 1996; Stock and Uhrhammer, 2010) and left a flat valley floor that aggraded only about 5 m subsequent to glacier retreat. Rock-fall deposits and individual boulders that have traveled beyond the limits of continuous talus have been mostly undisturbed by natural erosion, or by construction or maintenance activities due to the management of the park as a natural landscape. Because of this, the spatial and temporal distribution of these outlying boulders should represent a reasonable approximation of the temporal hazard beyond the talus edge. We note that there may have been changes in the type, density and spatial distribution of trees on the talus slope through time, which could affect boulder runout distances, but as we have no specific information on the nature of these potential changes, we have not attempted to account for that in this analysis.

4.7.1 Cosmogenic nuclide exposure dating of outlying boulders

A variety of methods have been used to date rock-falls that occurred prior to historic documentation (typically hundreds to thousands of years before the present). These include tree-ring analysis (e.g., Clague, 2010; Stoffel et al., 2010), and lichenomtery (e.g., Bull et al., 1994; Luckman and Fisk, 1995; McCarroll et al., 1998), both of which have been applied to rock-fall deposits in Yosemite (Bull, 2004; Huber et al., 2007). However, considering that Yosemite Valley was deglaciated ~15,000-17,000 years ago, there is potential for many boulders to have fallen many thousands of years ago, typically beyond the range of these dating techniques.

For dating outlying boulders, we utilized terrestrial cosmogenic ^{10}Be exposure dating. This technique utilizes the fact that quartz in rocks exposed near (within ~ 1 m) of the Earth's surface will accumulate cosmogenic isotopes such as ^{10}Be at known rates due to cosmic ray bombardment (e.g., Lal, 1991; Gosse and Phillips, 2001). The amount of ^{10}Be measured in a boulder sample can therefore be used to calculate the amount of time that boulder has been exposed to cosmic rays. Rock-fall deposits are generally well suited for cosmogenic ^{10}Be exposure dating because rock falls tend to instantaneously excavate rocks from within cliffs and expose them on the surface (e.g., Ballantyne and Stone, 2004; Ivy-Ochs et al, 2009; Stock and Uhrhammer, 2010). Vertical cliffs receive relatively low doses of cosmic rays due to topographic shielding, and most rock falls >1 m in thickness were likely shielded within the cliff prior to failure. Nevertheless, outlying boulders must be carefully sampled to ensure reliable exposure dates. Complicating factors can include significant cosmic ray exposure on the cliff prior to failure (termed "inheritance"), surface erosion of the boulder, rotation of boulders after deposition, rock spallation due to forest fires, and topographic, vegetation, and snow shielding of cosmic rays (e.g., Gosse and Phillips, 2001; Ivy-Ochs et al., 2009).

To address these issues, we sampled the tops of large which were unlikely to have been exposed on the cliff prior to failure (see discussion below) and are generally positioned above the influence of fire-induced spalling. We made detailed measurements of the angle to the skyline from each boulder to account for the topographic shielding of cosmic rays, which is significant beneath the ~1 km tall cliffs of Yosemite Valley (Table 2). Following the rationale described in Stock and Uhrhammer (2010), we consider snow and vegetation shielding to be negligible, and assume a boulder erosion rate of 0.00065 cm/yr, a typical value for erosion of granitic boulders and bare bedrock surfaces in the Sierra Nevada (e.g., Small et al., 1997; Stock et al., 2005).

Samples were chemically isolated for beryllium-10 at the Georgia Institute of Technology following standard methods (Kohl and Nishiizumi, 1992), and ^{10}Be/^{9}Be ratios measured by accelerator mass spectrometry at Lawrence Livermore National Laboratories. Beryllium-10 exposure ages for 33 outlying boulders range from 720 ± 90 to 25,070 ± 2,620 years (Table 2; Figure 24). Overall, the exposure ages for outlying boulders are relatively old, considering that the oldest they could likely be is about 15,000-17,000 years, the approximate age of deglaciation of Yosemite Valley. Several ages from the Rhombus Wall – Ahwahnee study region approach this maximum age (approximately 12,000 to 14,000 years), and many ages from other study regions are in the 9,000- to 10,000-year-range (Table 2; Figure 25).

As a check on the external reproducibility of boulder exposure ages, we collected two samples from the top of one boulder, an outlying boulder below LeConte Gully in Housekeeping Camp. We assume that samples from the planar top of this boulder have the same exposure history, and thus should yield the same exposure age. The two samples collected from this boulder (HKC-1a, 1b) yield exposure ages of 9,200 ± 900 and 9,400 ± 900 years, and are therefore indistinguishable within analytical uncertainty. Thus, our assumption that a sample from the top of the boulder accurately characterizes the exposure history of that boulder appears valid.

A more challenging assumption to test is whether sampled boulders experienced exposure to cosmic rays prior to being deposited on the valley floor, that is, that the boulders have no "inherited" ^{10}Be from exposure prior to failure (Gosse and Phillips, 2001). For an idealized cube-shaped boulder >1 m thick that has fallen from a vertical cliff face, there is roughly a one-in-six chance of sampling a surface that was exposed on the cliff prior to failure. Of all of the outlying boulders sampled, only one boulder clearly showed inheritance; this boulder, located beneath the eastern portion of Middle Brother near Wahhoga, yielded an exposure age of 25,000 ± 2,600 ka (Table 2), which is older than the inferred timing of deglaciation in Yosemite Valley. The best explanation for this anomalously old age is that the sampled boulder experienced some inventory of ^{10}Be on the cliff face prior to failure. Accordingly, we exclude this date from consideration.

It is difficult to directly evaluate whether other outlying boulders with ages younger than deglaciation experienced some pre-failure exposure on the cliff, but results from elsewhere in Yosemite Valley provide some insight. Stock and Uhrhammer (2010) dated five boulders within the El Capitan rock avalanche in western Yosemite Valley. Unlike the sampled outlying boulders, every sampled boulder in this case originated from the instantaneous failure of a 2.2 million m^3 rock avalanche, and thus should yield the same exposure age. Stock and Uhrhammer (2010) found that four of the five samples yielded consistent ages of between 3,500 and 3,800 years B.P. However, the fifth sample yielded a much older age of about 21,000 years, inconsistent with the history of deglaciation. In this example, one out of the five boulders sampled was affected by inheritance. Five samples collected from a smaller rock avalanche deposit near Curry Village yield similar ages of 2,000 years, suggesting no inheritance in those boulders. Thus, existing data indicate that one out of ten sampled boulders from rock avalanche deposits showed some inheritance. Recognizing that the outlying boulders sampled here represent a different type of event (individual fragmental rock falls rather than large rock avalanches), the existing data nevertheless suggest a relatively low probability that inheritance might be encountered in outlying boulders. However, because the possibility of inheritance cannot be excluded, the boulder exposure ages presented here should properly be considered to be maximum ages.

Cosmogenic ^{10}Be exposure ages yield two important results with respect to outlying boulder deposition: (1) Exposure ages suggest that most of the sampled boulders were deposited thousands of years ago, with several ages exceeding 10,000 years and a few approaching the inferred timing of last deglaciation approximately 15,000 to 17,000 years ago (Table 2); and (2) exposure ages within sampled study regions show significant variability (Table 2; Figure 25), implying that the sampled boulders fell at different times. This tends to confirm the assumption that most outlying boulders result from several independent fragmental rock fall events rather than from a single event, a key finding with respect to the frequency of outlying boulder deposition.

Table 2. Analytical results of terrestrial cosmogenic nuclide ^{10}Be geochronology of outlier rock-fall boulders in Yosemite Valley (continued on next page)

Sample	Location	Lat/Long (°N/°W)	Elevation (m above sea level)	Thick-ness[a] (cm)	^{10}Be Production rate (atoms g^{-1} yr^{-1})		Shield-ing[d] factor	Erosion rate (cm yr^{-1})	Mass quartz[e] (g)	Be carrier (mg)	^{10}Be/^{9}Be[f,g] (x 10^{-13})	^{10}Be concentration[g,h,i] (10^{4} atoms g^{-1} SiO$_2$)	Exposure age[g,j,k] (ka)
					Spallation[b]	Muons[c]							
ICC-1	Wahhoga	37.7404/ 119.6057	1216	2	9.23	0.269	0.86653	0.00065	36.000	0.3555	1.03 ± 0.07	6.65 ± 0.44	7.29 ± 0.83
ICC-2	Wahhoga	37.7403/ 119.6059	1215	2.5	9.10	0.269	0.85795	0.00065	100.226	0.4181	7.37 ± 0.18	20.46 ± 0.53	25.07 ± 2.64
ICC-3	Wahhoga	37.7400/ 119.6059	1213	4	9.07	0.268	0.86749	0.00065	99.636	0.4230	0.87 ± 0.04	2.37 ± 0.13	2.58 ± 0.27
ICC-4	Wahhoga	37.7397/ 119.6056	1212	3	9.14	0.268	0.86781	0.00065	99.997	0.4223	2.19 ± 0.04	6.09 ± 0.14	6.72 ± 0.63
ICC-5	Wahhoga	37.7406/ 119.6054	1217	1	9.21	0.270	0.85685	0.00065	99.985	0.4212	0.27 ± 0.01	0.68 ± 0.06	0.72 ± 0.09
C4-1	Camp 4	37.7417/ 119.6030	1213	3	9.31	0.268	0.88323	0.00065	100.180	0.4185	3.36 ± 0.06	9.30 ± 0.20	10.28 ± 0.98
C4-2	Camp 4	37.7409/ 119.6034	1213	4	9.34	0.268	0.89336	0.00065	100.329	0.4116	1.13 ± 0.03	3.00 ± 0.09	3.19 ± 0.30
C4-3	Camp 4	37.7408/ 119.6046	1217	1.5	9.53	0.270	0.88982	0.00065	100.614	0.4173	3.02 ± 0.06	8.27 ± 0.19	8.87 ± 0.84
C4-4a	Camp 4	37.7417/ 119.6034	1215	3.5	9.34	0.268	0.88834	0.00065	99.647	0.4230	1.50 ± 0.04	4.16 ± 0.13	4.44 ± 0.42
C4-5	Camp 4	37.7421/ 119.6029	1214	2	9.46	0.269	0.88942	0.00065	100.363	0.4230	3.11 ± 0.06	8.66 ± 0.19	9.37 ± 0.89
YFT-1	Yosemite Falls	37.7462/ 119.5965	1212	3.5	9.52	0.268	0.90785	0.00065	100.015	0.4100	1.88 ± 0.04	5.06 ± 0.12	5.32 ± 0.49
LH-1	Sunnyside Bench	37.7505/ 119.5924	1217	4	9.00	0.268	0.85796	0.00065	99.750	0.4090	0.87 ± 0.05	2.31 ± 0.15	2.53 ± 0.28
LH-2	Sunnyside Bench	37.7505/ 119.5927	1218	3.5	9.16	0.268	0.86891	0.00065	100.806	0.4100	1.16 ± 0.02	3.06 ± 0.07	3.31 ± 0.31
MC-1	Sunnyside Bench	37.7509/ 119.5878	1230	2	9.59	0.270	0.89062	0.00065	101.0754	0.4176	0.59 ± 0.01	1.53 ± 0.06	1.57 ± 0.15
MC-2	Sunnyside Bench	37.7508/ 119.5897	1227	2	9.28	0.270	0.86365	0.00065	100.9565	0.4207	1.41 ± 0.04	3.83 ± 0.12	4.11 ± 0.39
MC-3	Sunnyside Bench	37.751/ 119.5896	1230	2	9.34	0.270	0.86722	0.00065	100.790	0.3830	2.83 ± 0.05	7.10 ± 0.16	7.72 ± 0.73
AHW-1	Rhombus - Ahwahnee	37.7472/ 119.5757	1212	2	9.33	0.269	0.8783	0.00065	90.8759	0.4200	0.49 ± 0.02	1.43 ± 0.07	1.50 ± 0.15
AHW-2	Rhombus - Ahwahnee	37.7471/ 119.5747	1212	2	9.27	0.269	0.87321	0.00065	89.075	0.4256	3.44 ± 0.06	10.88 ± 0.24	12.20 ± 1.17
AHW-3	Rhombus - Ahwahnee	37.7472/ 119.5747	1213	2.5	9.15	0.268	0.86405	0.00065	100.017	0.4217	3.27 ± 0.09	9.13 ± 0.27	10.27 ± 1.00
AHW-4	Rhombus - Ahwahnee	37.74727/ 119.5742	1214	2	9.32	0.269	0.87597	0.000653	83.376	0.4222	3.69 ± 0.10	12.37 ± 0.37	13.94 ± 1.39
CV-CC-1	Glacier Point - Curry Village	37.73716/ 119.5750	1217	2	8.99	0.269	0.84345	0.00065	85.154	0.4090	0.57 ± 0.02	1.76 ± 0.07	1.92 ± 0.18

Sample	Location	Lat/Long (°N/°W)	Elevation (m above sea level)	Thick-ness[a] (cm)	^{10}Be Production rate (atoms g^{-1} yr^{-1})		Shield-ing[d] factor	Erosion rate (cm yr^{-1})	Mass quartz[e] (g)	Be carrier (mg)	^{10}Be/^{9}Be[f,g] (x 10^{-13})	^{10}Be concentration[g,h,i] (10^{4} atoms g^{-1} SiO_2)	Exposure age[g,j,k] (ka)
					Spallation[b]	Muons[c]							
CV-CC-2	Glacier Point - Curry Village	37.7371/ 119.5744	1218	4	8.86	0.268	0.84440	0.00065	100.076	0.4038	0.46 ± 0.02	1.17 ± 0.06	1.29 ± 0.13
CV-CC-3	Glacier Point - Curry Village	37.7368/ 119.5726	1219	1.8	9.22	0.270	0.86211	0.00065	66.874	0.4086	1.37 ± 0.03	5.47 ± 0.15	5.96 ± 0.56
CV-CC-4	Glacier Point - Curry Village	37.7362/ 119.5714	1221	3	9.26	0.269	0.87353	0.00065	100.700	0.4031	2.90 ± 0.11	7.68 ± 0.29	8.45 ± 0.84
CV-CC-5	Glacier Point - Curry Village	37.7366/ 119.5711	1218	4	9.39	0.268	0.89470	0.00065	100.396	0.4070	1.90 ± 0.04	5.07 ± 0.12	5.41 ± 0.50
CV-DRM-1	Glacier Point - Curry Village Res. Area	37.7378/ 119.5772	1216	2	8.95	0.269	0.84002	0.00065	100.211	0.4250	2.12 ± 0.05	5.94 ± 0.16	6.69 ± 0.63
CV-DRM-2	Glacier Point - Curry Village Res. Area	37.7377/ 119.5766	1214	2	8.90	0.269	0.83664	0.00065	56.539	0.4100	1.37 ± 0.04	6.48 ± 0.23	7.37 ± 0.72
CV-DRM-3	Glacier Point - Curry Village Res. Area	37.738/ 119.5766	1214	2	8.78	0.269	0.82555	0.00065	99.956	0.4088	2.61 ± 0.01	0.64 ± 0.04	0.71 ± 0.08
CV-DRM-4	Glacier Point - Curry Village Res. Area	37.7374/ 119.5756	1215	2	9.00	0.269	0.84517	0.00065	99.854	0.4126	1.64 ± 0.03	4.44 ± 0.10	4.93 ± 0.46
LEC-1	LeConte - Housekeeping	37.739/ 119.5792	1220	2	9.65	0.269	0.90286	0.00065	99.596	0.4181	1.44 ± 0.03	3.95 ± 0.10	4.07 ± 0.38
LEC-2	LeConte – Housekeeping	37.7402/ 119.5793	1214	3	9.52	0.268	0.90279	0.00065	100.809	0.3858	2.99 ±0.09	7.56 ± 0.25	8.08 ± 0.79
HKC-1a	LeConte – Housekeeping	37.7412/ 119.5797	1210	4	9.50	0.267	0.91070	0.00065	101.4367	0.4200	3.12 ± 0.07	8.53 ± 0.21	9.20 ± 0.88
HKC-1b	LeConte – Housekeeping	37.7412/ 119.5797	1210	4	9.50	0.267	0.91070	0.00065	100.0808	0.4183	3.15 ± 0.06	8.70 ± 0.19	9.40 ± 0.89
CHPL-1	Chapel Wall	37.7400/ 119.591	1207	1.5	9.44	0.269	0.88823	0.00065	100.284	0.4250	0.92 ± 0.02	2.52 ± 0.08	2.63 ± 0.25

[a]The tops of all samples were exposed at the boulder surface.
[b]Constant (time-invariant) local production rates based on Lal (1991) and Stone (2000). A sea level, high-latitude value of 4.8 ^{10}Be g^{-1} quartz was used.
[c]Constant (time-invariant) local production rate based on Heisinger et al. (2002a, 2002b).
[d]Geometric shielding correction for topography and sample surface orientation calculated with the Cosmic-Ray Produced Nuclide Systematics (CRONUS) Earth online calculator (Balco et al., 2008) version 2.2 (http://hess.ess.washington.edu/)..
[e]A density of 2.7 g cm^{-3} was used based on the granitic composition of the samples.
[f]Isotope ratios were normalized to ^{10}Be standards prepared by Nishiizumi et al. (2007) with a value of 2.85 x 10^{12} and using a ^{10}Be half-life of 1.36 x 10^{6} years.
[g]Uncertainties are reported at the 1σ confidence level.
[h]A mean blank value of 53,540 ± 10,845 ^{10}Be atoms (^{10}Be/^{9}Be = 3.33 x 10^{-15} ± 8.74 x 10^{-16}) was used to correct for background.
[i]Propagated uncertainties include error in the blank, carrier mass (1%), and counting statistics.
[j]Propagated error in the model ages include a 6% uncertainty in the production rate of ^{10}Be and a 4% uncertainty in the ^{10}Be decay constant.
[k]Beryllium-10 model ages were calculated with the Cosmic-Ray Produced Nuclide Systematics (CRONUS) Earth online calculator (Balco et al., 2008) version 2.2 (http://hess.ess.washington.edu).

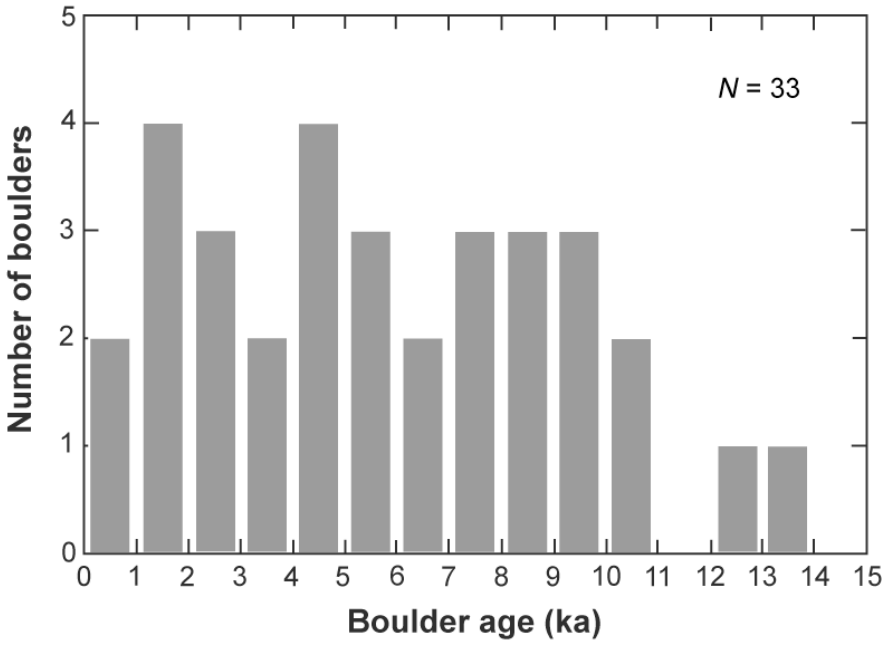

Figure 25. Histogram of cosmogenic beryllium-10 exposure ages (in thousands of years, or "ka") for sampled outlying boulders in Yosemite Valley.

4.7.2 Determining recurrence intervals for past outlying boulder deposition

To determine a recurrence interval (the inverse of annualized frequency) of outlying boulders entering each study region, an accumulation time over which the observed number of outlying boulders in the region has been deposited is needed. If all of the observed boulders were dated, the accumulation time could simply be taken as the oldest boulder age in each region. However, not all of the outlying boulders in the study regions were dated due to their prohibitively large number (258). Thus, instead of using the oldest boulder ages, which may not accurately depict the actual onset of outlying boulder deposition, we have used a maximum accumulation time based on the approximate time since glaciation of the Yosemite Valley, namely 15,000 years (Huber, 1987; Wieczorek and Jäger, 1996). Use of this maximum accumulation time is supported by the fact that the oldest ages amongst the relatively few boulders that we dated for each study region are close to the timing of deglaciation. Note, however, that the ages of all of the mapped outlying boulders spans from this time to the present, with at least some of the mapped outlying boulders deposited historically (past ~150 years).

With the maximum accumulation time defined, we calculate a recurrence interval for each study region by dividing the maximum accumulation time (15,000 years) by the corresponding number of outlying boulders in each study region (Table 3). We also calculate the recurrence interval across all the study regions, namely 15,000 years/258 (boulders) = 58 years. Thus, an outlying boulder should be deposited in the study regions approximately every 50-60 years on average.

Table 3. Outlying boulder deposition recurrence intervals and frequency ratings

Study region	Study region width (m)	Number observed boulders	Oldest boulder age (yr)[a]	Maximum accumulation time (yr)[b]	Outlying recurrence interval (yr)[c]	Outlying boulder annualized frequency (1/yr)
El Capitan	1,023	18	n/a	15,000	833	1.20×10^{-3}
Three Brothers	1,144	36	n/a	15,000	417	2.40×10^{-3}
Wahhoga	218	8	7,290	15,000	1,875	5.33×10^{-4}
Camp 4	391	12	10,280	15,000	1,250	8.00×10^{-4}
Yosemite Lodge	692	1	n/a	15,000	15,000	6.67×10^{-5}
Yosemite Falls	300	6	n/a	15,000	2,500	4.00×10^{-4}
Sunnyside Bench	179	9	n/a	15,000	1,667	6.00×10^{-4}
Castle Cliffs	218	1	7,100	15,000	15,000	6.67×10^{-5}
Church Bowl	208	3	n/a	15,000	5,000	2.00×10^{-4}
Rhombus Wall – Ahwahnee	447	11	13,940	15,000	1,364	7.33×10^{-4}
Royal Arches	303	36	n/a	15,000	417	2.40×10^{-3}
Glacier Point - Curry Village	415	25	n/a	15,000	600	1.67×10^{-3}
Glacier Point - Curry Village R.A.	215	26	n/a	15,000	577	1.73×10^{-3}
LeConte – Housekeeping Camp	480	16	9,400	15,000	938	1.07×10^{-3}
Chapel Wall	674	36	n/a	15,000	417	2.40×10^{-3}
Cathedral Rocks	506	14	n/a	15,000	1,071	9.33×10^{-4}

[a]Derived from ^{10}Be exposure dating of outlying boulders; see Table 2. Study regions with "n/a" are regions where no boulders were dated. Wahhoga study region excludes boulder ICC-2, which yields an exposure age of 25,070 years, inconsistent with the glacial history of Yosemite Valley and likely resulting from pre-failure cosmic ray exposure
[b]Assumed to be 15,000 yrs, the approximate time of deglaciation of Yosemite Valley
[c]Calculated as the maximum accumulation time (15,000 yrs) /number of outlying boulders

Based on historic rock-fall activity, most of the talus slopes in Yosemite Valley could reasonably be expected to accumulate rock fall debris yearly to every several decades (Stock et al., 2012b). In British Columbia, Evans and Hungr (1993) determined a recurrence interval on the order of 1,000 years for rock falls deposited beyond the edge of talus and within a particular 10 by 10 m section within the rock-fall shadow line. This generally agrees with our estimated recurrence intervals for outlying boulder deposition for each of the studied regions in Yosemite Valley (Table 3), although the range is large and the mean (3058 years) rather high because some study regions only had one outlying boulder, yielding a boulder deposition recurrence interval of 15,0000 years for those regions.

4.8 Determining the frequency of potential future outlying boulder deposition

The approach described in Section 4.7.2 uses the observed frequency of outlying boulders that have already fallen to estimate the frequency of boulder deposition beyond the base of talus slopes. However, it is plausible that future rock falls could produce different patterns of deposition, or produce more outlying boulders per event, than those that have occurred in the past 15,000 years. This could be due simply to detachment of larger rock masses than has previously occurred, or due to changes in cliff and/or talus slope morphology through time; for example, accumulation of talus at the base of cliffs has changed the morphology of the transition between cliff faces and the valley floor, promoting longer runout distances. To account for the possibility that future rock falls

could produce a different number and/or distribution of outlying boulders in the study regions than that preserved in the geologic record, we developed a second frequency estimate that makes use of information from computer model simulations of rock-fall trajectories.

4.8.1 Computer simulations of rock-fall runout

As discussed in Section 2, quantitative estimation of rock-fall hazard can be informed through the use of computer programs that simulate the spatial distribution of rock fall runout. A number of different rock-fall simulations exist, ranging from two-dimensional runout models (e.g., Jones et al., 2000) to full three-dimensional trajectory models (e.g., Guzzetti et al., 2002, 2003; Lan et al., 2007, 2010; Dorren, 2003, 2012). These models differ, sometimes considerably, in their operating platforms, input parameters, and output results. Evaluation and comparison of different model results is ongoing (e.g., Tagliavini et al., 2009).

For assessing potential future rock-fall runout extents and trajectories in Yosemite Valley, we utilized the STONE model, a physically based computer program that simulates rock fall events in three dimensions (e.g., Guzzetti et al., 2002, 2003; Agliardi and Crosta, 2003). We chose to use the STONE model because (1) it is a three-dimensional model that operates on a digital elevation model (DEM), (2) it has a range of output parameters that are easily incorporated into a GIS, and (3) it has previously been used to simulate rock falls in Yosemite Valley (Guzzetti et al., 2003; Wieczorek et al., 2008), and therefore has had the greatest level of site-specific calibration of any of the existing models at this time. The STONE model has also been used to assess rock-fall hazard in numerous other locations in the United States and worldwide (e.g., Crosta and Agliardi, 2003; Guzzetti et al., 2004; Tagliavini et al., 2009; Katz et al., 2010; Harp et al., 2010). The STONE model simulations were performed by the Research Institute for Geo-Hydrological Protection (CNR-IRPI) in Perugia, Italy.

The input data required by the STONE model include: (1) a DEM of the rock-fall detachment area(s) and potential runout area(s); (2) the location(s) and size(s) of the rock-fall source area(s); (3) the initial velocity and the starting angle (degrees from horizontal) for each rock fall; (4) a velocity threshold below which the block stops; and (5) the coefficients of dynamic rolling friction (the frictional resistance to rolling) and the normal and tangential energy restitution (fractional values representing the ratio of speeds after and before an impact) used to simulate the loss of energy when rolling and at impact points (e.g., Chau et al., 2002).

The STONE model uses a lumped mass approach to simulate rock falls, where each rock fall block is considered dimensionless with all of the mass concentrated in a point (the center of mass). This contrasts with other models that allow users to specify block shape and volume (e.g., Dorren, 2012). The ability to specify block shape and volume is particularly useful for slope-scale simulations, i.e., simulations of past rock falls, or of potential future failures of an unstable block of known dimensions, from

specific source areas on a cliff; it is less useful for simulating numerous potential future rock falls at the regional scale whose dimensions cannot be known (Guzzetti et al., 2002).

The STONE model accounts for the inherent natural variability in the input data by "launching" a variable number of particles from each cell of the source area, and by randomly varying the starting angle, the dynamic rolling friction coefficient, and the normal and tangential energy restitution coefficients (Guzzetti et al., 2002, 2003; Wieczorek et al., 2008). For each DEM cell, the STONE model produces results in raster maps that are easily incorporated into a GIS. These maps contain information on: (1) the cumulative count of rock-fall trajectories that passed through each cell, (2) the maximum computed velocity, and (3) the maximum height of a block from the ground computed along the rock-fall trajectories (i.e., the particle bounce height). The STONE model does not consider the collision of boulders falling along intersecting trajectories.

For the STONE simulations, we used input values for dynamic rolling friction, normal and tangential restitution, initial model conditions, and model parameters previously used by Guzzetti et al. (2003) and Wieczorek et al. (2008) for Yosemite Valley (Table 4). Although the values in Table 4 were not empirically determined for Yosemite Valley, they are within published ranges from experimental results (Chau et al., 2002) and values used by other models (Lan et al., 2007). These values were calibrated for Yosemite Valley using the terrain types (bedrock and surficial geology) described in Section 3.1 (Table 4). The calibrations performed by Guzzetti et al. (2003) and Wieczorek et al. (2008) consisted of modeling 15 actual rock falls in Yosemite Valley for which the source areas and runout extents were known, and adjusting the input values and initial model conditions until the extent and shape of the simulation matched those of the actual event, the number of rock-fall trajectories falling outside the mapped area was restricted, and the model parameters and initial conditions were within reasonable values.

To uniformly evaluate potential future rock-fall trajectories across the study regions, we performed simulations of rock falls from likely source areas throughout Yosemite Valley. Here we consider every DEM cell with a slope angle $\geq 60°$ to be a potential rock-fall source, which covers an area of approximately 19 km^2 (Figure 26; Guzzetti et al., 2003). Although rock falls can originate from lower-angle slopes, and have originated from slopes in Yosemite Valley as low angle as 35°, evaluation of recent (post-1980) rock falls in Yosemite Valley (Stock et al., 2012b) indicate that more than 70% of rock falls occurred from slopes > 60°. A $\geq 60°$ slope angle was also used as initiation points for the STONE model simulations of Yosemite Valley published by Guzzetti et al. (2003).

Because of limitations in computing power, the valley-wide simulations were performed on a 10 x 10 m DEM rather than the 1 x 1 m DEM. For the valley-wide simulations, 10 dimensionless particles were "launched" from each 10 x 10 m DEM cell, for a total of approximately 61,440 simulated particles (Figure 27). For simulations at the regional scale, where the dimensions of potential future rock fall particles are expected to vary widely, a dimensionless approach is appropriate. Because the results are ultimately used in a relative sense as discussed below, the hazard assessment in this case is not

particularly sensitive to the DEM cell size or the number of particles launched. The particles were launched using initial starting velocities of 1.5 meters/second.

Table 4. Values of dynamic rolling friction and normal and tangential energy restitution assigned to each terrain type in Yosemite Valley (from Guzzetti et al., 2003).

Terrain type	Rolling friction	Normal restitution	Tangential restitution
Recent debris flow[a]	0.65	30	50
Recent rock fall and rock slide[a]	0.75	35	55
Rock fall path[a]	0.30	65	80
Landslide scar[a]	0.20	65	80
Historical debris slide[a]	0.60	30	55
Historical rock fall and rock slide[a]	0.75	40	60
Prehistorical debris flow[a]	0.60	35	60
Prehistorical rock fall and rock slide[a]	0.70	35	55
Prehistorical rock avalanche[a]	0.60	40	60
Talus deposit[b]	0.70	35	55
Granitic bedrock[b]	0.30	65	80
Alluvial deposit[b]	0.85	15	20

[a]Landslide types obtained from Wieczorek et al. (1998).
[b]Lithological types obtained from Matthes (1930) and Calkins et al. (1985).

Wieczorek et al. (2008) compared runout extents associated with actual rock falls from Glacier Point against STONE simulations of those rock falls. Overall, they found that simulated rock-fall trajectories matched well the mapped distribution of rock debris in the field. The majority of simulated trajectories fell within the zone of mapped rock debris deposition, and many observed dynamic attributes of the rock falls (e.g., topographic steering and concentration) were displayed in the simulations. However, Wieczorek et al. (2008) also found that some trajectories, typically with total counts of <10, extended farther from the base of the cliff than the mapped distribution of rock debris. This apparent "overshoot" of the simulated trajectories may be due to several factors. First, some values assumed for input data may not accurately represent the full range of rock-fall dynamics. Second, and perhaps more importantly, the STONE model does not account explicitly for certain factors such as block shape, air drag, block fracturing, and/or energy dissipation by vegetation in the impact zone (e.g., Stokes et al., 2005; Dorren et al., 2006; Lundström et al., 2009). Even 1 x 1 m DEMs do not capture certain roughness elements in the landscape that can diminish the distance that boulders travel beyond the base of the cliff. It should be noted that only those trajectories resulting from the most unfavorable combination of modeling parameters and local topography reach these maximum runout positions; thus, these trajectories (typically trajectory counts of ≤ 10) represent low probability events. Nevertheless, the uncertainty of runout extent in the simulations is a primary reason why we use the STONE results in a relative (as opposed to absolute) manner, as discussed below.

Because the STONE model tracks the spatial distributions of rock-fall trajectories, it is possible to calculate the number of trajectories entering each study region, a proxy for potential future outlying boulder deposition; by definition, any trajectory extending beyond the edge of talus line is an outlying boulder. We used the valley-wide simulations to evaluate the number of trajectories entering each study region (Figures 28-34). The study regions that we use to evaluate trajectories are roughly rectangular in

shape (Figures 28-34). The longer sides, which are only used in conjunction with the STONE simulations, are bounded on the upslope side by the edge of talus line and on the downslope side by the 90th-percentile distance of mapped outlying boulders. The shorter sides are bounded by natural breaks in the topography and/or the morphology of the adjacent talus slope. In most cases one or both of the shorter sides abuts another study region (e.g., the Yosemite Lodge study region shares shorter sides with the Camp 4 study region to the west and the Yosemite Falls Trail study region to the northeast). The width of each study region is defined as the approximate straight-line distance along the longer side, i.e., roughly parallel to the edge of talus line and the 90th-percentile distance line. Note that the edge of talus line is often irregular (see, for example, Figure 32) and would exaggerate the study region width if taken as a line distance, which is why we use an approximate straight-line distance for the width.

For each study region, we approximate the number of simulated rock-fall trajectories entering each region, per unit width of the region, by summing the number of trajectories crossing pixels within the study region and dividing by the area of that region; alternative calculations of the number of trajectories entering each study area were deemed to be unjustifiably difficult to implement. As explained below, we normalize the number of trajectories entering each study region by the total trajectories entering all study regions, in order to predict the number of outlying boulders in each region in the next (as opposed to the past) 15,000 years. This normalization allows the STONE simulation results to be used in a relative sense, diminishing the impact of the uncertainties in the model input parameters.

The valley-wide STONE model simulations utilized here yielded two important results: (1) all study regions in Yosemite Valley containing outlying boulders beyond the base of talus also show modeled particle trajectories extending beyond the base of talus (Figures 27-34), with the number of outlying boulders in a region generally proportional to the number of model trajectories in that region, and (2) there is significant variation in the number of the STONE model trajectories within the 90th-percentile distance (between the edge of the talus and the 90th-percentile distance line) for each study region, ranging from 97 simulated trajectories for the Church Bowl study region to 16,642 simulated trajectories for the Three Brothers study region (Table 5). Some of this variation is due to the size of the study region, so normalizing by study region provides a more objective measure of comparison between the study regions (Table 5). Nevertheless, significant variation between study regions remains after this normalization, with study regions beneath the Three Brothers (Three Brothers and Wahhoga) and Glacier Point (Curry Village and the Curry Village Residential Area) showing greater numbers of modeled trajectories (Table 5). This is primarily a result of the steepness and height of the cliffs above these study regions and the topography of the cliffs and talus slopes that tend to steer and concentrate rock-fall trajectories.

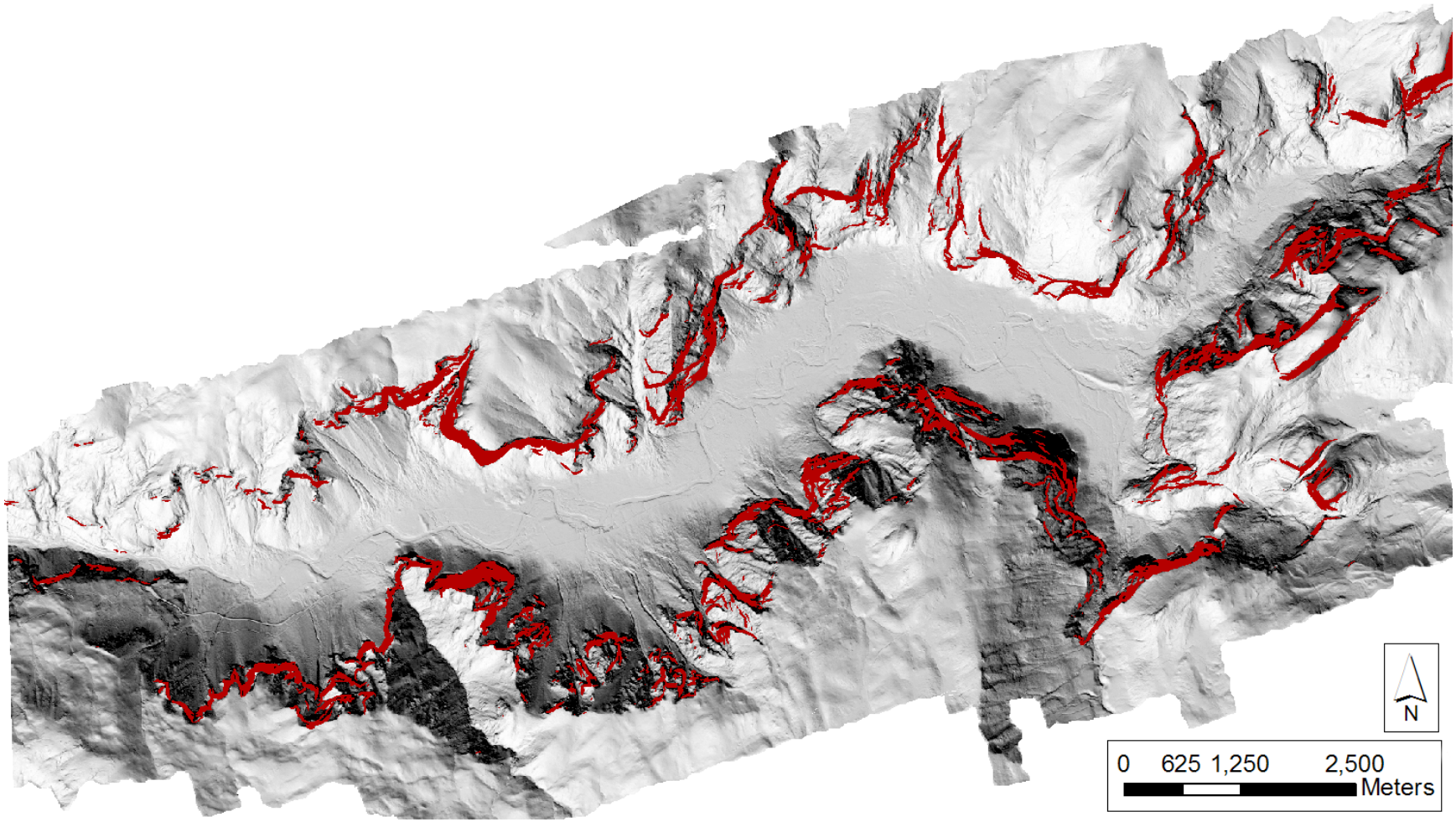

Figure 26. Shaded relief map showing DEM cells in Yosemite Valley with slopes ≥ 60° (red), representing approximately 19 km^2 of the three-dimensional surface region of Yosemite Valley (Guzzetti et al., 2003). Based on examination of recent rock-fall source areas, these areas were considered the most likely potential rock-fall source areas for the valley-wide STONE model simulations.

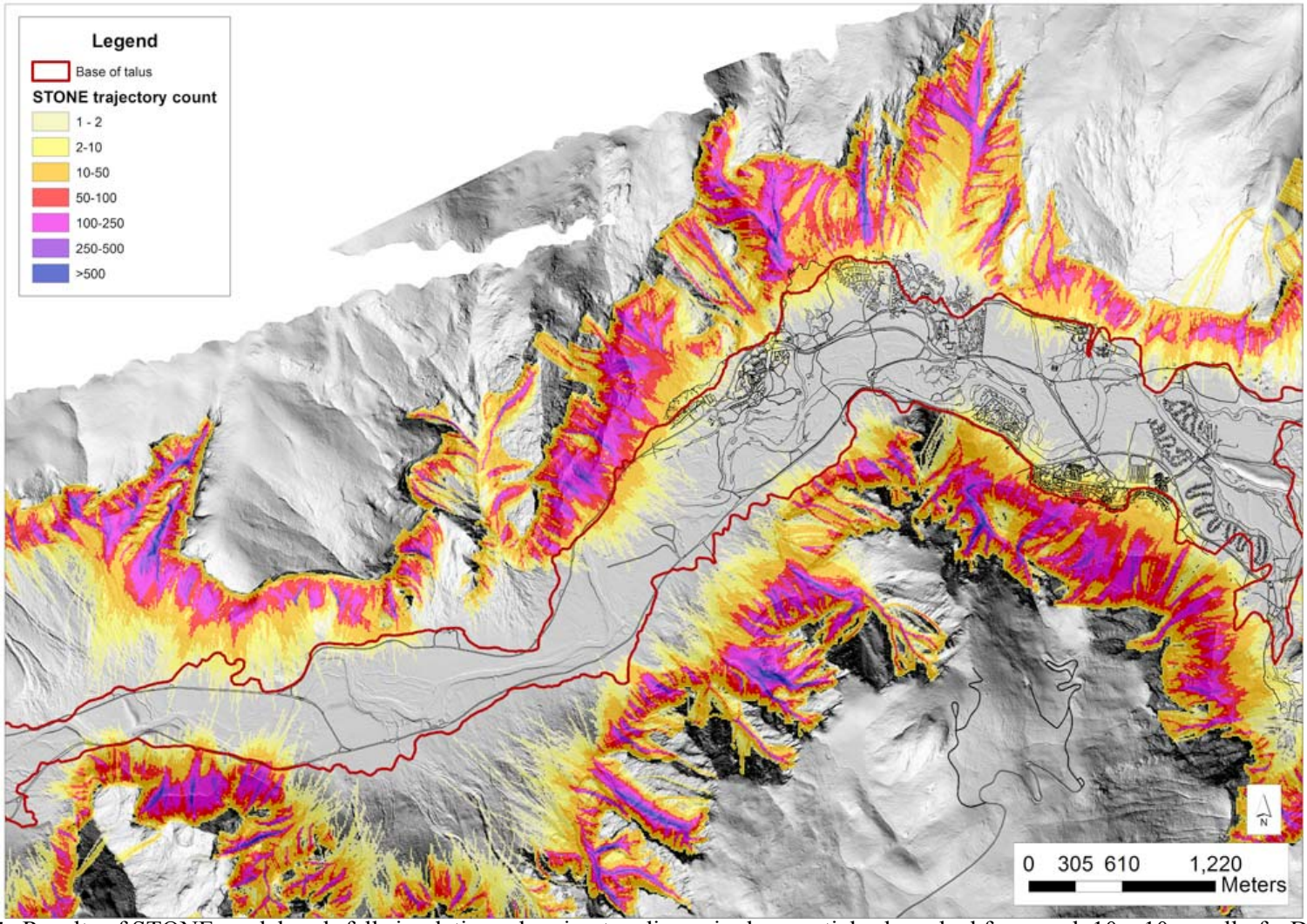

Figure 27. Results of STONE model rock-fall simulations showing ten dimensionless particles launched from each 10 x 10 m cell of a Digital Elevation Model (DEM) with slopes ≥ 60°. Each particle moves down the slope according to physical parameters producing a unique trajectory. Colors represent categories of trajectory counts per DEM cell.

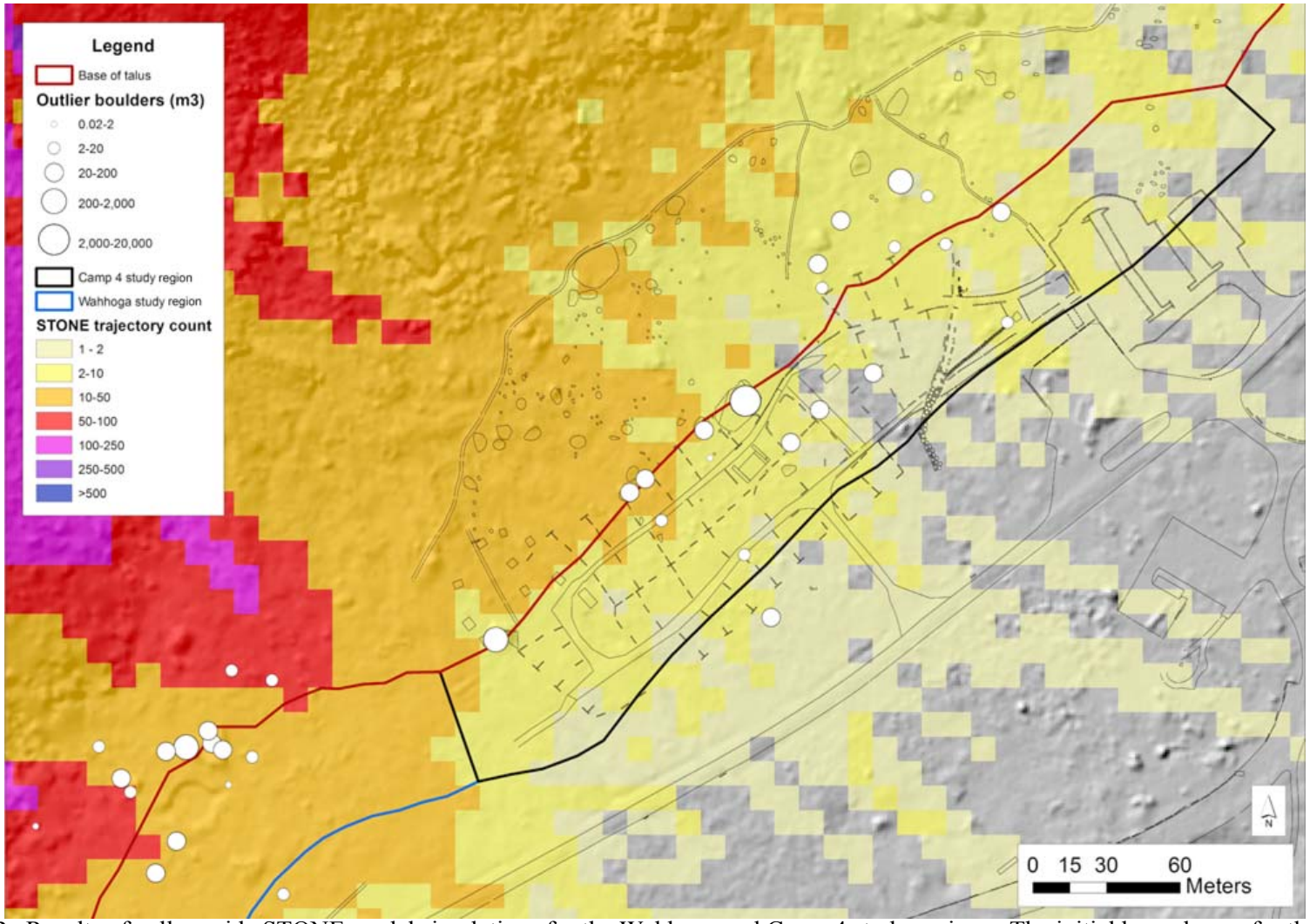

Figure 28. Results of valley-wide STONE model simulations for the Wahhoga and Camp 4 study regions. The initial hazard zone for the Wahhoga (blue line) and Camp 4 (black line) study regions is defined by the base of talus line (red) and 90th-percentile outlying boulder distance line. The Camp 4 study region contains 915 STONE model trajectories.

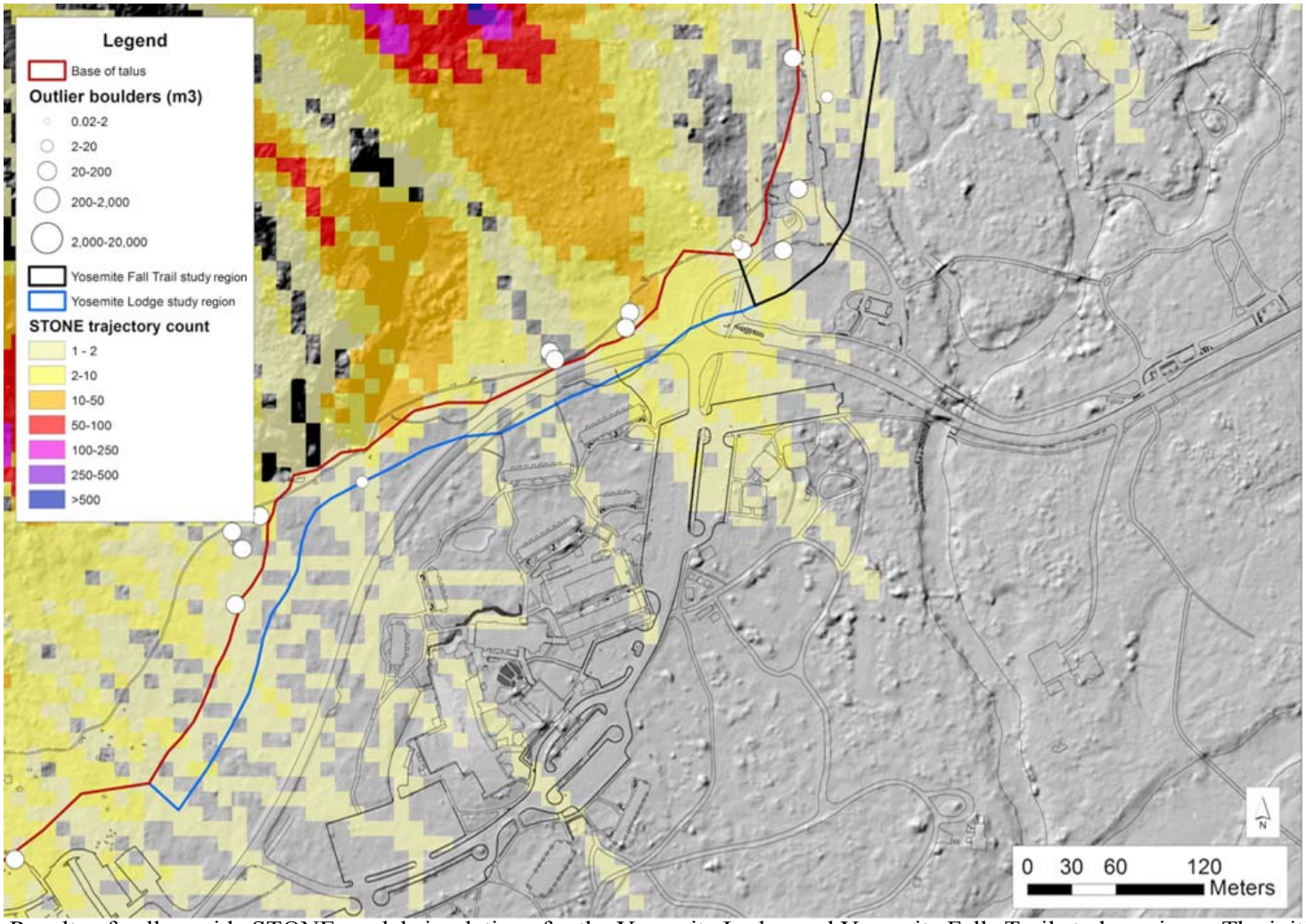

Figure 29. Results of valley-wide STONE model simulations for the Yosemite Lodge and Yosemite Falls Trail study regions. The initial hazard zones for the Yosemite Lodge (blue line) and Yosemite Falls Trail (black line) study regions are defined by the base of talus line (red) and 90th-percentile outlying boulder distance line. The Yosemite Lodge study region contains 377 STONE model trajectories, and the Yosemite Falls Trail study region contains 575 trajectories.

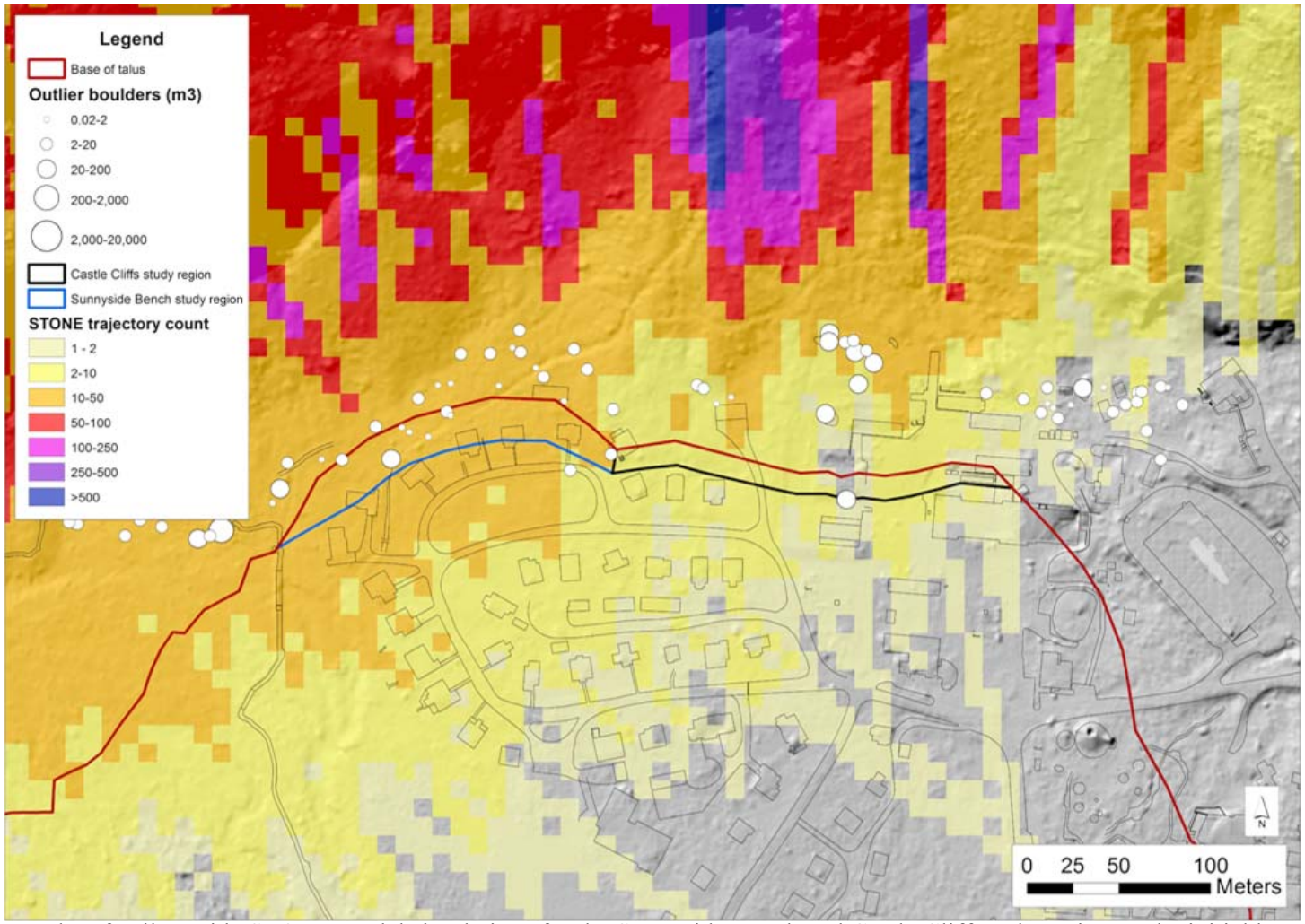

Figure 30. Results of valley-wide STONE model simulations for the Sunnyside Bench and Castle Cliff study regions. The initial hazard zones for the Sunnyside Bench (blue line) and Castle Cliffs (black line) study regions are defined by the base of talus line (red) and 90th-percentile outlying boulder distance line. The Sunnyside Bench study region contains 1,000 STONE model trajectories, and the Castle Cliffs study region contains 106 trajectories.

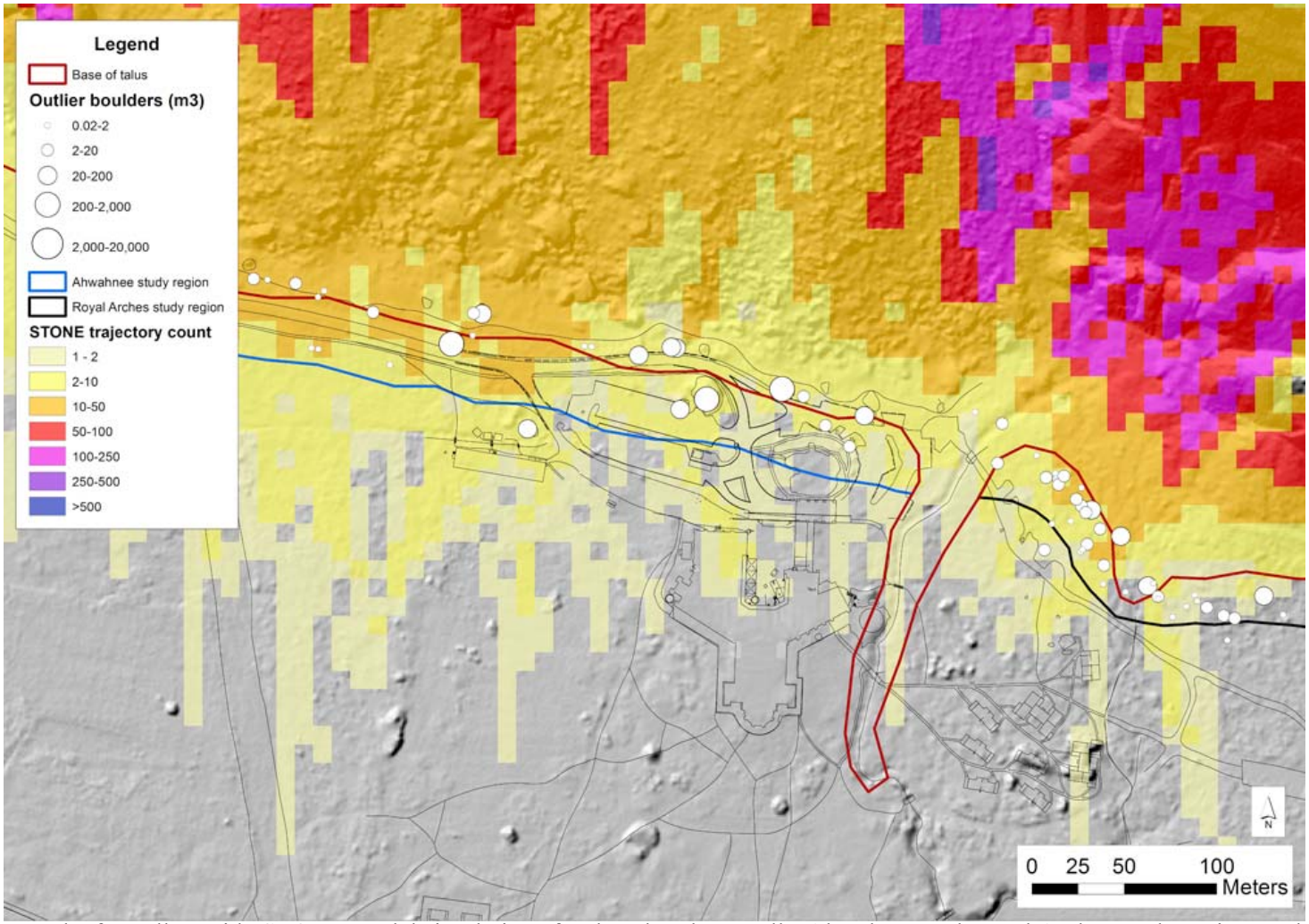

Figure 31. Results for valley-wide STONE model simulations for the Rhombus Wall - Ahwahnee and Royal Arches study regions. The initial hazard zones for the Rhombus Wall - Ahwahnee (blue line) and Royal Arches (black line) study regions are defined by the base of talus line (red) and 90th-percentile outlying boulder distance line. The Rhombus Wall - Ahwahnee study region contains 1,252 STONE model trajectories, and the Royal Arches study region contains 303 trajectories.

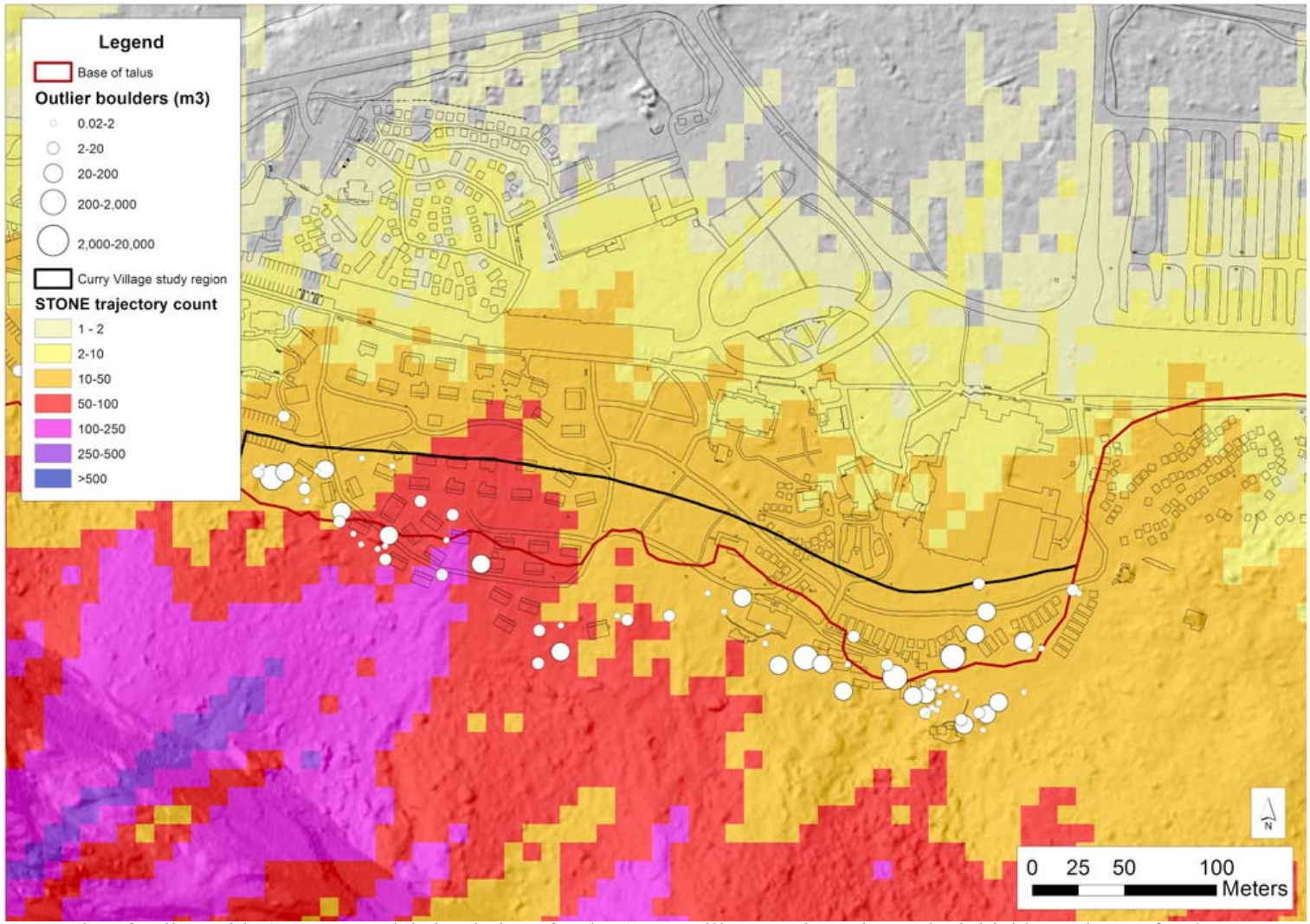

Figure 32. Results of valley-wide STONE model simulations for the Curry Village study region. The initial hazard zone for the Curry Village study region (black line) is defined by the base of talus line (red) and 90th-percentile outlying boulder distance line. The Curry Village study region contains 7,227 STONE model trajectories.

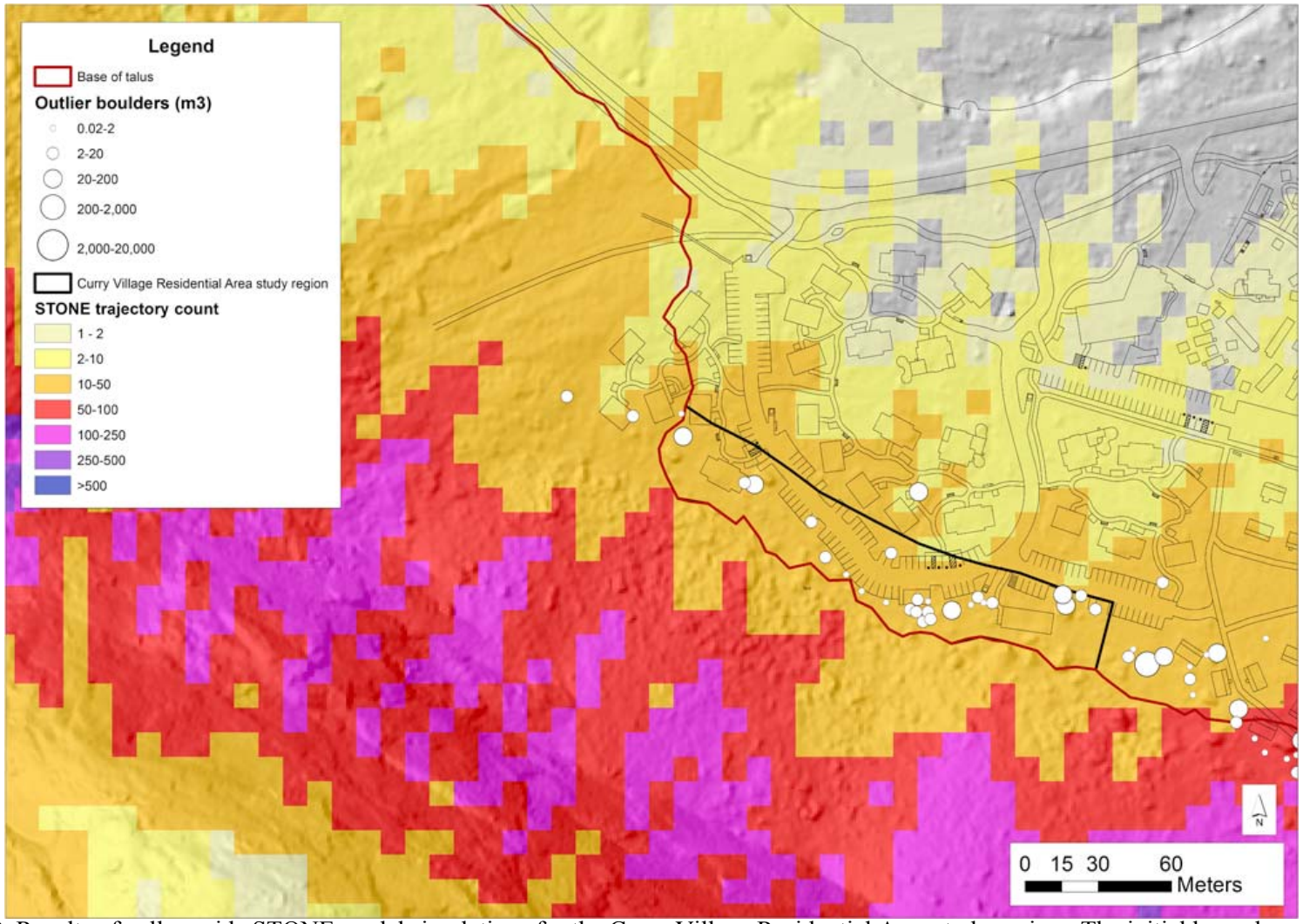

Figure 33. Results of valley-wide STONE model simulations for the Curry Village Residential Area study region. The initial hazard zone for the Curry Village Residential Area study region (black line) is defined by the base of talus line (red) and 90th-percentile outlying boulder distance line. The Curry Village Residential Area study region contains 1,554 trajectories.

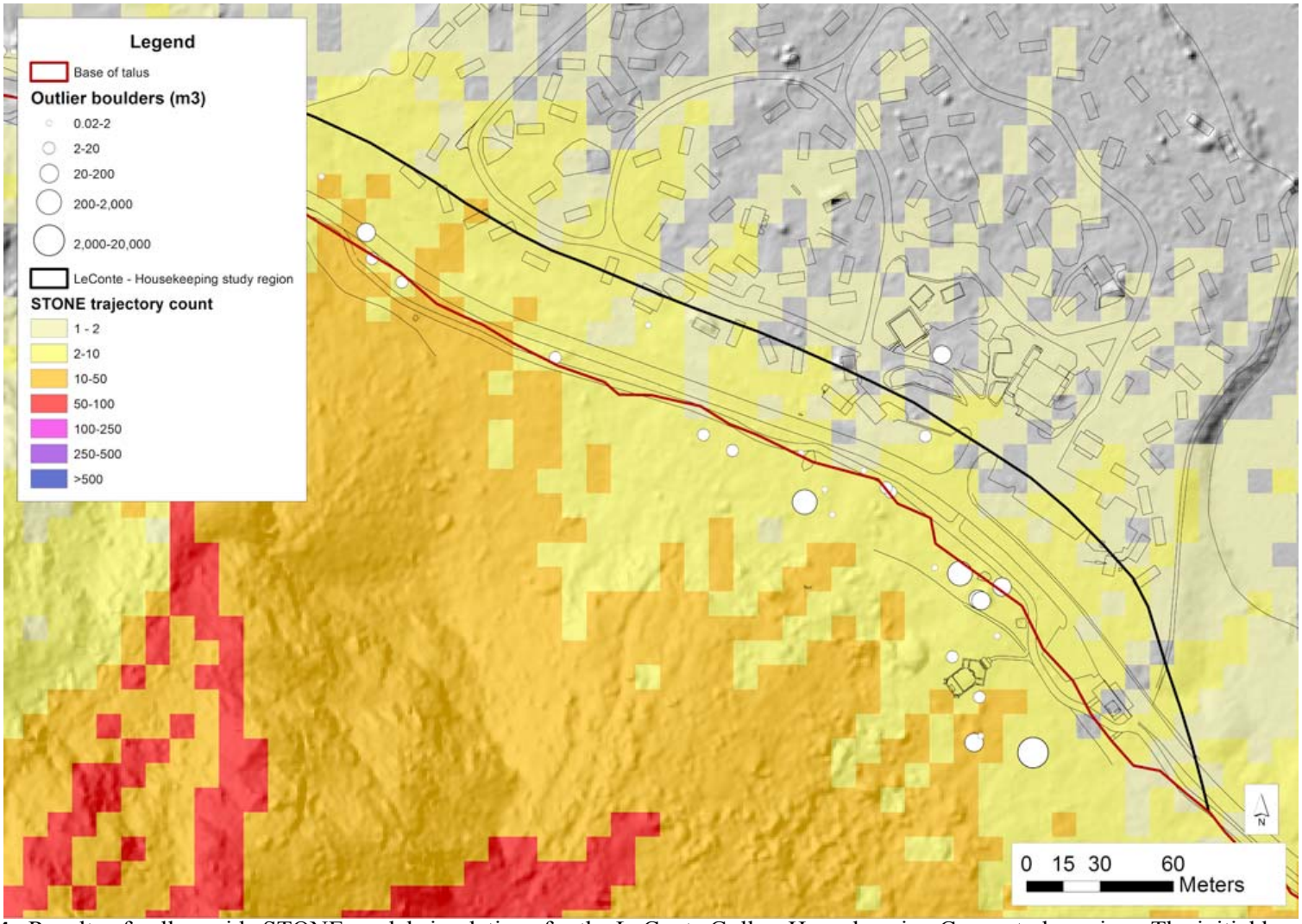

Figure 34. Results of valley-wide STONE model simulations for the LeConte Gully - Housekeeping Camp study region. The initial hazard zone for the LeConte - Housekeeping Camp study region (black line) is defined by the base of talus line (red) and 90th-percentile outlying boulder distance line. The LeConte - Housekeeping Camp study region contains 972 STONE model trajectories.

Table 5. STONE model trajectory counts for Yosemite Valley study regions

Study region	Planimteric area (m^2)	90th-percentile distance (m)	Study region width (m)	Number of STONE trajectories	STONE trajectories/ m^2	Normalized STONE trajectories
El Capitan	32,936	32	1,023	1,206	0.04	0.02
Three Brothers	52,839	48	1,144	16,642	0.31	0.15
Wahhoga	11,757	54	218	3,013	0.26	0.13
Camp 4	22307	57	391	915	0.04	0.02
Yosemite Lodge	14,652	21	692	377	0.03	0.01
Yosemite Falls Trail	16,394	55	300	575	0.04	0.02
Sunnyside Bench	3,444	23	179	1,000	0.24	0.12
Castle Cliffs	2,918	12	218	106	0.04	0.02
Church Bowl	1,453	7	208	97	0.07	0.03
Rhombus Wall - Ahwahnee	15,653	35	447	1,252	0.08	0.04
Royal Arches	8,172	27	303	303	0.04	0.02
Glacier Point - Curry Village	17,486	42	415	7,227	0.41	0.20
Glacier Point - Curry Village R.A.	6,113	28	215	1,554	0.25	0.12
LeConte Gully – Housekeeping Camp	19,811	41	480	972	0.05	0.02
Chapel Wall	28,104	42	674	1,417	0.05	0.02
Cathedral Rocks	21,363	42	506	1,983	0.09	0.04
				Total	**2.04**	**1.00**

4.8.2 Determining recurrence intervals for potential future outlying boulder deposition

Due to the potential sources of uncertainty associated with the model simulations discussed above and in Wieczorek (2008), we rely solely on actual observed outlying boulders for quantifying the distribution of outlying boulder distances beyond the base of talus, as described in Sections 4.4 and 4.6, and use the STONE results only in a relative sense. As there is no time component to the STONE simulations, it is not possible to directly calculate recurrence intervals for future deposition events. However, because the number of trajectories/m^2 varies substantial between study regions, we use the STONE simulation results to develop additional estimates of the recurrence intervals for potential future outlying boulder deposition by apportioning the total number of observed outlying boulders in all study regions according to the modeled trajectories.

Specifically, we use the valley-wide STONE simulations to apportion to each study region the total observed annualized frequency (inverse of recurrence interval) of outlying boulders across all the study regions, i.e. 1/58 yrs. We do this by first taking, from the results of the STONE simulations, the number of simulated STONE trajectories that go beyond the edge of talus line in each study region (Table 5). These numbers are then normalized by the total number of STONE trajectories predicted to travel beyond the edge of talus line across all study regions. The result is the relative proportion of expected outlying boulders in each study region that may be possible from potential future events as suggested by the STONE trajectories (Table 5). Although this does not directly provide an estimate of future recurrence intervals, it does provide necessary information for developing integrated past-and-future recurrence intervals. Our approach acknowledges that future outlying boulder deposition is likely to be similar to the long-term deposition experienced by all study regions (i.e., 258 boulders in 15,000 years), but

also acknowledges that individual study regions may experience more or less frequent deposition in the future, consistent with the STONE simulation results.

4.9 Integrating rock-fall hazard assessment methods

As explained in Section 4.6, the 90th-percentile outlying boulder distances for the 16 study regions in Yosemite Valley (Table 1) are such that when a future rock fall generates an outlying boulder, the chance that it will travel beyond the 90th-percentile distance is expected to be 1/10, assuming a steady rate of outlying boulder deposition since 15,000 years ago. However, how often future rock falls will generate outlying boulders within each study region is not taken into account by the 90th-percentile distances. To explicitly account for the frequency of outlying boulders deposited within each study region – again, a key component of hazard assessment (Varnes, 1984) – we adjusted the 90th-percentile distances by frequency-related factors derived from Sections 4.7 and 4.8, and integrated as described below (Figure 35). The final result is that the overall hazard beyond the scaled distances is the same for all the study regions.

We estimate the frequencies of outlying boulders that are used to adjust the 90th-percentile distances in two different ways; both estimates are plausible and are given equal weighting in our hazard assessment. The first frequency estimate for each study region is that explained in Section 4.7.2, i.e., the observed number of outlying boulders in the study region (e.g., 18 outlying boulders in the El Capitan study region) divided by an accumulation time of 15,000 years. This approach essentially uses the geological record of past rock falls to estimate the frequency of outlying boulder deposition. However, it is plausible that future rock falls may extend farther, or produce more outlying boulders per event, than those that have occurred in the past 15,000 years. To accommodate this possibility, we developed a second frequency estimate that makes use of information from the STONE model simulations described in Section 4.8.2. This second frequency estimate is based on the relative numbers of simulated boulder trajectories entering the study regions (i.e., the normalized number of trajectories described in Section 4.8.2). The product of this relative number for each region and the total observed frequency of outlying boulders across all 16 study regions (i.e., 258 boulders/15,000 years from Section 4.7.2) provides the second estimate of the frequency of outlying boulders in the region. In effect, the valley-wide STONE simulations are used to apportion the total observed frequency of all outlying boulders in all study regions to each of the individual study regions.

The two different frequency estimates for each study region are presented in Table 6. Also presented in Table 6 is the average of the two estimates, which represents an equally weighted estimate of hazard base on both past observations and future expectations. This average was used to adjust the initial 90th-percentile distances. Note that the estimated frequencies differ between study regions by one order of magnitude or more (Table 6).

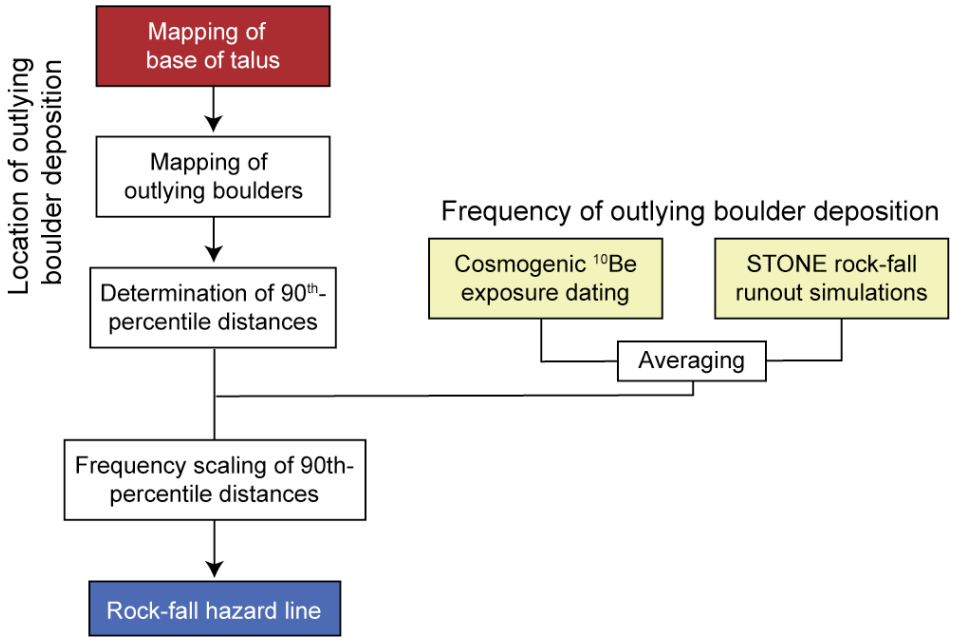

Figure 35. Flow chart illustrating the key components of the hazard assessment methodology used to determine the final rock-fall hazard line.

As previously stated, the adjusted 90th-percentile distances are such that the overall hazard of outlying boulders going beyond each distance will be the same for all the study regions. The resulting exceedance frequency of a boulder going beyond the scaled distances is 258/15,000 boulders/year multiplied by 1/10 (i.e., a 10% exceedance threshold), which results in 1/581 boulders/year. This exceedance frequency of 1/581 exceedance/year is close to the 1/500 exceedance/year that has often been specified for natural hazard assessments such as earthquake (e.g. Giardini et al., 1999) and floods (e.g., USGS, 1982; CFR 2010). A 1/500 exceedance/year translates to a 0.2% probably that such an event will occur in any given year, or an approximately 10% probability that such an event will occur in the next 50 years.

To distribute the exceedance frequency equally to all of the study regions, we normalize it by the total width of the study regions measured along the talus edge (7,412 m) such that the hazard should be identical at all locations once the initial 90th-percentile lines are adjusted. The normalized exceedance frequency is thus ([1/581 boulders/year]/7,412 m) = 2.32 x 10^{-7} boulders/year/m). With this normalized exceedance frequency as the specified target, we calculated the adjusted 90th-percentile outlying boulder distance for each study region according to the following procedure:

(1) We first determined the ratio of the normalized (by width) exceedance frequency for the study region to the specified target exceedance frequency, e.g., (1/10 x [9.24 x 10^{-7} boulders/year/m/ 2.32 x 10^{-7} boulders/year/m]) = 0.40 for the El Capitan study region; see Table 6.

(2) We then scaled the 1/10 chance of exceeding the 90^{th}-percentile distance by the inverse of the ratio from Step 1 (e.g., 1/10 / 0.40 = 1/4 for the El Capitan study region). We denote this scaled chance as p for Step 3.

(3) Lastly we read the $(1-p)^{th}$ percentile from the cumulative distribution function of outlying boulder distances for the study region (e.g., 20 m from Figure 21 for the El Capitan study region).

For all of the study regions, the scaled outlying boulder distance from Step 3 above is presented in Table 6 as a scale factor with respect to the corresponding 90^{th}-percentile distance (e.g., 20 m / 32 m = 0.62 for the El Capitan study region). Note that if the normalized exceedance frequency of boulders going beyond the 90^{th}-percentile distance in a region is relatively low or high compared to the specified target (e.g., ratios from Step 1 above of 0.40 for the El Capitan study region and 2.75 for the Curry Village Residential Area study region), the resulting scale factor will be relatively small or large, respectively (e.g., 0.62 for the El Capitan study region and 1.69 for the Curry Village Residential Area study region; Table 6). Final scaled distances of the hazard line from the talus edge are shown in Table 7 and Figure 36. The scaled distance is never larger than the maximum observed outlying boulder distance in a region. This is because the scaled distance corresponds to a percentile of the cumulative distribution function of observed outlying boulder distances in the region, as indicated in Step 3 above. The new percentile distance is simply smaller or larger than the 90^{th}-percentile distance when the frequency of outlying boulders in the region is relatively low or high, respectively. Where the estimated frequency is relatively low, a smaller percentile distance (e.g., 75^{th}-percentile distance for the El Capitan study region) is allowed; where it is relatively high, a larger percentile distance (e.g., 96^{th}-percentile distance for the Curry Village Residential Area study region) is required. To reiterate, the scaled hazard line everywhere represents the same level of hazard, i.e., a 1/500 boulders/year frequency of exceedance (approximately a 1/500, or 0.2%, annual probability that a boulder will be deposited beyond this line). Final scaled hazard lines are shown for representative study regions in Figures 37-43.

The scaled distances from the talus edge that were calculated according to this procedure are the basis for a final rock-fall hazard line. The line is thereby based on observable, measurable evidence of previous rock falls in the form of the spatial distribution of outlying boulders, but also incorporates additional data on the frequency of occurrence of outlying boulder deposition, and simulated trajectories of potential future rock falls from the STONE model. Thus, by representing a spatial probability, this hazard line incorporates the key information identified by Varnes (1984) regarding rock-fall hazards, namely information about location (where an event will occur) and time (when or how frequently an event will occur).

Table 6. Derivation of hazard line scaling factors for Yosemite Valley study regions

Study region	Area (m^2)	90^{th}-percentile distance (m)	Width (m)	Number STONE trajectories in study region	Number STONE trajectories/ distance	Number estimated outlying boulders	Number observed outlying boulders	Average number outlying boulders	Average outlying boulders/ 15,000 yrs/width	Estimated outlying boulders/mean estimated outlying boulders	Scaling factor
El Capitan	32,936	32	1,023	1,206	37	10	18	14	9.24×10^{-7}	0.29	0.62
Three Brothers	54,356	48	1,144	16,642	350	97	36	66	3.87×10^{-6}	2.43	1.18
Wahhoga	11,757	54	218	3,013	56	15	8	12	3.59×10^{-6}	2.04	1.19
Camp 4	22,307	57	391	915	16	4	12	8	1.40×10^{-6}	0.33	0.84
Yosemite Lodge	14,524	21	692	377	18	5	1	3	2.88×10^{-7}	0.21	1.00
Yosemite Falls Trail	16,394	55	300	575	11	3	6	4	9.90×10^{-7}	0.28	0.38
Sunnyside Bench	4,115	23	179	1,000	43	12	9	11	3.92×10^{-6}	1.93	1.16
Castle Cliffs	2,611	12	218	106	9	2	1	2	5.28×10^{-7}	0.32	1.00
Church Bowl	1,453	7	208	97	14	4	3	3	1.10×10^{-6}	0.53	1.00
Rhombus Wall-Ahwahnee	15,653	35	447	1,252	36	10	11	10	1.56×10^{-6}	0.64	0.82
Royal Arches	8,172	27	303	303	11	3	36	20	4.31×10^{-6}	0.29	1.30
Glacier Point - Curry Village	17,486	42	415	7,227	172	48	25	36	5.82×10^{-6}	3.29	1.34
Glacier Point - Curry Village R.A.	61,13	28	215	1,554	55	15	26	21	6.37×10^{-6}	2.02	1.69
LeConte – Housekeeping Camp	19,811	41	480	972	24	7	16	11	1.56×10^{-6}	0.39	0.70
Chapel Wall	28,104	42	674	1,417	34	9	36	23	2.25×10^{-6}	0.40	0.99
Cathedral Rocks	21,363	42	506	1,983	47	13	16	14	1.78×10^{-6}	0.74	0.98

Table 7. Final scaled distances beyond the base of talus for Yosemite Valley study regions

Study region	90th-percentile outlying boulder distance (m)[a]	Scaling factor[b]	Final hazard zone distance (m)
El Capitan	32	0.62	20
Three Brothers	48	1.18	56
Wahhoga	54	1.19	64
Camp 4	57	0.84	48
Yosemite Lodge	21	1.00	21
Yosemite Falls Trail	55	0.38	21
Sunnyside Bench	23	1.16	27
Castle Cliffs	12	1.00	12
Church Bowl	7	1.00	7
Rhombus Wall - Ahwahnee	35	0.82	29
Royal Arches	27	1.30	35
Glacier Point - Curry Village	42	1.34	56
Glacier Point - Curry Village R.A.	28	1.69	48
LeConte – Housekeeping Camp	41	0.70	29
Chapel Wall	42	0.99	41
Cathedral Rocks	42	0.98	41

[a]From Table 1
[b]From Table 6.

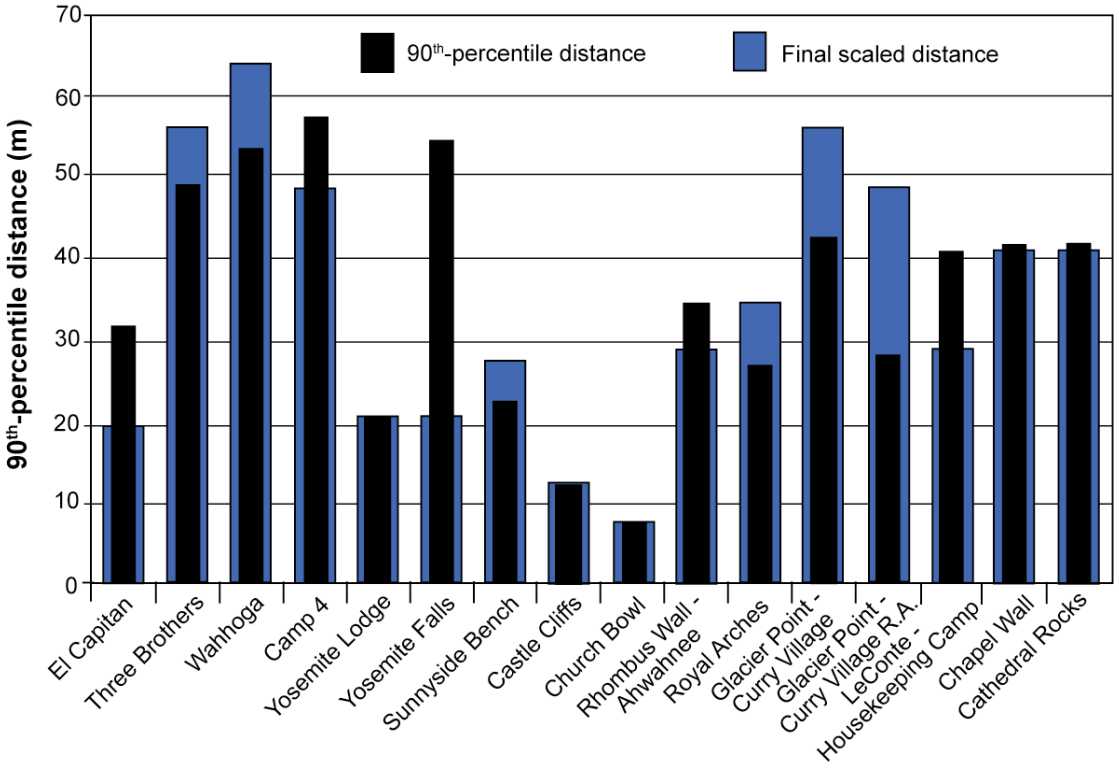

Figure 36. Comparison of the 90th-percentile distances for boulders beyond the talus edge and final scaled distances beyond the talus edge for the different study regions in Yosemite Valley. Scaled distances incorporate frequency information derived from boulder dating and rock-fall simulations.

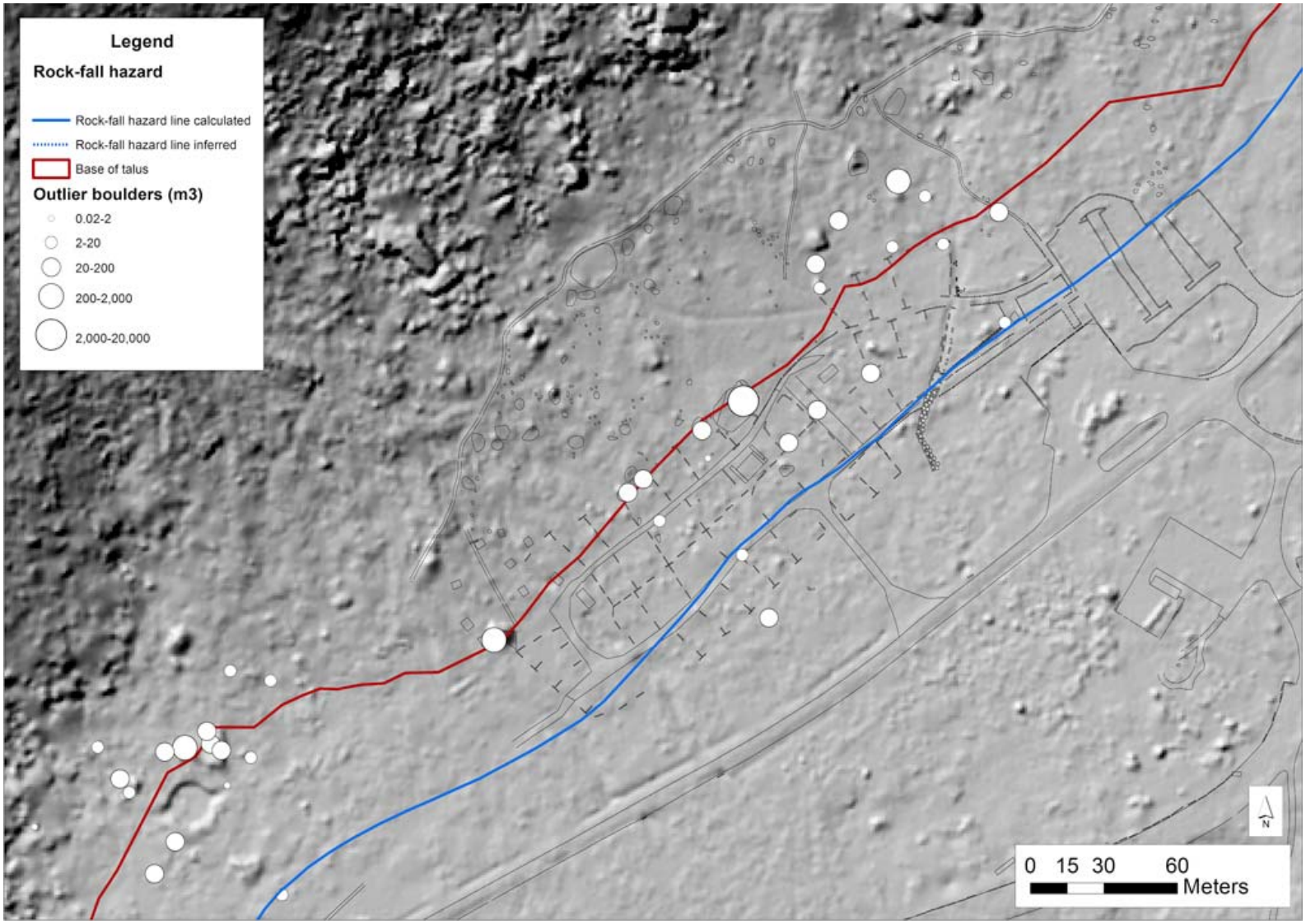

Figure 37. The final adjusted rock-fall hazard line developed by this study (blue line) for the Wahhoga and Camp 4 study regions.

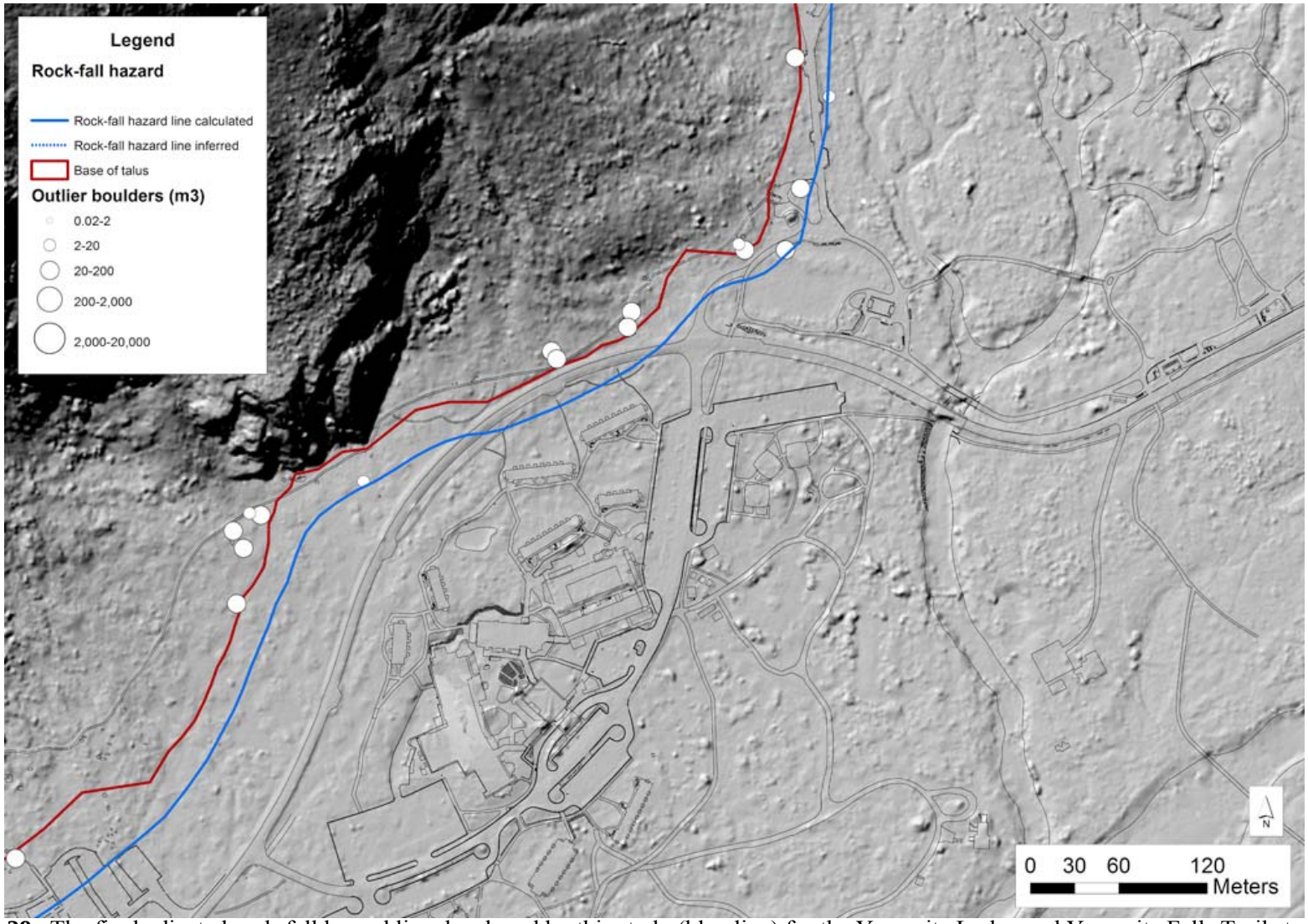

Figure 38. The final adjusted rock-fall hazard line developed by this study (blue line) for the Yosemite Lodge and Yosemite Falls Trail study regions.

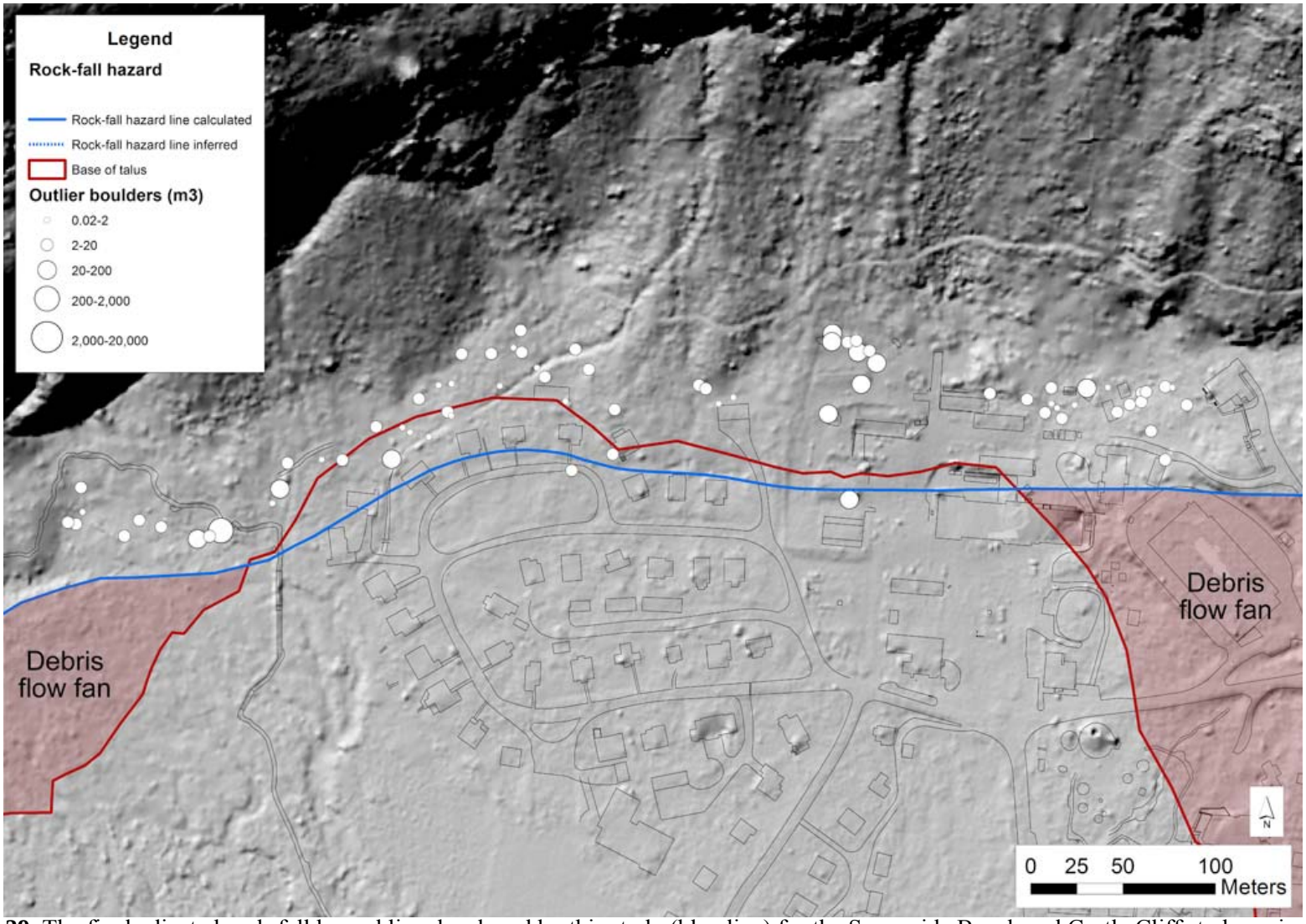

Figure 39. The final adjusted rock-fall hazard line developed by this study (blue line) for the Sunnyside Bench and Castle Cliff study regions. Red shaded regions are debris flow fans that are not accounted for in this analysis.

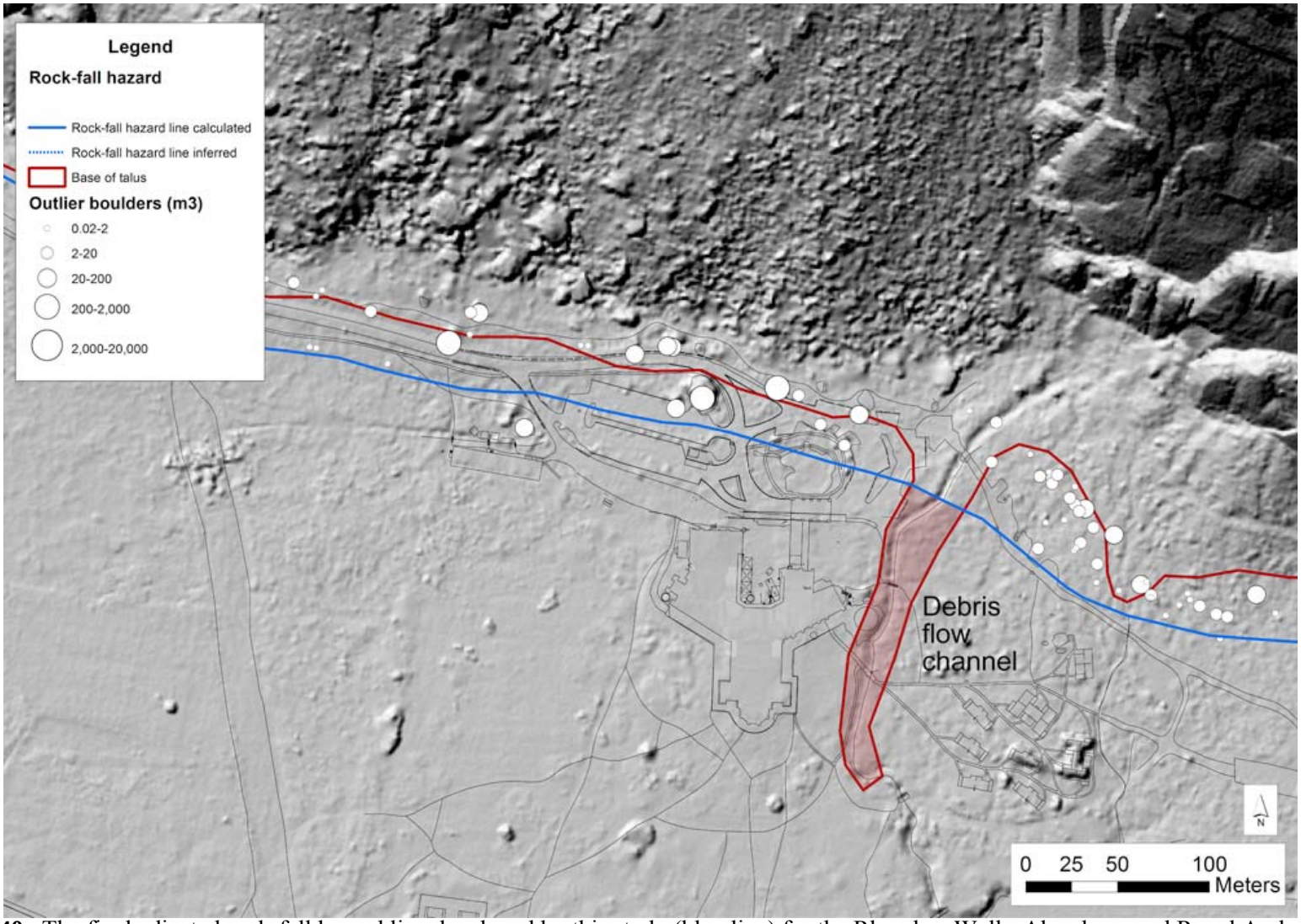

Figure 40. The final adjusted rock-fall hazard line developed by this study (blue line) for the Rhombus Wall - Ahwahnee and Royal Arches study regions. The red shaded region is a debris flow channel that is not accounted for in this analysis.

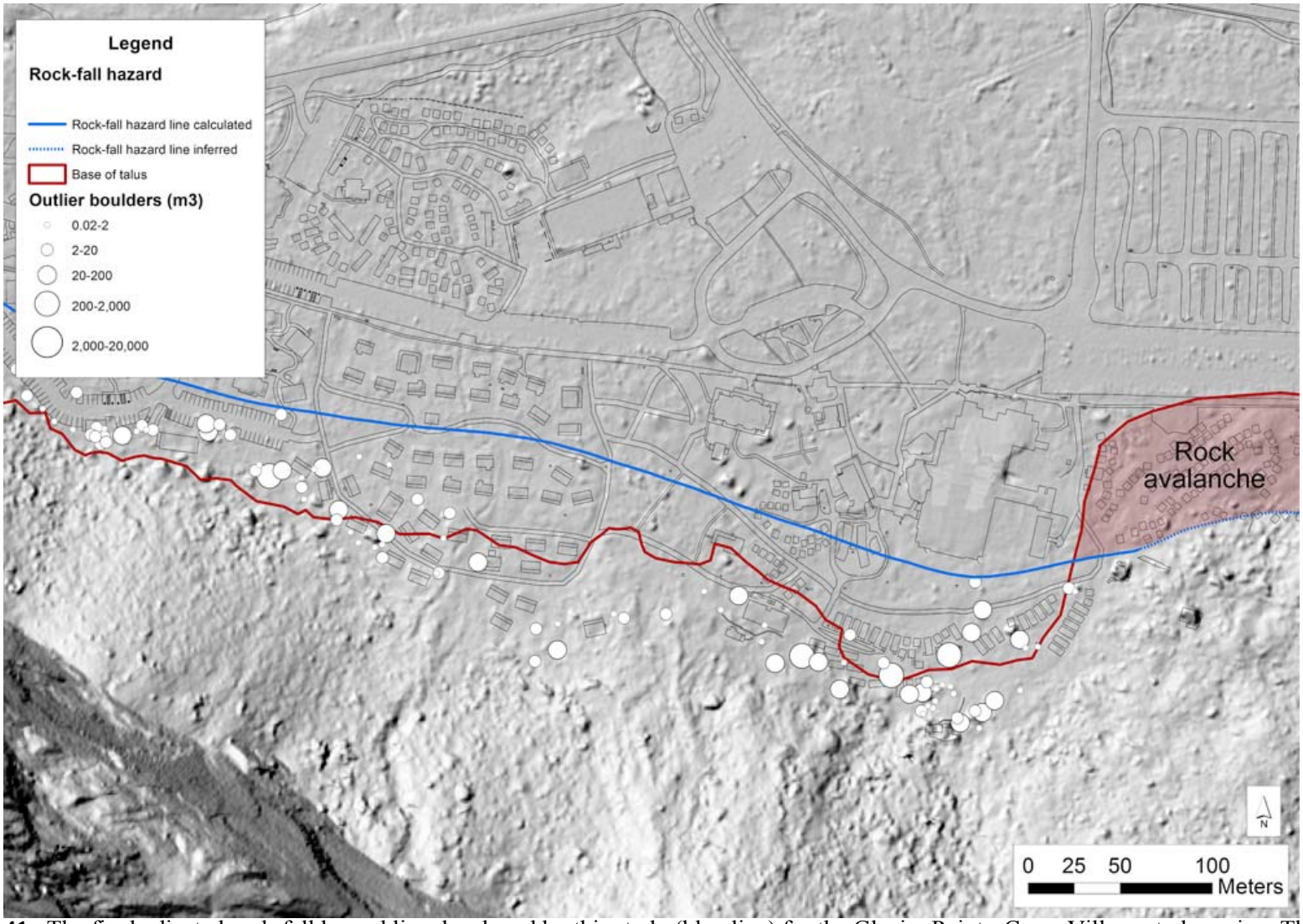

Figure 41. The final adjusted rock-fall hazard line developed by this study (blue line) for the Glacier Point - Curry Village study region. The red shaded region is a prehistoric rock avalanche deposit that is not accounted for in this analysis.

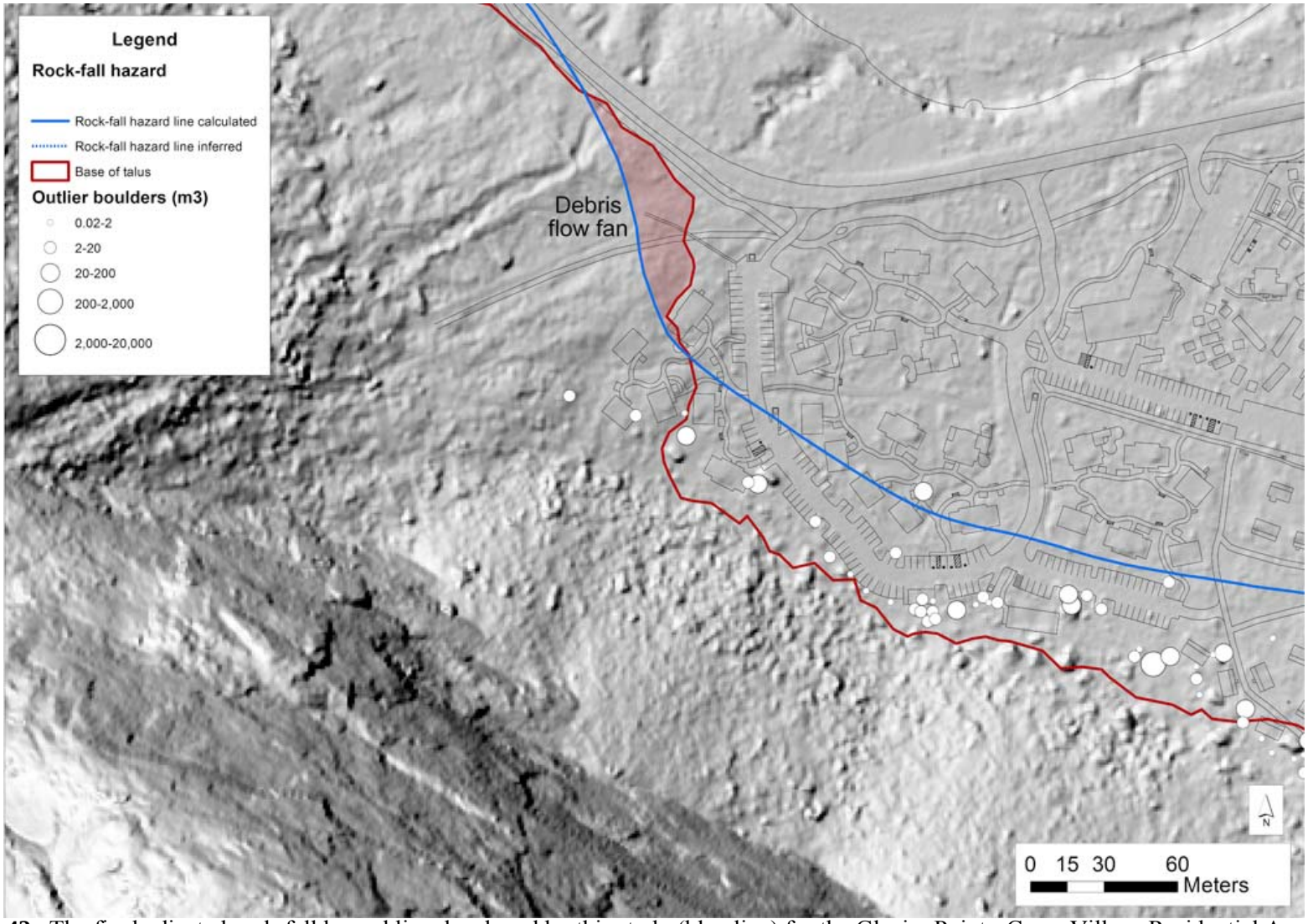

Figure 42. The final adjusted rock-fall hazard line developed by this study (blue line) for the Glacier Point - Curry Village Residential Area study region. The red shaded region is a debris flow fan that is not accounted for in this analysis.

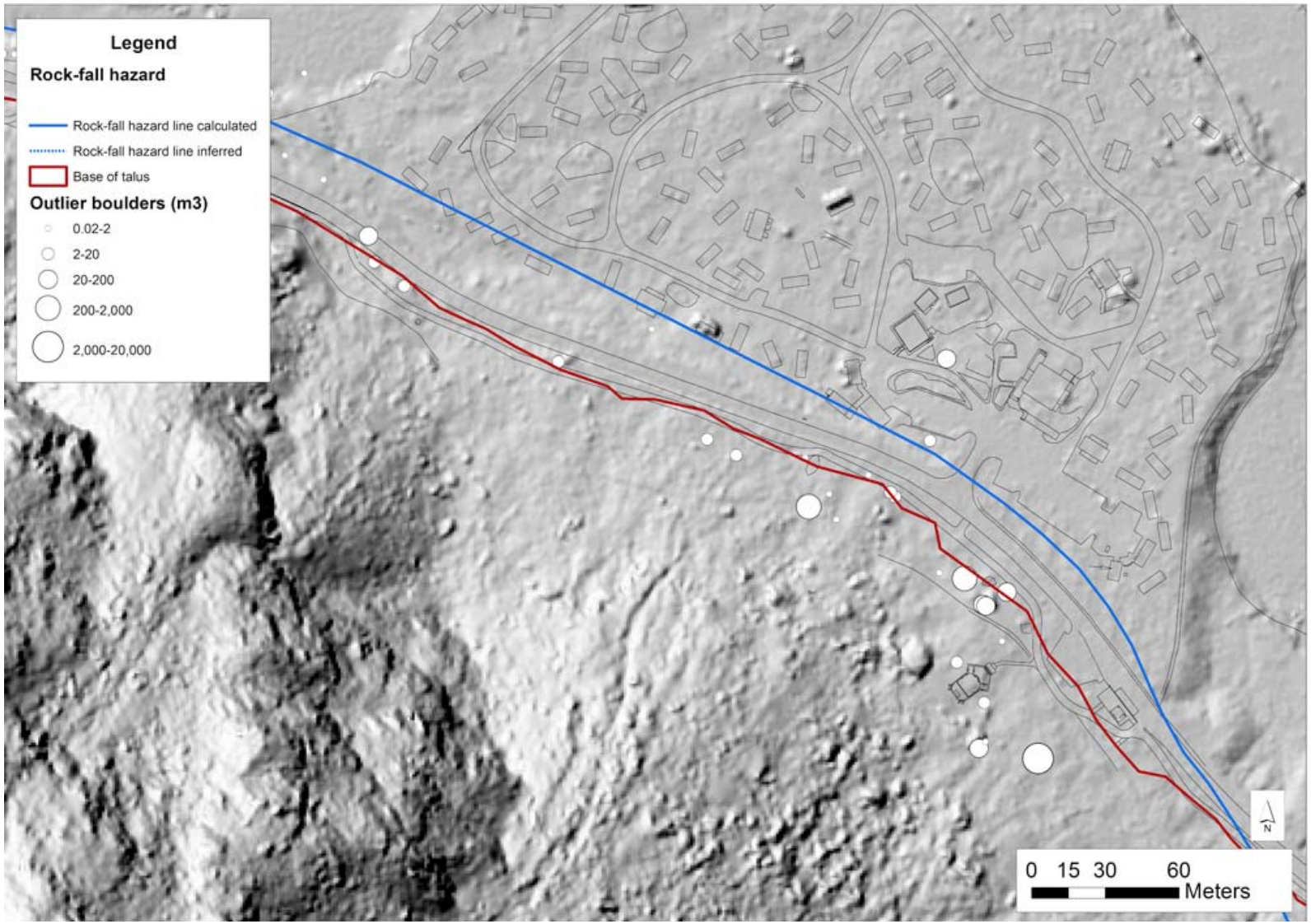

Figure 43. The final adjusted rock-fall hazard line developed by this study (blue line) for the LeConte – Housekeeping Camp study region.

5.0 Rock-fall risk assessment

Risk from rock-fall hazards was investigated by determining the likelihood of persons being struck by rock-fall boulders within the previously delineated hazard zones, including both the talus slopes and the adjacent outlying boulder zones. This risk assessment focused on the inventory of buildings , structures, and other facilities such as campsites, lodges, and amphitheaters where people congregate (see Section 3.4). In this assessment, we assume that all structures in the study regions are equally vulnerable to penetration by rock fall boulders. This assumption is based on the fact that the mean observed outlying boulder volume is 67 m^3, equivalent to a spherical boulder with a radius of 2.5 m, and that boulder fall heights can be as much as approximately 1 km, leading to extremely large impact energies. These energies would be capable in almost all cases of penetrating the structures within the hazard zone.

As will be explained below, the risk level for each structure or facility was quantified as a combination of its distance from the hazard line and its expected occupancy. More specifically, the risk level, here termed the risk metric, was calculated as the product of an annualized frequency of outlying boulders striking the structure or facility and the annualized expected number of people within the structure or facility Figure 44). This risk metric is proportional to an annualized expected number of people struck by outlying boulders in each structure.

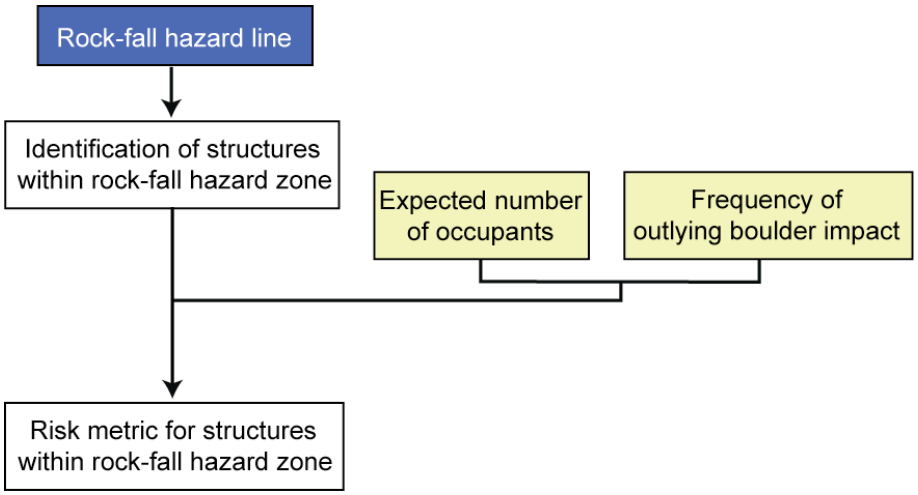

Figure 44. Flow chart illustrating the key components of the risk assessment methodology used to calculate risk metrics for buildings or other facilities within the hazard line.

5.1 Annualized frequency of outlying boulder striking each structure

In Section 4.9 we calculated an annualized frequency for the possibility of outlying boulders traveling beyond (exceeding) a particular distance from the talus edge; this is calculated as the product of:

(1) the annualized frequency of outlying boulders entering the region, and

(2) the probability of exceeding the particular outlying distance, from a probability distribution of distances (e.g., Figure 23 for the El Capitan study region).

Here, to calculate an annualized frequency of outlying boulders striking a particular structure, we have simply applied the calculation from Section 4.8 using the distance of the structure or facility from the talus edge (or, similarly, the distance of the structure from the hazard line).

As an example, the restroom structure in the El Capitan study region is 2.5 m from the talus edge, and from Figure 23 the probability of exceeding this outlier distance is 1 - 0.1 = 0.9. From Table 6, the annualized frequency of outlier boulders entering the El Capitan study region, per unit width along the talus edge (width is measured along the talus edge), is 9.24×10^{-7} boulders/yr/m. Hence, the annualized frequency of an outlier boulder striking the El Capitan restroom structure, per unit width, is ($[9.24 \times 10^{-7}] \times 0.9$) = 8.32×10^{-7} boulders/year/m. This is approximately 3.6 times larger than the corresponding annualized frequency of outlying boulders traveling beyond the hazard line, namely ([1/581 boulders/yr]/7,412 m) = 2.32×10^{-7} boulders/year/m. Note that this ratio can be thought of as a hazard multiplier that depends on the distance of the structure from the hazard line; the farther inboard of the hazard line, or the closer to the talus edge from the outside, the larger the multiplier. How much larger depends on the probability distribution of observed outlying boulder distances at each study region (e.g., Figure 23 for the El Capitan study region).

5.2 Expected number of people in each structure

As described in Section 3.4, we obtained data on (or, in some cases, estimated) the typical number of occupants in each structure or other facility (e.g., maximum two people for the El Capitan restroom structure), and on the number of hours per year the structure is occupied (e.g., 3.3 hours per day in May through October = 607 hours for the El Capitan restroom structure). By multiplying the number of occupants by the occupancy rate (i.e., fraction of year), we calculated the expected number of people in each structure at any given moment in time, e.g., (2 people x 607 hours)/(24 hours/days)/(365 days/year) = 0.14 people/year for the El Capitan restroom structure. This yields a measure of the human exposure to rock-fall hazard in each structure.

5.3 Risk metric for each structure

By multiplying the annualized frequency of outlier boulders striking each structure (e.g., 8.32×10^{-7} boulders/year/m for the El Capitan study region from Section 5.1) by the annualized expected number of people in it (e.g., 0.14 people/year for the El Capitan study region restroom structure from Section 5.2), we calculated the annualized expected number of people struck by a boulder in the structure, which we refer to as the risk metric after normalization by the annualized frequency of outlying boulders traveling beyond the hazard line (2.32×10^{-7} boulders/year/m). Calculated risk metrics range from 0.1 to 32.6. Maps of the inventory of buildings or other facilities color-coded by their risk metrics are shown in Figures 45-51.

Although we purposefully focus here on the structures and similar facilities that are presently occupied, we also calculated risk metrics for structures in Curry Village that were closed in November of 2008 following the October 2008 Glacier Point rock falls (Stock et al., 2011). Figure 52 shows sorted risk metrics for all structures within the hazard zone, including both presently open structures (black dots) and those that were permanently closed in 2008 (red dots). This figure shows that the highest risk metrics calculated for all structures within the hazard zone in Yosemite Valley are associate with those structures in Curry Village that were closed in 2008; closure of those structures in 2008 reduced the overall risk to structures in Yosemite Valley from rock falls by at least 87% (Table 8). This finding demonstrates the significant risk reduction associated with that management action, and shows consistency between the present risk assessment and past management actions designed to reduce rock-fall related risk.

The focus in this report on those structures that are presently open provides a risk-based means of evaluating infrastructure within the hazard zone (Figure 53; Table 8). Following the 2008 closures, the remaining rock-fall related risk associated with structures in Yosemite Valley is highest in the Curry Village (40.7% of the total remaining risk), Camp 4 (26.9%), and the Curry Village Residential Area (20.6%) study regions (Table 8). Lower amounts of risk are associated with structures in the LeConte-Housekeeping Camp (5.8%), Sunnyside Bench (3.2%), Castle Cliffs (1.7%), Wahhoga (1.0%), and El Capitan (0.1%) study regions (Table 8).

The quantitative risk information presented here can assist the National Park Service in prioritizing future planning and mitigation actions to further reduce rock-fall related risk. If it is determined that some existing infrastructure must remain within the hazard zone defined by this report, or that new infrastructure must be placed within the hazard zone, additional investigations will likely be required to evaluate the site-specific geological hazard and related risk.

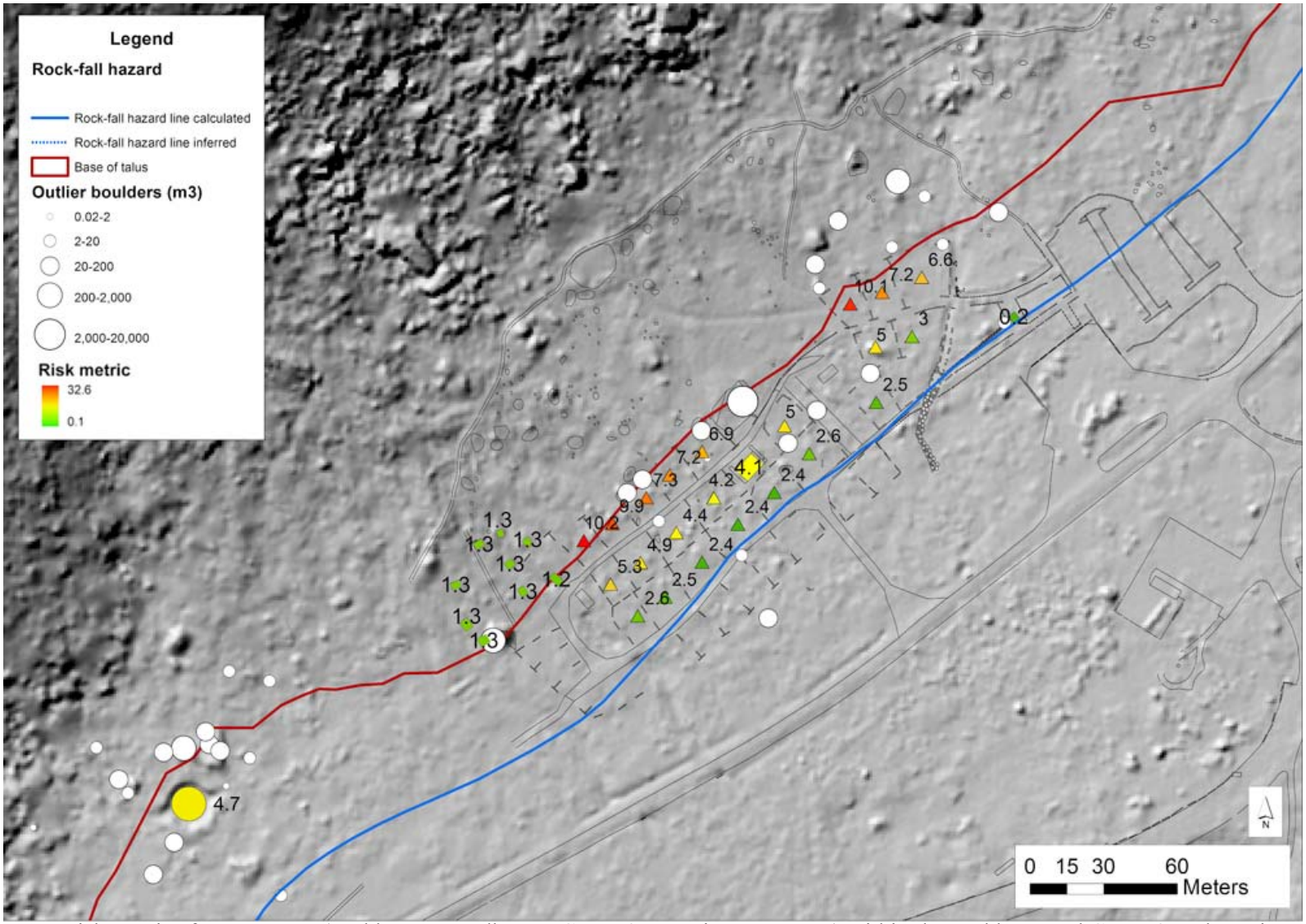

Figure 45. Risk metrics for structures (Wahhoga Roundhouse, Camp 4 campsites, restroom) within the Wahhoga and Camp 4 study regions.

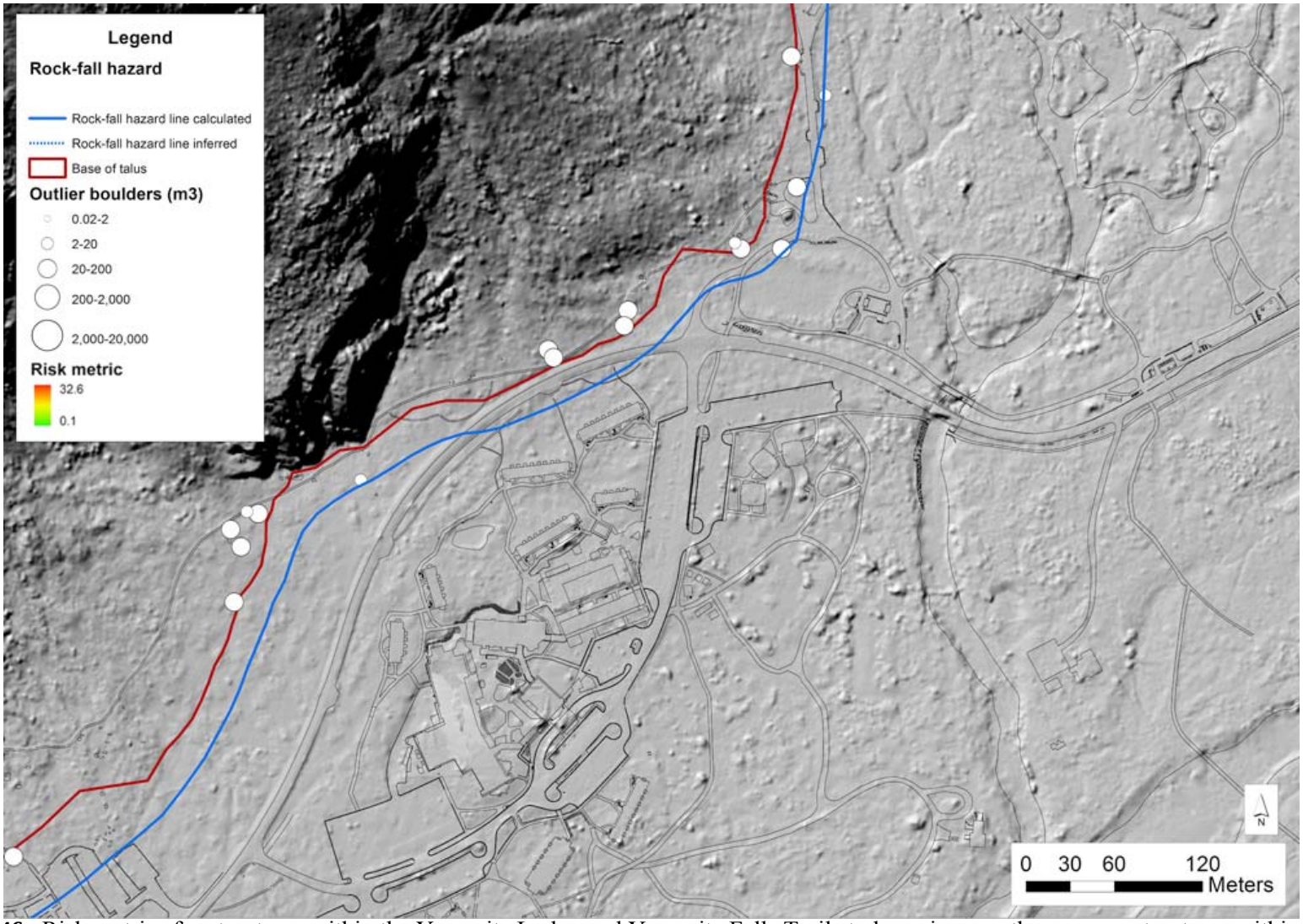

Figure 46. Risk metrics for structures within the Yosemite Lodge and Yosemite Falls Trail study regions; as there are no structures within these study regions, there are no calculated risk metrics.

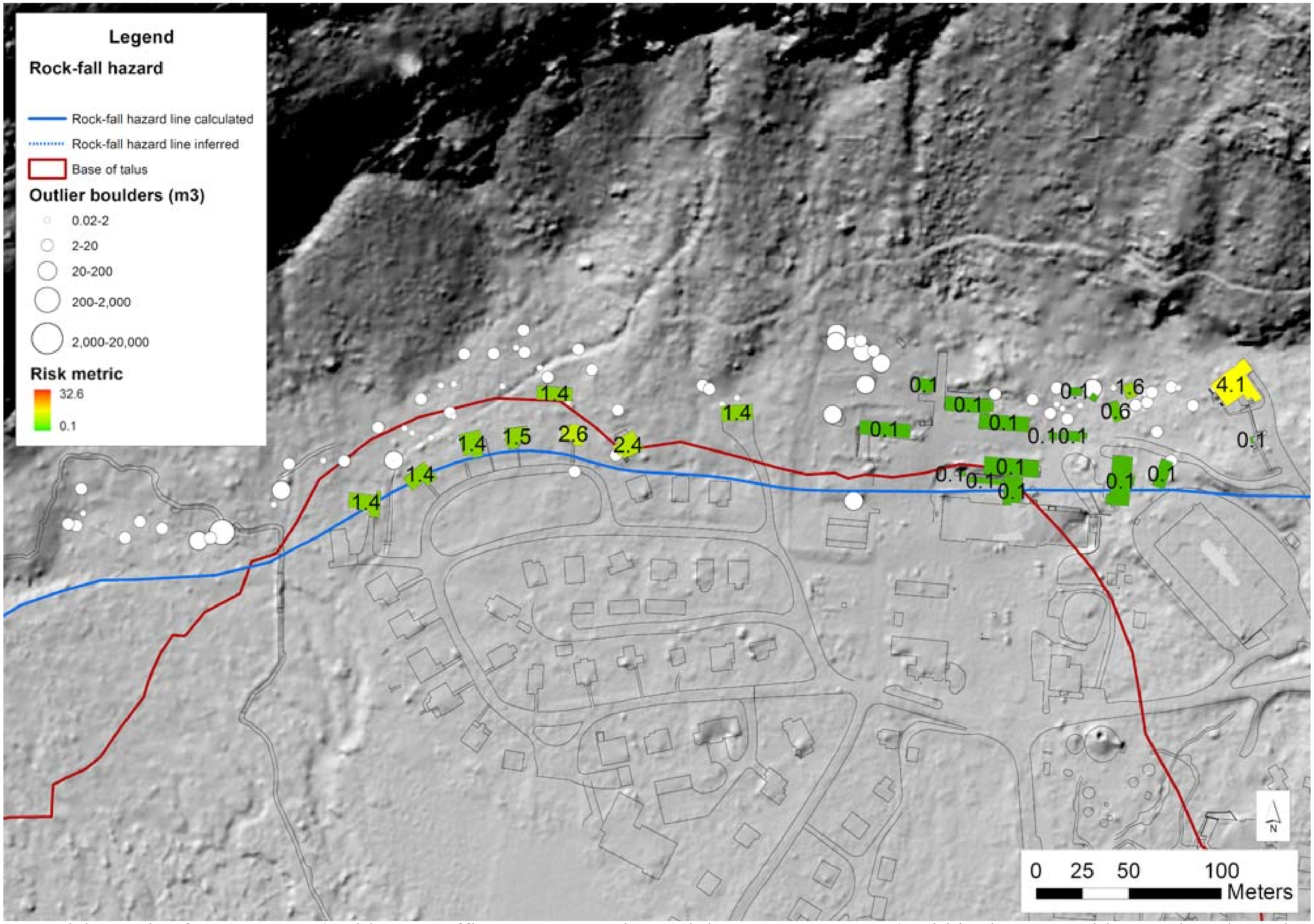

Figure 47. Risk metrics for structures (residences, offices, storage units, and the US Court House) within the Sunnyside Bench and Castle Cliffs study regions.

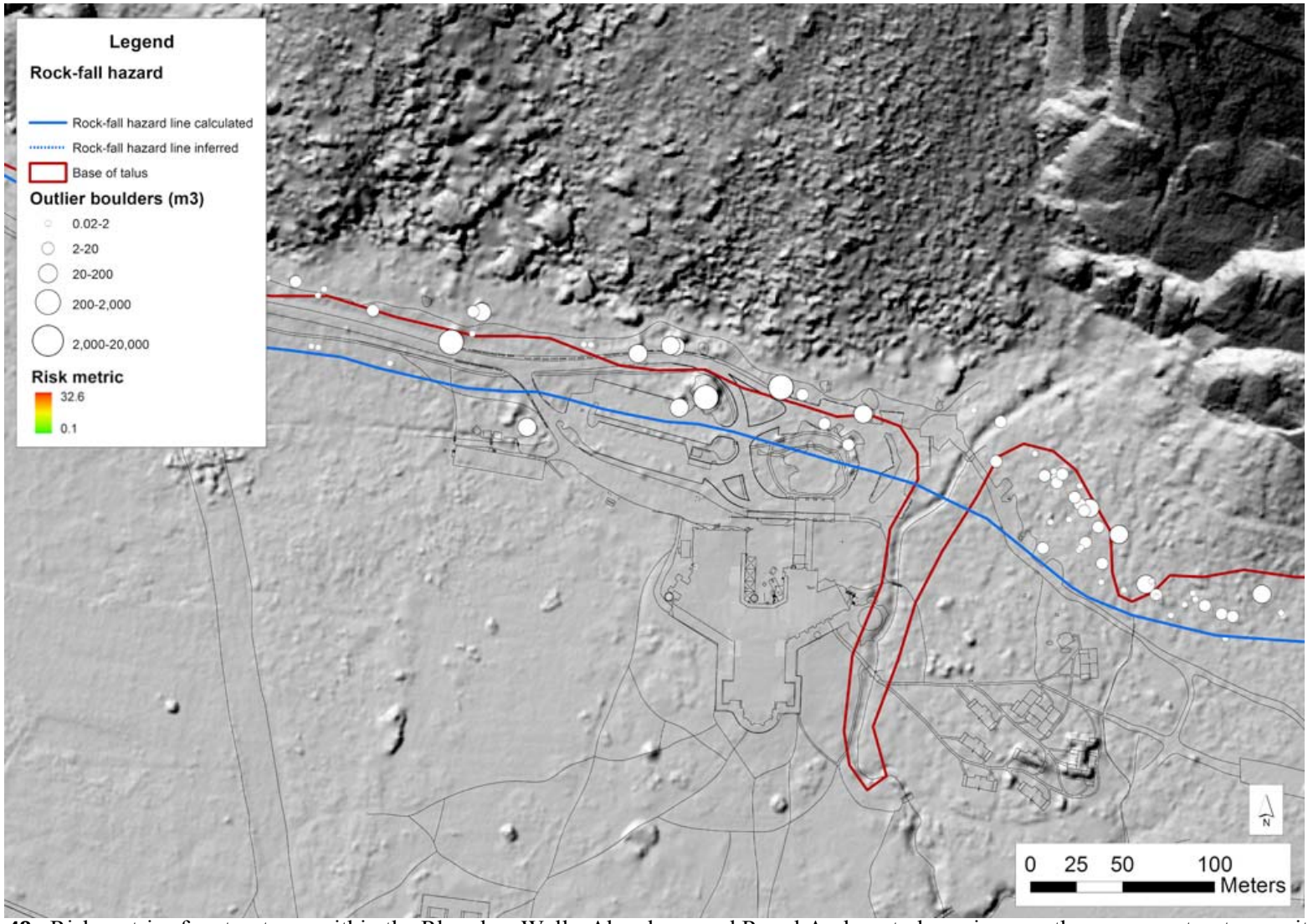

Figure 48. Risk metrics for structures within the Rhombus Wall - Ahwahnee and Royal Arches study regions; as there are no structures within these study regions, there are no calculated risk metrics.

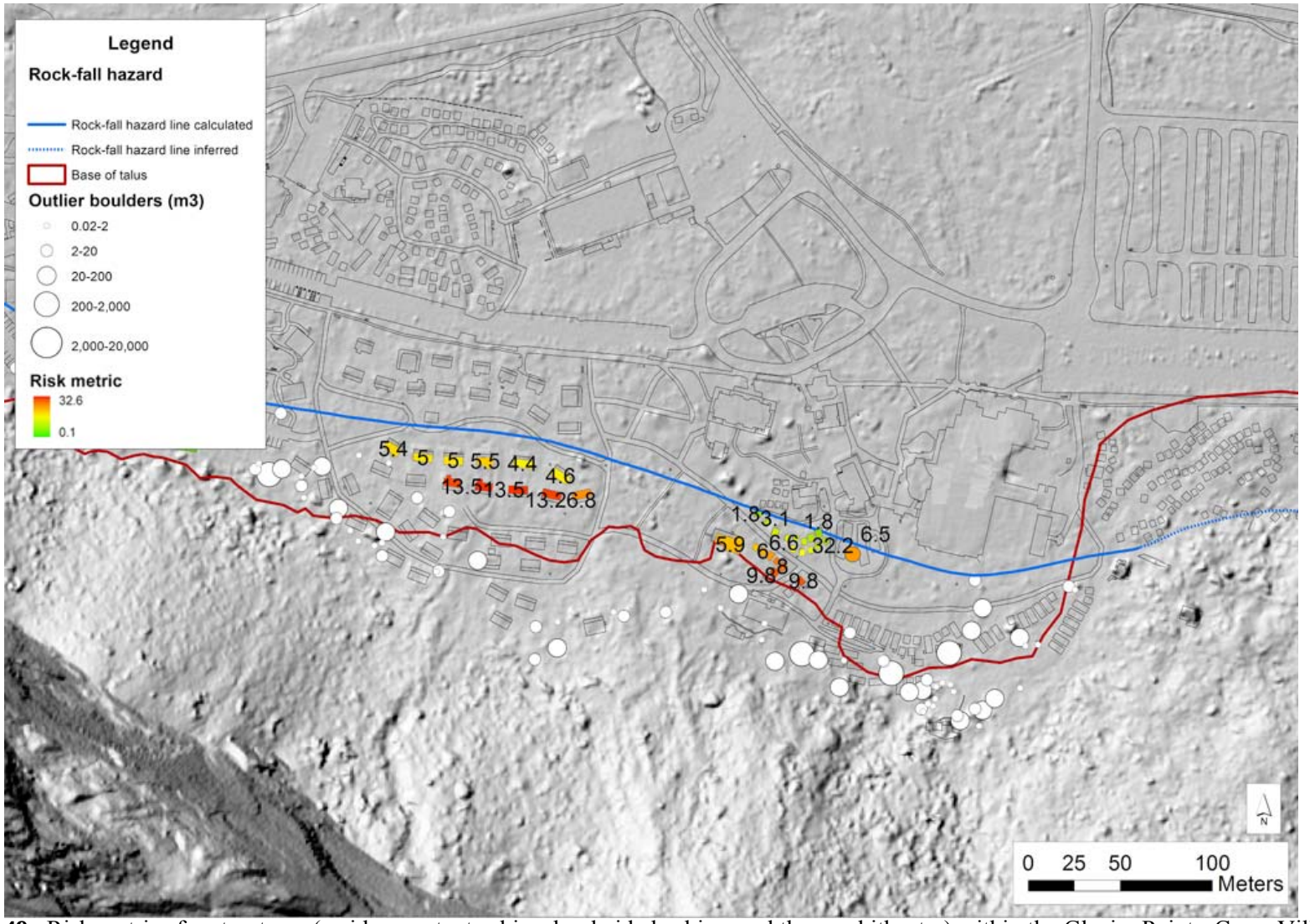

Figure 49. Risk metrics for structures (residences, tent cabins, hard-sided cabins, and the amphitheater) within the Glacier Point - Curry Village study region. Buildings within the hazard line with no reported risk metrics were permanently closed in 2008 following Glacier Point rock falls.

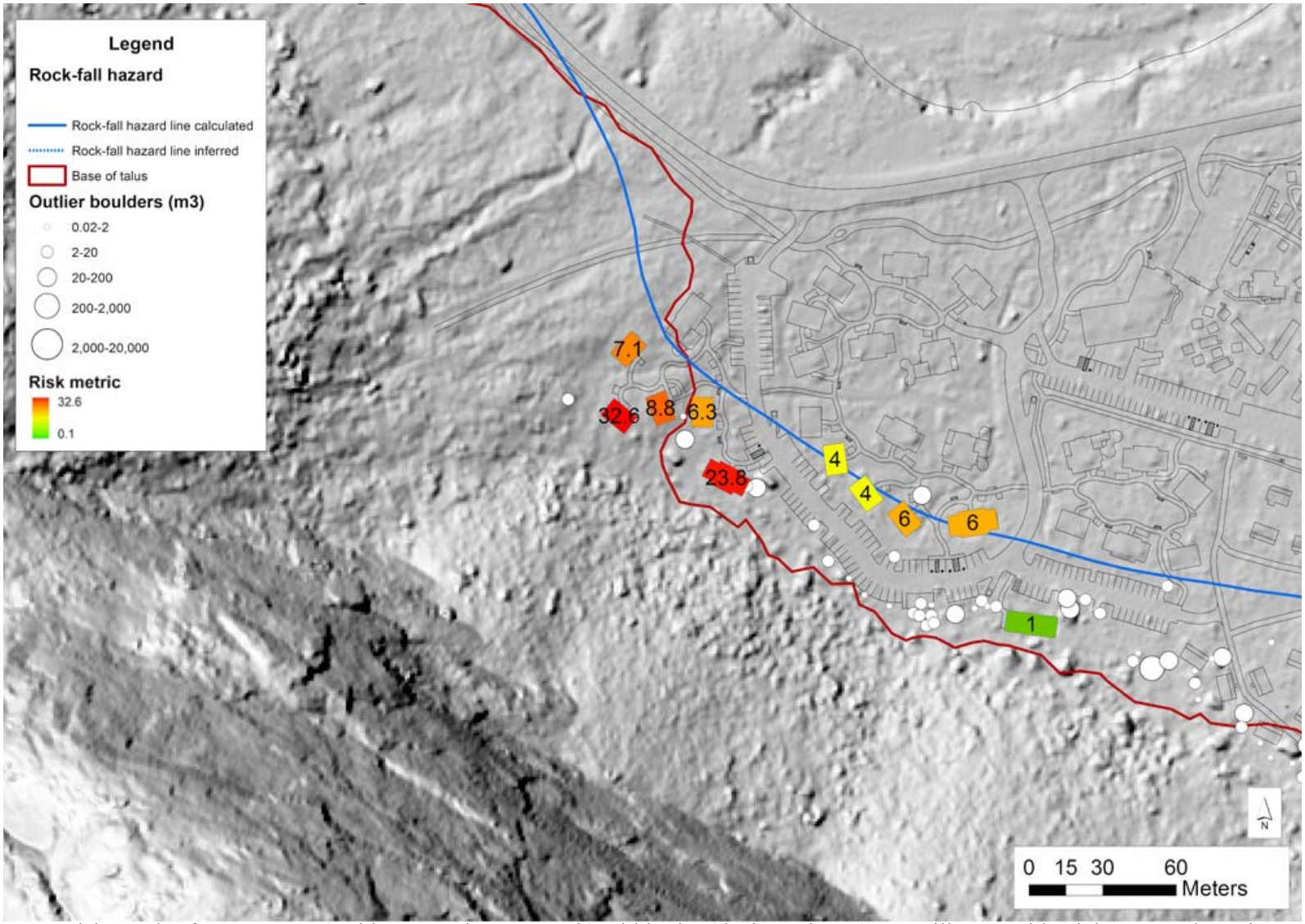

Figure 50. Risk metrics for structures (residences and storage unit) within the Glacier Point - Curry Village Residential Area study region.

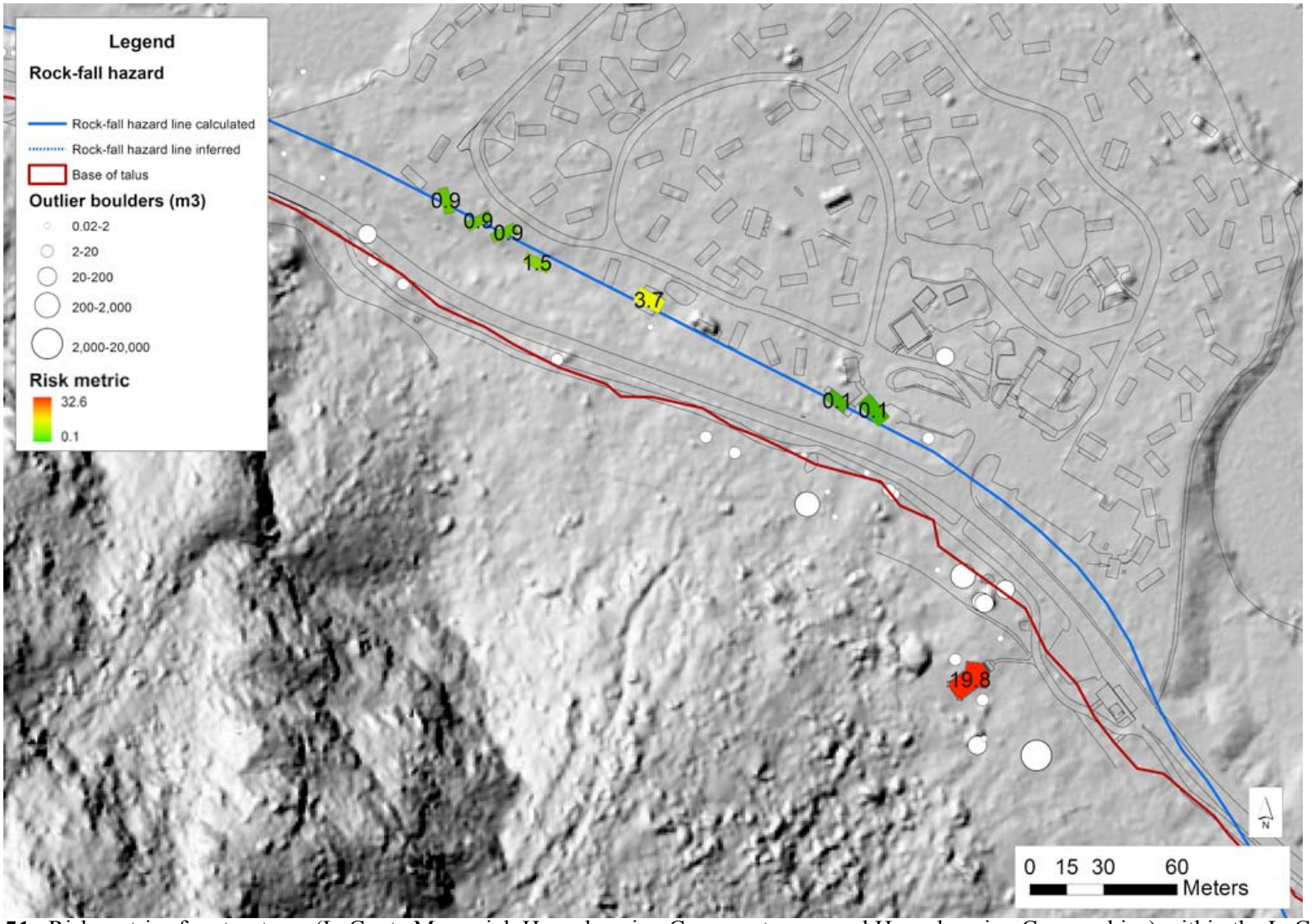

Figure 51. Risk metrics for structures (LeConte Memorial, Housekeeping Camp restroom, and Housekeeping Camp cabins) within the LeConte - Housekeeping Camp study region.

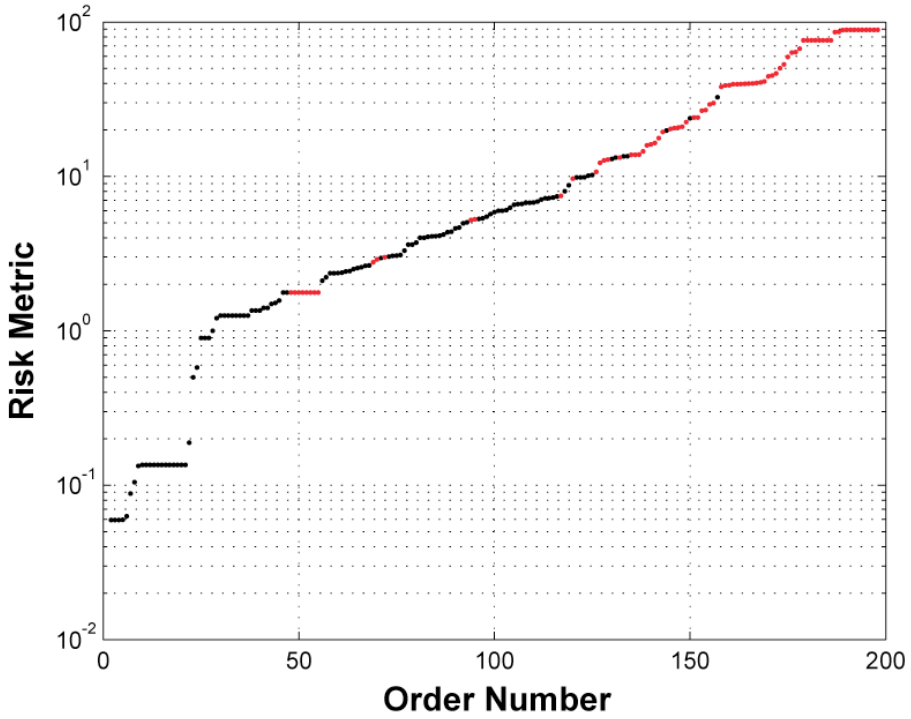

Figure 52. All structures within the rock-fall hazard line in Yosemite Valley ordered according to their risk metric. Buildings in Curry Village that were permanently closed following the 2008 Glacier Point rock fall are shown in red.

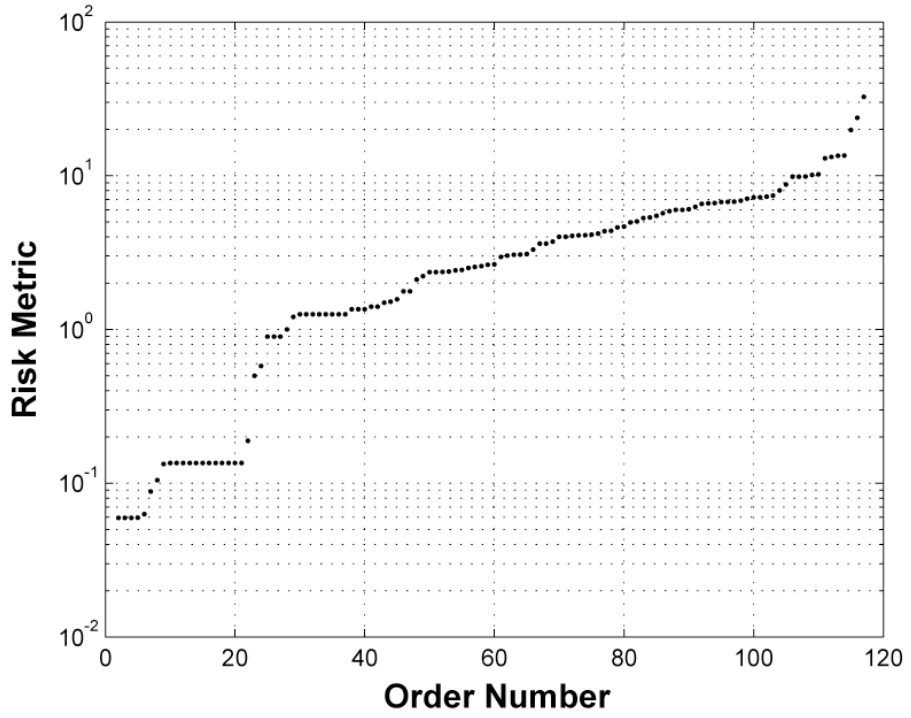

Figure 53. Open structures within the rock-fall hazard line in Yosemite Valley ordered according to their risk metric.

Table 8. Aggregated risk metrics and percent-of-total-risk for structures pre- and post-2008 closures located within Yosemite Valley study regions

Study region	Aggregated risk metric (pre-2008 closure)	Percent of total risk (pre-2008 closure) (%)	Aggregated risk metric (post-2008 closure)	Percent of total risk (post-2008 closure) (%)
El Capitan	0.5	0.01	0.5	0.1
Three Brothers	0	0	0	0
Wahhoga	4.7	0.1	4.7	1.0
Camp 4	130.4	3.3	130.4	26.9
Yosemite Lodge	0	0	0	0
Yosemite Falls Trail	0	0	0	0
Sunnyside Bench	15.5	0.4	15.5	3.2
Castle Cliffs	8.3	0.2	8.3	1.7
Church Bowl	0	0	0	0
Rhombus Wall - Ahwahnee	0	0	0	0
Royal Arches	0	0	0	0
Glacier Point - Curry Village	3589.5	92.9	197.1	40.7
Glacier Point - Curry Village Residential Area	99.5	2.5	99.5	20.6
LeConte - Housekeeping Camp	27.8	0.7	27.8	5.8
Chapel Wall	0	0	0	0
Cathedral Rocks	0	0	0	0
Total	**3864.8**	**100**	**483.7**	**100**

6.0 Conclusions

Rock falls are common in Yosemite Valley, California, posing substantial hazard and risk to the approximately four million people that visit Yosemite National Park each year. The assessment presented here, building upon previous work by the U.S. Geological Survey, focuses on hazard and risk in developed regions in Yosemite Valley posed by individual fragmental rock falls up to approximately 100,000 m^3 in volume. Previous hazard assessments identified two primary hazard zones in Yosemite Valley defined by: (1) a line delineating the base of talus and other slope movement debris, and (2) a line delineating the shadow angle limit (Wieczorek et al., 1998, 1999). The hazard line presented here is based on observable, measurable evidence of previous rock falls in the form of the spatial distribution of outlying boulders, but also incorporates additional data on the frequency of occurrence of outlying boulder deposition, and simulated trajectories of potential future rock falls from computer modeling.

We initially define a new rock-fall hazard zone using the distribution of "outlying" boulders beyond the base of talus slopes. We used a statistical approach to define outlying boulder distances beyond the base of talus that encompass 90% of the outlying boulders in each region. 90^{th}-percentile distances for the study regions range from 7 to 57 m beyond the mapped base of talus slopes. This zone defines a probability of outlying boulder deposition, with a 90% probability that boulders resulting from future fragmental rock falls will be deposited within this zone, and a 10% probability that boulders will be deposited beyond this zone. The 90^{th}-percentile distances are subsequently scaled by frequency-related factors to account for the frequency of outlying boulder deposition in each study region.

Cosmogenic beryllium-10 exposure dating of outlying boulders indicates that outlying boulders tend to result from numerous individual events through time rather than a single event. The oldest boulder exposure ages approach the timing of deglaciation for Yosemite Valley (~15,000-17,000 years), suggesting that 15,000 years is a reasonable time period for the accumulation of outlying boulders for each study region. We calculate annualized frequency of outlying boulders for each study region, and for the union of all of the study regions, by dividing the corresponding number of outlying boulders by 15,000 years.

To evaluate outlying boulder deposition from potential future rock falls, we utilized STONE, a three-dimensional computer program that simulates rock-fall runout, in a relative sense. We performed rock-fall trajectory modeling in which rock falls were simulated from every slope ≥60° in Yosemite Valley. We calculated the total number of simulated trajectories into each study region as a function of the total number of simulated trajectories across all study regions and compared these with the corresponding number of actual mapped outlying boulders in each study region. Based on this comparison, we used the STONE trajectories to apportion the total (across all study regions) annualized frequency of outlying boulders to the individual study regions.

We used the average of the annualized frequencies from the STONE simulations, each normalized by the width of the respective study region, and the frequencies based on the observed outlying boulders, to adjust the 90^{th}-percentile distance line inward or outward. The adjusted hazard line is such that the average recurrence interval of outlying boulders beyond the line is projected to be approximately 500 years, an interval commonly used for assessing other natural hazards (e.g., earthquakes and floods). Assuming steady deposition through time, this translates to 0.2% probability of outlying boulder deposition beyond the hazard line in a given year, or an approximately 10% probability of this occurring in 50 years.

With the hazard zone defined, we investigated the risk of people being struck by boulders within the zone, focusing on buildings and other structures such as campsites and amphitheaters where people congregate. First, we quantified the human exposure to rock-fall hazard in each building or other structure in terms of an expected number of people in each structure at any given moment in time when a rock fall could occur. This was calculated by multiplying the typical number of occupants in each structure by its occupancy rate (i.e., the fraction of year that the structure is occupied).

We assumed that all structures in the study regions are equally vulnerable to penetration by rock-fall boulders. A risk metric for each structure that is proportional to an annualized expected number of people struck by outlying boulders was then calculated, as the product of an annualized frequency of an outlying boulder striking the structure and the expected number of people in it. Calculated risk metrics range from 0.06 to 32.56. Finally, we sorted structures according to their risk metric. The sorted list will assist the NPS in evaluating infrastructure within the hazard line and in prioritizing management actions to reduce risk.

This hazard line encompasses zones of relatively frequent (<1/500 annualized exceedance) talus and outlying boulder deposition for fragmental rock falls in Yosemite Valley; based on the extents of historic rock falls, this approximately corresponds to rock falls up to about 100,000 m^3 in volume. It does not include potential deposition zones of infrequent extremely large rock falls (>100,000 m^3) or airblasts produced by rock-fall impacts, due to their low inferred frequencies. As previously stated by Wieczorek et al. (1998), because of the configuration of the steep, tall (~ 1 km) valley walls and the relatively narrow (~1 km) valley, there are no absolutely safe or zero probability regions for extremely large rock falls within Yosemite Valley. This hazard also does not explicitly account for flyrock, rock "shrapnel" produced by impacts on talus slopes (Wieczorek and Snyder, 1999), because of uncertainty in modeling these type of behavior; however, based on flyrock distributions resulting from recent rock falls, the hazard zone identified here is likely to encompass most flyrock deposition for typical fragmental-type rock falls in Yosemite Valley. If rock-fall frequencies and/or magnitudes change through time due to changing geological and/or environmental conditions, or due to improved understanding of those conditions, then the rock-fall hazard line presented here should be re-evaluated.

Acknowledgements

David Santaniello (GeoCorps America) assisted with field mapping of outlying boulders, calculating shadow angles, and collecting samples for cosmogenic ^{10}Be exposure dating. Tina Marstellar (Georgia Institute of Technology) performed the chemical preparation of cosmogenic ^{10}Be, and Dr. Dylan Rood (Lawrence Livermore National Laboratories) measured ^{10}Be/^{9}Be ratios, from which ^{10}Be concentrations were derived. Greg Smoczyk (U.S. Geological Survey) assisted with ArcGIS analyses of infrastructure within the hazard zone. Dr. Dave Perkins (U.S. Geological Survey) assisted with the statistical analyses of outlying boulder distances and recurrence intervals.

Dr. Jonathan Godt (U.S. Geological Survey), Sandra Melzner (Geological Survey of Austria), Michael Moelk (Austrian Service for Torrent and Avalanche Control), and Dr. Robert Wesson (U.S. Geological Survey) provided helpful internal reviews. Dr. John Clague (Simon Fraser University), Dr. Fausto Guzzetti (CNR-IRPI), and Dr. Oldrich Hungr (University of British Columbia) provided constructive external reviews that greatly improved the final report. Dr. Jan van Wagtendonk (U.S. Geological Survey, emeritus) facilitated the external review process.

References

Agliardi, F., and Crosta, G.B., 2003, High resolution three-dimensional numerical modeling of rockfalls: International Journal of Rock Mechanics and Mineral Science, v. 40, p. 455-471.

Balco, G., Stone, J.O, Lifton, N.A., and Dunai, T.J., 2008, A complete and easily accessible means of calculating surface exposure ages or erosion rates from ^{10}Be and ^{26}Al measurements: Quaternary Geochronology, v. 3, p. 174-195, doi: 10.1016/j.quageo.2007.12.001.

Ballantyne, C.K., and Stone, J.O., 2004, The Beinn Alligin rock avalanche, NW Scotland: Cosmogenic ^{10}Be dating, interpretation and significance, The Holocene, v. 14, p. 448-453.

Bateman, P.C., 1992, Plutonism in the central part of the Sierra Nevada Batholith, California: U.S. Geological Survey Professional Paper 1483, 186 p.

Bertolo, P., and Wieczorek, G.F., 2005, Calibration of numerical models for small debris flows in Yosemite Valley, California, USA: Natural Hazards and Earth System Sciences, v. 5, p. 993-1001.

Bull, W.B., 2004, Sierra Nevada earthquake history from lichen on rockfall blocks: Sierra Nature Notes, v. 4, p. 8-21.

Bull, W.B., King, J., Kong, F., Moutoux, T., and Phillips, W.M., 1994, Lichen dating of coseismic landslide hazards in alpine mountains: Geomorphology, v. 10, p. 253-264.

Bunce, C.M., Cruden, D.M., and Morgenstern, N.R., 1997, Assessment of the hazard from rockfall on a highway: Canadian Geotechnical Journal, v. 34, p. 344-356.

Bursik, M.I., and Gillespie, A.R., 1993, Late Pleistocene glaciation of Mono Basin, California: Quaternary Research, v. 39, p. 24-35.

Calkins, F.C., Huber, N.K., and Roller, J.A., 1985, Geologic bedrock map of Yosemite Valley, Yosemite National Park, California: U.S. Geological Survey Map I-1639.

Chau, K.T., Wong, R.H.C., Liu, J., and Lee, C.F., 2003, Rockfall hazard analysis for Hong Kong based on rockfall inventory: Rock Mechanics and Rock Engineering, v. 36, p. 383-408.

Chau, K.T., Wong, R.H.C., and Wu, J.J., 2002, Coefficient of restitution and rotational motions of rockfall impacts: International Journal of Rock Mechanics and Mineral Sciences, v. 39, p. 69-77.

Clague, J.J., 2010, Dating landslides with trees, *in* Stoffel, M., Bollschweiler, M., Butler, D.R.., and Luckman, B.H., eds, Tree Rings and Natural Hazards: A State-of-the-Art: Advances in Global Change Research, v. 41, Springer, p. 81-89.

Code of Federal Regulations (CFR), 2010, Federal Emergency Management Agency, DHS, 44 CFR 9.4, p. 70.

Coe, J.A., Harp, E.L., Tarr, A.C., and Michael, J.A., 2005, Rock-Fall Hazard Assessment of Little Mill Campground, American Fork Canyon, Uinta National Forest, Utah: U.S Geological Survey Open-File Report 2005-1229.

Copons, R., and Vilaplana, J.M., 2008, Rockfall susceptibility zoning at a large scale: From geomorphological inventory to preliminary land use planning: Engineering Geology, v. 102, p. 142-151.

Corominas, J., 1996, The angle of reach as a mobility index for small and large landslides: Canadian Geotechnical Journal, v. 33, p. 260-271.

Corominas, J., and Moya, J., 2008, A review of assessing landslide frequency for hazard zoning purposes: Engineering Geology, v. 102, p. 193-213.

Crosta, G.B., and Agliardi, F., 2003, A methodology for physically based rockfall hazard assessment: Natural Hazards and Earth System Sciences, v. 3, p. 407-422.

Dai, F.C., Lee, C.F., and Ngai, Y.Y., 2002, Landslide risk assessment and management: an overview: Engineering Geology, v. 64, p. 65-87.

Davies, M.C.R., Hamza, O., and Harris, C., 2001, The effect of rise in mean annual temperature on the stability of rock slopes containing ice-filled discontinuities: Permafrost and Periglacial Processes, v. 12, p. 137-144.

Derron, M.H., Blikra, L.H., and Jaboyedoff, M., 2005, Preliminary assessment of landslide and rockfall hazards using a DEM (Oppstadhornet, Norway): Natural Hazards and Earth System Sciences, v. 5, p. 285-292, www.nat-hazards-earth-syst-sci.net/5/285/2005/.

Dorren, L.K.A., 2003, A review of rockfall mechanics and modeling approaches: Progress in Physical Geography, v. 27, p. 69-87.

Dorren, L.K.A., 2012, Rockyfor3D (v.5.0) revealed – Transparent description of the complete 3D rockfall model: ecorisQ paper, www.ecorisq.org, 30 p.

Dorren, L.K.A., Seijmonsbergen, A., 2003, Comparison of three GIS-based models for predicting rockfall runout zones at a regional scale: Geomorphology, v. 56, p. 49-64.

Dorren, L.K.A., Maier, B., Putters, U.S., and Seijmonsbergen, A.C., 2004, Combining field and modeling techniques to assess rockfall dynamics on a protection forest hillslope in the European Alps: Geomorphology, v. 57, p. 151-167.

Dorren, L.K.A., Berger, F., and Putters, U.S., 2006, Real size experiments and 3D simulation of rockfall on forested and non-forested slopes: Natural Hazards and Earth System Sciences, v. 6, p. 145-153.

Dussauge-Peisser, C., Helmstetter, A., Grasso, J.-R., Hantz, D., Desvarreaux, P., Jeannin, M., and Giraud, A., 2002, Probabilistic approach to rock fall hazard assessment: potential of historical data analysis: Natural Hazards and Earth System Sciences, v. 2, p. 15-26.

Dussauge, C., Grasso, J.-R., and Helmstetter, A., 2003, Statistical analysis of rockfall volume distributions: Implications for rockfall dynamics: Journal of Geophysical Research, v. 108, 2286, doi: 10.1029/2001JB000650.

Evans, S.G., and Hungr O., 1993, The assessment of rockfall hazard at the base of talus slopes, Canadian Geotechnical Journal, v. 30, p. 620-636.

Fell, R., 1994, Landslide risk assessment and acceptable risk: Canadian Geotechnical Journal, v. 31, p. 261-272.

Fell, R., Corominas, J., Bonnard, C., Cascini L., Leroi, E., and Savage, W.Z., 2008, Guidelines for landslide susceptibility, hazard and risk zoning for land use planning: Engineering Geology, v. 102, p. 85-98.

Frattini, P., Crosta, G., Carrara, A., and Agliardi, F., 2008, Assessment of rockfall susceptibility by integrating statistical and physically-based approaches: Geomorphology, v. 94, p. 419-437.

Gardner, J.S., 1983, Rockfall frequency and distribution in the Highwood Pass area, Canadian Rocky Mountains: Zeitschrift für Geomorphologie, v. 27, p. 311-324.

Giardini, D., Grünthal, G., Shedlock, K.M., and Zhang, P., 1999, The GSHAP global seismic hazard map: Annali di Geofisica, v. 42, p. 1225-1230.

Gosse, J.C., and Phillips, F.M., 2001, Terrestrial in situ cosmogenic nuclides: Theory and application: Quaternary Science Reviews, v. 20, p. 1475-1560.

Guzzetti, F., Crosta, G., Detti, R., and Agliardi, F., 2002, STONE: A computer program for the three-dimensional simulation of rock-falls: Computers and Geoscience, v. 28, p. 1079-1093.

Guzzetti, F., Reichenbach, P., Wieczorek, G.F., 2003, Rockfall hazard and risk assessment in the Yosemite Valley, California, USA: Natural Hazards and Earth System, Sciences, v. 3, p. 491-503, www.nat-hazards-earth-syst-sci.net/3/491/2003/

Guzzetti, F., Reichenbach, P., and Ghigi, S., 2004, Rockfall hazard and risk assessment along a transportation corridor in the Nera Valley, Central Italy: Environmental Management, v. 34, p. 191-208, doi: 10.1007/s00267-003-0021-6.

Harp, E.L., and Wilson, R.C., 1995, Shaking intensity thresholds for rock falls and slides: Evidence from 1987 Whittier Narrows and Superstition Hills earthquake strong motion records: Bulletin of the Seismological Society of America, v. 85, p. 1739-1757.

Harp, E.L., Dart, R.L., and Reichenbach, P. 2010, Rock fall simulation at Timpanogos Cave National Monument, American Fork Canyon, Utah, USA: Landslides, doi: 10.1007/s10346-010-0251-7.

Heim, A., 1932, Bergsturtz und Menschenleben: Fretz und Wasmuth, Zurich, 218 pp.
Heisinger, B., Lal, D., Jull, A.J.T., Kubik, P., Ivy-Ochs, S., Neumaier, S., Kniew K., Lazarev, V., and Nolte, E., 2002a, Production of selected cosmogenic radionuclides by muons: 1. Fast muons: Earth and Planetary Science Letters, v. 200, p. 345-355.
Heisinger, B., Lal, D., Jull, A.J.T., Kubik, P. Ivy-Ochs, S., Knie, K., and Nolte, E., 2002b, Production of selected cosmogenic radionulcides by muons: 2. Capture of negative muons: Earth and Planetary Science Letters, v. 200, p. 357-369.
Hsu, K.J., 1975, On sturzstroms – catastrophic debris streams generated by rockfalls: Geological Society of America Bulletin, v. 86, p. 129-140.
Huber, N.K., 1987, The Geologic Story of Yosemite National Park: U.S. Geological Survey Bulletin 1595.
Huber, N.K., Phillips, W.M., and Bull, W.B., 2007, The Slide, *in* Huber, N.K., Geological Ramblings in Yosemite, Heyday Books, Berkeley, California, p. 115-121.
Hungr, O., Evans, S.G., Hazzard, J., 1999, Magnitude and frequency of rock falls along the main transportation corridors of southwestern British Columbia: Canadian Geotechnical Journal, v. 36, p. 224-238.
Ivy-Ochs, S., Poschinger, A.V., Synal, H.-A., and Maisch, M., 2009, Surface exposure dating of the Flims landslide, Graubünden, Switzerland: Geomorphology, v. 103, p. 104-112, doi: 10.1016;j.geomorph.2007.10.024.
Jaboyedoff, M., and Labiouse, V., 2003, Preliminary assessment of rockfall hazard based on GIS data: ISRM 2003, Technology Roadmap for Rock Mechanics, South African Institute of Mining and Metallurgy, 2003.
Jaboyedoff, M., Baillifard, F., Couture, R., Locat, J., and Locat, P., 2004, New insight of geomorphology and landslide prone area detection using DEMs, in Landslides Evaluation and Stabilization, Lacerda, W.A., Ehrlich, M., Fontoura, A.B., and Sayo, A., eds., Balkema, 199-205.
Jones, C.L., Higgins, J.D., and Andrew, R.D., 2000, Colorado rockfall simulation program, version 4.0: Colorado Department of Transportation, Denver, Colorado, 127 p.
Katz, O., Reichenbach, P., and Guzzetti, F., 2010, Rock fall hazard along the railway corridor to Jerusalem, Israel, in the Soreq and Refaim valleys: Natural Hazards, v. 56, p. 649-665.
Keefer, D.K., 1984, Landslides caused by earthquakes: Geological Society of America Bulletin v. 95, p. 406-421.
Kohl, C.P., and Nishiizumi, K., 1992, Chemical isolation of quartz for measurement of in-situ-produced cosmogenic nuclides: Geochimica et Cosmochimica Acta, v. 56, p. 3583-3587.
Lal, D., 1991, Cosmic ray labeling of erosion surfaces: In situ nuclide production rates and erosion models: Earth and Planetary Science Letters, v. 104, p. 424-439.
Lan, H., Martin, C.D., and Lim, C.H., 2007, RockFall analyst: A GIS extension for three-dimensional and spatially distributed rockfall hazard modeling: Computers and Geosciences, v. 33, p. 262-279.
Lan, H., and Martin, D.C., Zhou, C., and Lim, C.H., 2010, Rockfall hazard analysis using LiDAR and spatial modeling: Geomorphology, v. 118, p. 213-223.
LeConte, J.N., 1875, A Journal of Ramblings through the High Sierras of California: Francis & Valentine, San Francisco, California, 103 p.
Loye, A., Jaboyedoff, M., and Pedrazzini, A., 2009, Identification of potential rockfall source areas at a regional scale using a DEM-based geomorphometric analysis: Natural Hazards and Earth System Sciences, v. 9, p. 1643-1653, www.nat-hazards-earth-syst-sci.net/9/1643/2009/.
Luckman, B.H., and Fiske, C.J., 1995, Estimating long-term rockfall accretion rates by lichenometry, in Slaymaker, O., (ed), Steepland Geomorphology, Wiley, Chichester, pp. 233-255.

Lundström, T., Johsson, M.J., Volkwien, A., and Stoffel, M., 2009, Reactions and energy absorption of trees subject to rockfall: A detailed assessment using a new experimental method: Tree Physiology, v. 29, p. 345-359.

Matasci, B., Carrea, D., Jaboyedoff, M., Pedrazzini, A., Stock, G.M., and Oppikofer, T., 2011, Structural characterization of rockfall sources in Yosemite Valley from remote sensing data and field surveys: Proceedings of the 2011 Pan-Am Canadian Geological Survey Geotechnical Conference, Toronto, Ontario, Canada.

Matsuoka N., and Sakai, H., 1999, Rockfall activity from an alpine cliff during thawing periods: Geomorphology v. 28, p. 309-328.

Matthes, F.E., 1930, Geologic history of the Yosemite Valley: U.S. Geological history of the Yosemite Valley, U.S. Geological Professional Paper 504.

McCarroll, D., Shakesby, R.A., and Matthews, J.S., 1998, Spatial and temporal patterns of late Holocene rockfall activity on a Norwegian talus slope: lichenometry and simulation-modelling approach: Artic and Alpine Research, v. 30, p. 51-60.

Morrissey, M.M., Savage, W.Z., and Wieczorek, G.F., 1999, Air blasts generated by rockfall impacts: Analysis of the 1996 Happy Isles event in Yosemite National Park: Journal of Geophysical Research, v. 104, B10, p. 23,189-23,198.

Muir, J., 1912, The Yosemite: Century Company, 284 pp. (Reprinted 1962, Garden City, New York, Anchor Books, Doubleday & Company, Inc., 225 p.)

National Park Service, 2006, Management Policies 2006, U.S. Department of the Interior, 168 p., www.nps.gov/policy/mp2006.pdf

Nicoletti, P.G., and Sorriso-Valvo, M., 1991, Geomorphic controls on the shape and mobility of rock avalanches: Geological Society of America Bulletin, v. 103, p. 1365-1373.

Nishiizumi, K., Imamura, M., Caffee, M.W., Southon, J.R., Finkel, R.C., and McAninch, J., 2007, Absolute calibration of ^{10}Be AMS standards: Nuclear Instrumentation and Methods in Physics Research B, v. 258, p. 403-413, doi: 10.1016/j.nimb.2007.01.297

Phillips, F. M., Zreda, M., Plummer, M. A., Elmore, D., Clark, D. H., 2009, Glacial geology and chronology of Bishop Creek and vicinity, eastern Sierra Nevada, California: Geological Society of America Bulletin, v. 121, p. 1013-1033, doi: 10.1130/B26271.1.

Ruff, M., and Czurda, K., 2008, Landslide susceptibility analysis with a heuristic approach in the Eastern Alps (Vorarlberg, Austria): Geomorphology, v. 94, p. 314-324.

Scheidegger, A.E., 1973, On the prediction of the reach and velocity of catastrophic landslides: Rock Mechanics, v. 5, p. 231-236.

Selby, M.J., 1993, Hillslope Materials and Processes (2nd edition): Oxford University Press, New York, 451 p.

Small, E.E., Anderson, R.S., Repka, J.L., and Finkel, R., 1997, Erosion rates of alpine bedrock summit surfaces deduced from in situ ^{10}Be and ^{26}Al: Earth and Planetary Science Letters, v. 150, p. 413-425.

Smith, D.G, and Anderson, R.S., 1992, Late Wisconsin paleoecologic record from Swamp Lake, Yosemite National Park, California: Quaternary Research, v. 38, p. 91-102.

Stock, G.M., and Uhrhammer, R.A., 2010, Catastrophic rock avalanche 3,600 years B.P. from El Capitan, Yosemite Valley, California: Earth Surface Processes and Landforms, v. 35, p. 941-951.

Stock, G.M., Anderson, R.S., and Finkel, R.C., 2005, Rates of erosion and topographic evolution of the Sierra Nevada, California, inferred from cosmogenic ^{26}Al and ^{10}Be concentrations: Earth Surface Processes and Landforms, v. 30, p. 985-1006.

Stock, G.M., Bawden, G.W., Green, J.K., Hanson, E., Downing, G., Collins, B.D., Bond, S., and Leslar, M., 2011a, High-resolution three-dimensional imaging of rock falls in Yosemite Valley, California, Geosphere, v. 7, p. 573-581.

Stock, G.M., Martel, S.J., Collins, B.D., and Harp, E.L., 2012a, Progressive failure of sheeted rock slopes: The 2009-2010 Rhombus Wall rock falls in Yosemite Valley, California, USA: Earth Surface Processes and Landforms, v. 37, p. 546-561, doi: 10.1002/esp.3192.

Stock, G.M., Collins, B.D., Santaniello, D.J., Zimmer, V.L., Wieczorek, G.F., and Snyder, J.B., 2012b, Historical rock falls in Yosemite National Park (1857-2011): U.S. Geological Survey Open-File Report (in review).

Stoffel, M., Schneuwly, D.M., and Bollschweiler, M., 2010, Assessing rockfall activity in a mountain forest – Implications for hazard assessment, *in* Stoffel, M., Bollschweiler, M., Butler, D.R., and Luckman, B.H., eds, Tree Rings and Natural Hazards: A State-of-the-Art: Advances in Global Change Research, v. 41, Springer, p. 139-155.

Stokes, A., Salin, F., Kokutse, A.D., Berthier, S., Jeannin, H., Mochan, S., Dorren, L., Kokutse, N., Ghani, M.A., and Fourcaud, T., 2005, Mechanical resistance of different tree species to rockfall in the French Alps: Plant and Soil, v. 278, p. 107-117.

Stone, J.O., 2000, Air pressure and cosmogenic isotope production: Journal of Geophysical Research, v. 105, p. 23,753-23,759.

Tagliavini, F., Reichenbach, P., Maragna D., Guzzetti, F., and Pasuto, A., 2009, Comparison of 2-D and 3-D computer models for the M. Salta rock fall, Vajont Valley, northern Italy: Geoinformatica, v. 13, p. 323-337.

U.S. Geological Survey (USGS), 1982, Guidelines for Determining Flood Flow Frequency, Bulletin #17B of the Hydrology Subcommittee, Interacency Dvisory Committee on Water Data, Office of Water Data Coordination, Reston, Virgina, 194 p.

Vargas Jr., E.A., Chavez, E., Gusmão, L., and Amaral, C., 2009, Is thermal fatigue a possible mechanism for failures of some rock slopes in Rio de Janeiro, Brazil? American Rock Mechanics Association, 43rd US Rock Mechanics Symposium and 4th U.S.-Canada Rock Mechanics Symposium, Asheville, NC.

Varnes, D.J., 1978, Slope movement types and processes, *in* Schuster, R.L., and Krizek, R.J., Landslides analysis and control: Washington, D.C., Transportation Research Board, National Academy of Science, Special Report 176, p. 12-33.

Varnes, D.J., 1984, Landslide hazard zonation: A review of principles and practice: Natural Hazards, v. 3, UNESCO, Paris.

Wieczorek, G.F., 2002, Catastrophic rockfalls and rockslides in the Sierra Nevada, USA, *in* Evans, S. G. and DeGraff, J.V., eds., Catastrophic Landslides: Effects, occurrence, and mechanisms: Boulder, Colorado, Geological Society of America Reviews in Engineering Geology, v. XV, p. 165-190.

Wieczorek, G.F., and Jäger, S., 1996, Triggering mechanisms and depositional rates of postglacial slope-movement processes in the Yosemite Valley, California: Geomorphology, v. 15, p. 17-31.

Wieczorek, G.F., and Snyder, J.B., 1999, Rock falls from Glacier Point above Camp Curry, Yosemite National Park, California: U.S. Geological Survey Open-file Report 99-385.

Wieczorek, G.F., and Snyder, J.B., 2004, Historical rock falls in Yosemite National Park: U.S. Geological Survey Open-File Report 03-491.

Wieczorek, G.F., Snyder, J.B., Alger, C.S., and Isaacson, K.A., 1992, Rock falls in Yosemite Valley, California: U.S. Geological Survey Open-File Report 92-387.

Wieczorek, G.F., Nishenko, S.P., and Varnes, D.J., 1995, Analysis of rock falls in the Yosemite Valley, California, *in* Daemen, J.J.K, and Schultz, R.A., Rock Mechanics, Proceedings of the 35th U.S. Symposium, p. 85-89.

Wieczorek, G.F., Morrissey, M.M., Iovine, G., and Godt, J., 1998, Rock-fall hazards in Yosemite Valley: U.S. Geological Survey Open-File Report 98-467.

Wieczorek, G.F., Morrissey, M.M., Iovine, G., and Godt, J., 1999, Rock-fall potential in the Yosemite Valley, California: U.S. Geological Survey Open-File Report 99-578.

Wieczorek, G.F., Snyder, J.B., Waitt, R.B., Morrissey, M.M., Uhrhammer, R., Harp, E.L., Norris, R.D., Bursik, M.I., and Finewood, L.G., 2000, The unusual air blast and dense sandy cloud triggered by the July 10, 1996, rock fall at Happy Isles, Yosemite National Park, California: Geological Society America Bulletin, v. 112, p. 75-85.

Wieczorek, G.F., Stock, G.M., Reichenbach, P., Snyder, J.B., Borchers, J.W., Godt, J.W., 2008, Investigation and hazard assessment of the 2003 and 2007 Staircase Falls rock falls, Yosemite National Park, California, USA: Natural Hazards and Earth System Sciences, v. 8, p. 421-432, www.nat-hazards-earth-syst-sci.net/8/421/2008/

Zimmer, V.L., Collins, B.D., Stock, G.M., and Sitar, N., 2012, Rock fall dynamics and deposition: An integrated analysis of the 2009 Ahwiyah Point rock fall, Yosemite National Park, USA: Earth Surface Processes and Landforms, v. 37, p. 680-691, doi: 10.1002/esp.3206.